Heidelberg University

Faculty of Chemistry and Earth Sciences

Institute of Geography

Master Thesis

Remote sensing analyses for open-pit mine area computation

– A comparative study on the implementation of multi-spectral classifications and crowdsourcing to compute the spatial extent of four open-pit mines in Indonesia, Australia, Canada and Brazil –

Silvana Bürck

Matriculation number: 3469917

Buerck@stud.uni-heidelberg.de

1st supervisor: **Prof. Dr. Bernhard Höfle**

2nd supervisor: **Prof. Dr. Olaf Bubenzer**

Ruprecht-Karls-Universität Heidelberg

Date: 2019-06-21

„The first day or so we all pointed to our countries.

The third or fourth day we were pointing to our continents.

By the fifth day, we were aware of only one Earth. "

Astronaut Sultan bin Salman Al-Saud about his space flight 1985

(Kelley 1988)

Statutory declaration

I declare that I have authored this thesis independently, that I have not used other than the declared sources / resources and that I have explicitly marked all material which has been quoted either literally or by content from the used sources.

This paper was not previously presented to another examination board and has not been published.

…………………………… ………………………………………………..

Date Signature

Acknowledgements

First of all, I would like to thank Prof. Dr. Bernhard Höfle for his supervision and providing me with inspirations and valuable feedback. In addition, I want to thank his 3D GEO Group for constructive feedback during the seminar.

Further, I would like to thank Prof. Dr. Olaf Bubenzer for being my second supervisor.

I sincerely want to thank ifeu GmbH, especially Claudia Kämper, Regine Vogt and Horst Fehrenbach, for giving me the opportunity to work on this topic within ifeu GmbH, for providing me with ideas and for support.

Moreover, I would like to thank Judith Levy for support in SAR pre-processing.

Furthermore, I would like to thank Benjamin Herfort, Elisabeth Brzoska and Raffael Lutz for participating in the crowdsourcing pre-test and all volunteers who joined the crowdsourcing project.

A big thank you goes to my family for their support during this period. Especially I would like to thank Reinhold and Anneliese Bürck for providing me with this working place.

In addition, I would like to thank to my friends Jonas Werle, Elisabeth Brzoska and Amelie Kramer for proofreading, as well as Paul Sudrat, Jan Sennekamp and Michel Allekotte for support and food provision.

At this point, I also want to thank Hekla Udho for inspiring me to go into the field of Geography and Karoline Maretzke for support during this way.

Abstract

Increasing awareness is dedicated to environmental impacts of mining activities around the world. In this context, Environmental Hazard Potential (EHP) is considered to be an appropriate way to assess all environmental impacts related to mining activities. A holistic EHP requires detailed knowledge about the spatial extent of the mining area. Even though several studies have already been conducted in the domain of mine detection and mapping, no comparative study has yet been carried out that investigates several remote sensing analyses, which are transferable to other geographic regions. The aim of this study is thus to compare remote sensing analyses that can be applied in order to determine the area that is subject to open-pit mining in different geographic regions. Therefore, this study examines strengths and weaknesses of remote sensing analyses, among them index-based, pixel-based and object-based multi-spectral classifications on single- and multi-source level, as well as crowdsourcing. Data sets comprise freely available Sentinel-2 optical imagery, Aster GDEM V2 elevation model and Sentinel-1 synthetic aperture radar imagery. Four copper or iron ore open-pit mines in Indonesia (Grasberg-Ertsberg Gold Copper Mine), Australia (Hamersley Iron Ore Mines), Canada (Highland Valley Copper Mine) and Brazil (Mariana Iron Ore Complex) constitute the study sites. Index-based, pixel-based and object-based classifications are applied on the datasets for each study site, whereby index-based classifications are conducted on single-source level, pixel-based and object-based classifications on multi-source level. Simultaneously, a crowdsourcing project is launched, where volunteers are asked to digitize the delineation of the four open-pit mines. First, classifications and crowdsourcing are investigated individually by visual interpretation, accuracy assessment and area computation. Secondly, both methods are compared by Intersection over Union (IoU), by area values, accuracy values and visual interpretation. Acquired new findings regarding the implementation of the methods and the achieved results support the final derivation of strengths and weaknesses of classifications and crowdsourcing.

Classifications and crowdsourcing can both be applied in order to detect, classify and digitize open-pit mines in different geographic regions with an overall accuracy ≥ 77.41 % and to compute their spatial extent. Overall accuracy ranges for all methods from 77.41 % up to 97.73 %. The comparison of these methods reveals that classification and crowdsourcing results are not congruent, indicated by a mean IoU of 0.49 for all conducted comparisons. Classifications and crowdsourcing results differ among their respective area values, accuracy values and visual impression. Regarding area and accuracy values, crowdsourcing results have an intermediate position between the three considered classifications. Final derivation of strengths and weaknesses, as well as opportunities and threats shows that classifications and crowdsourcing differ further regarding effort, transferability, completeness, implementation, quality and credibility as well as their potential for automatization and further development. This study strongly supports decision making regarding method selection by providing strengths and weaknesses of remote sensing analyses for mine area computation. It contributes thus to the development of a holistic EHP of open-pit mines in different geographic regions. Future research recommendations are primarily related to the detection of unknown mines with classification approaches, to the development of a crowdsourcing project for global mine mapping and to the investigation of the potential of a combined application of classifications and crowdsourcing.

Table of contents

List of figures

List of tables

List of abbreviations

AOI	Area of Interest
CMI	Clay Mineral Index
DEM	Digital Elevation Model
EHP	Environmental Hazard Potential
ENVI	Environment for Visualizing Images (Software)
EPSG	European Petroleum Survey Group Geodesy
ESA	European Space Agency
FMI	Ferrous Mineral Index
GDEM	Global DEM
GIS	Geographic Information System
GRD	Ground Range Detected
IND	Index-based Classification
IoU	Intersection over Union
IW	Interferometric Wide Swath
LR	Lower-Right (Coordinates)
MAJ	Majority polygon
MAX	Maximum (Maximum polygon)
MIN	Minimum (Minimum polygon)
NASA	National Aeronautics and Space Administration
NDVI	Normalized Difference Vegetation Index
NIR	Near Infrared
OBIA	Object-based image analysis/classification
OCN	L2 Ocean Product
PCA	Principal Component Analysis
PIX	Pixel-based Classification
QGIS	Quantum GIS (software)
RGB	Red Green Blue (True color image)
ROI	Region of Interest
SAR	Synthetic Aperture Radar
SCP	Semi-Automatic-Classification Plugin
SLC	Single Look Complex
SNAP	Sentinel Application Platform (Software)
SVM	Support Vector Machine (Algorithm)
SWIR	Short Wavelength Infrared
UBA	Umweltbundesamt (Federal Environment Agency)
UL	Upper-Left (Coordinates)
UTM	Universal Transverse Mercator
VH	Vertical Horizontal Polarization
VV	Vertical Polarization

1 Introduction

The most recent dam failure, known as the Brumadinho dam disaster, occurred in 2019 on January 25th in Minas Gerais, a state in the southeast of Brazil. A tailing dam collapsed and a total of 13 million m^3 of tailings were released. More than 200 people were killed, agricultural areas and subsequently local markets were destroyed and aquatic ecosystems were contaminated by heavy metals, exceeding accepted heavy metal thresholds by factor 21 (Cionek et al. 2019). In the last years, a number of similar dam failures occurred, such as the Mount Polley dam failure of 2014 in Canada or the Mariana dam failure of 2015 in Brazil (Santamarina et al. 2019). However, dam failures constitute only one potential consequence of mining activities. Other environmental consequences range from local land degradation and subsequent impacts on ecosystems, the water balance and soil conditions to emissions impacting the environment and climate on a global scale (Manhart et al. 2017).

Global mining activities will further increase, as the current world population of 7.6 billion will increase to 8.6 billion by the year 2030 (United Nations, Department of Economic and Social Affairs, Population Division 2017). This global population growth manifests itself in a growing demand for consumer goods, which is related to an increasing depletion of resources. Additionally, the permanent process of global industrialization requires large amounts of raw materials. Germany in particular, focusses heavily on the resource intensive production and export of non-agriculture products, with motor cars being the top exported product (World Trade Organization 2017). In this context, abiotic raw materials, especially metals, among them iron ore, copper ore and bauxite, are of particular interest for industrialized countries, as they are most frequently used for industrial purposes (Neukirchen and Ries 2014).

Due to its importance for the economy and the involved environmental risks, the mining sector has come into the focus of political discussions. In order to mitigate environmental impacts of mining activities in countries exporting abiotic raw materials, the German Federal Environment Agency carries out a resource efficiency program for the sustainable use and conservation of natural resources since 2012 (Bundesministerium für Umwelt, Naturschutz, Bau und Reaktorsicherheit (BMUB) 2016). Within this context, the Federal Environment Agency (UBA) investigates the Environmental Hazard Potential (EHP) of mining, thereby considering all environmental impacts related to the mining of iron ore, copper ore and bauxite in different geographic regions (Manhart et al. 2017). The above mentioned raw materials are primarily extracted by open-pit mining. An open-pit mine is defined as an area that is subject to the extraction of raw materials at the earth's surface (Neukirchen and Ries 2014).

For the purpose of a comprehensive assessment of the EHP of open-pit mining, a sound knowledge of the spatial extent of each mining area and a thorough understanding of its correlation with environmental impacts is required. However, the possibility of such a comprehensive assessment remains limited, given the fact that information about the spatial extent is still unknown for a significant number of open-pit mines, and mapping approaches in this domain remain sporadic (Lobo et al. 2018).

In the case of spatial analysis of mining areas, remote sensing is considered to provide the required data. According to Lillesand et al. (2008), remote sensing is the science of generating information about a research object by analyzing data that have been obtained contactless, thereby sensing the object remotely. Given the fact that different objects reflect electromagnetic radiation differently, remote sensing analyses use the investigation of different spectral signals in order to acquire information about the research object. Different sensors and sensing methods, which constantly emerge, result in a large variety of remote sensing data. They comprise aerial photographs, multispectral, thermal and hyperspectral satellite imagery, which are referred to imagery from passive sensing methods, as well as Synthetic Aperture Radar (SAR) imagery and Light Detection and Ranging (LIDAR) point clouds from active sensing methods. Remote sensing data exhibit a wide range of spectral, spatial and temporal characteristics. For the spatial analysis of mining areas, remote sensing constitutes a suitable way to acquire data, given the fact that access to open-pit mines is frequently limited (Paull et al. 2006). Besides this, the wide spectral range, the high temporal and spatial resolution as well as the partially free availability of remote sensing data makes it a suitable data source (Basommi et al. 2015; Charou et al. 2010; Garai and Narayana, 2018; LaJeunesse Connette et al. 2016).

Remote sensing analyses which can be applied for area calculation range from pixel-based to object-based multi-spectral classifications and index-based feature detection. Classifications based on the multiple spectral characteristics of the investigated features and accordingly of the different bands, are referred to multi-spectral classifications. For pixel-based classification, the remote sensing imagery is classified according to the spectral information of each individual pixel. On the contrary, object-based classification considers spectral as well as spatial information by first segmenting the entire image into homogeneous objects and secondly classifying these objects separately. For the segmentation, characteristics such as shape, color and texture of each pixel are considered in order to group them to a homogeneous segment. In the case of multi-spectral band availability, spectral indices can be derived from mathematical band combinations, such as the Normalized Difference Vegetation Index (NDVI) for the detection of vegetated areas (Albertz 2009; Lillesand et al. 2008). Contrary to pixel-based and object-based classifications, feature detection based on spectral indices (Ma et al. 2018a) requires only a small amount of spectral bands from one sensor and demands no training, which makes them a fast classification method. On the other hand, pixel-based classification requires more bands for the classification, but it has the advantage of generating reliable results when only considering spectral information of individual pixels of a only single source, thus constituting a low-time expenditure classification method as well (Lobo et al. 2018). Object-based classification convinces through the integration of spatial, texture and contextual parameters in addition to spectral information, as well as the possibility to integrate ancillary datasets (multi-source) and the absence of the salt & pepper effect (Prudente et al. 2017; Qian et al. 2018). In addition, crowdsourcing provides a further approach of spatially analyzing data by a crowd of volunteers on the basis of remote sensing data (Heipke 2010). For such geospatial analyses, volunteers can participate either in digitization, classification or conflation tasks (Albuquerque et al. 2016). Albuquerque et al. (2016) demonstrated that crowdsourcing classifications constitutes a successful method for deriving geospatial information, thus crowdsourcing can be considered as an additional remote sensing analysis for mine area computation. Current applications of these methods in the domain of mining are presented in the following chapter.

The motivation to conduct this study is based on the general lack of information about the spatial extents of mining areas, while a wide variety of suitable remote sensing analyses and data sets are technically available. Therefore, the objective of this study is to compare different remote sensing analyses with regard to their suitability to compute the spatial extent of mining areas. According to the state of the art, this research objective will experience further precision within the following chapter.

By providing strengths and weaknesses of potential remote sensing analyses that can be applied to determine the missing parameter "mine area at earth surface", this study supports decision-making regarding the selection of appropriate methods and thereby contributes to a comprehensive EHP of open-pit mines in different geographic regions.

The content of this document is organized as follows: Chapter 2 gives an overview on the state of the art regarding the dimension of open-pit mines, remote sensing, classifications and crowdsourcing. After mapping the current research field, the research gap as well as the derived research question is presented. Subsequently, the choice of the study sites and datasets is described in chapter 3, including the required pre-processing of the datasets and information about the reference data and mine indicators. In order to give an overview of the methodology, the research design is presented first in chapter 4, followed by an in detail description of each single method. The obtained results for each method are presented in chapter 5. A discussion of these results follows in chapter 6. Thereby, main findings concerning the results and the methodology are identified and related to previous studies and conclusively strengths and weaknesses of each method are determined in order to answer the research question. Finally, chapter 7 gives a conclusion and outlines future research recommendations.

2 Related works

As mentioned in the introduction, the framework of this study is composed out of three dimensions. The object of research, the open-pit mine, constitutes the first dimension. Remote sensing represents the second dimension, meaning the data source, whereas remote sensing analyses, such as classifications and crowdsourcing, are considered as the third dimension. In the following, current studies related to these three dimensions are presented chronologically. First, an outline on current research about open-pit mines is presented. Secondly, the state of the art of remote sensing and remote sensing applications in the domain of mining is presented. Following, current studies on classifications and crowdsourcing are outlined as well as their application in the mining context. A sound knowledge about the current research in these three dimensions is crucial in order to recognize the research gap in this field and to fully understand the thereby derived research question.

2.1 Open-pit mines

In the literature on open-pit mines, two distinct research objectives were found. The first main research objective is related to mining optimization, whereas the second main research objective is the analysis of consequences of mining activities.

During the last years, several studies about short- and long term production scheduling (Blom et al. 2018; Ramazan and Dimitrakopoulos 2018), mining schedule optimization (Menabde et al. 2018) and cutoff grade optimization (Ahmadi and Bazzazi 2019; Ahmadi and Shahabi 2018) were conducted. The main focus of these studies was to optimize mining activity by strategic planning of the mining process (Navarra et al. 2018). In the same context, optimized methods for the extraction and processing of raw materials have been proposed by Abbaspour et al. (2019) and Froyland et al. (2018). Xu et al. (2018) investigated production scheduling optimization as well, but contrary to studies mentioned before they additionally conducted ecological cost considerations integrating costs from carbon emissions, costs related to damaged land, and lost value of direct and indirect ecological services. Accordingly, Xu et al. (2018) investigated the optimization of mining as well as mining consequences.

A wide range of studies have been conducted in order to assess the consequences related to mining activities. In this context, consequences associated with human health issues, such as genetic damage have also been investigated (Espitia-Pérez et al. 2018a; 2018b). The impact of current mining activity on vegetation has been thoroughly studied by Stachiw et al. (2019), who analyzed trace elements in berries in the proximity of the mine. Additionally, the development of ecological reclamation and ecological restauration areas has been investigated by vegetation and soil analysis (Domínguez-Haydar et al. 2019; Hou et al. 2019). A novel approach of ecological restoration evaluation by a non-scientific crowd has been conducted by Carabassa et al. (2019), who developed a methodology for self-evaluation of a quarry restoration by a heterogeneous crowd.

A part from consequences of mining activity on the natural or human environment, mining hazards and accidents, such as dam bursts have been investigated. Carmo et al. (2017) and Hatje et al. (2017) analyzed the dam burst of the Mariana mine in 2015, a dam collapse, which is considered to be one of the largest tailing dam failures worldwide. Whereas Carmo et al. (2017) analyzed the consequences of the hazard of this dam burst in a global context, Hatje et al. (2017) carried out an environmental impact assessment of the dam failure by studying toxic metals in water and sediments.

In order to mitigate such hazards, a variety of investigations have been dedicated to ground deformation analysis (Widzyk-Capehart et al. 2019), slope instability (Jiang et al. 2018; Morales et al. 2019; Ortega et al. 2018), rockslides (Li et al. 2019) and rock mass disturbance (Rose et al. 2018) of open-pit mines. Especially slope instability has been intensively investigated, given the fact that slope instability can be accompanied by rock slides (Ma et al. 2018b) or infrastructure damage, such as dam breaking.

First general screenings of mining activities in order to assess the EHP have been carried out by Manhart et al. (2017) and Castelo Branco et al. (2019). Whereas the latter reviewed risks by keyword search in specific databases and found out that risk was primarily related to the environment and geology, Manhart et al. (2017) developed a model for the evaluation of raw materials on the one hand and mining areas on the other hand.

2.2 Remote sensing

With the permanent enhancement of existing and the development of new sensors (Hossam 2015), a wide range of datasets with different potentials became available. This situation manifests itself in a constant development of fusion methods on the one hand and in a broad field of applications on the other hand.

In order to benefit from the large amount of different available sensors and their specific spectral and spatial characteristics, data fusion methods have been developed for multi-source applications (Chen et al. 2017; Dong et al. 2009; Ghassemian 2016; Pohl and Van Genderen 1998). Frequently, synthetic aperture radar (SAR) and optical sensor imagery have been fused for spectral and spatial optimization (Kuchma 2016). For example Whyte et al. (2018) applied Sentinel-1 and Sentinel-2 data for wetland mapping. In this context, Abdikan et al. (2014) presented a model for quality assessment of multi-sensor fusion methods for SAR and optical imagery, thereby revealing that the Ehlers fusion performs best regarding accuracy. In addition to multi-source fusion, multi-temporal fusion has been investigated for pan-sharpening fusion by Ehlers et al. (2010). An overview of spatiotemporal fusion techniques has been given by Xiaolin Zhu et al. (2018).

Besides the large number of data fusion methods, the field of remote sensing applications has widened. Current applications range from volcanic deposit monitoring (Ganci et al. 2018), mangrove monitoring (Duncan et al. 2018), archeology investigations (Borie et al. 2019), crop type classification (Cai et al. 2018) to water resource management (Sheffield et al. 2018). Even for distribution analysis of particulate matter concentrations (Chen et al. 2018a; Lin et al. 2018) or aerosol investigations (Eck et al.

2018), remote sensing data has been applied. Additionally, ecosystem functions (Pettorelli et al. 2018), as well as ecosystem risks (Murray et al. 2018) have recently been monitored by the application of remote sensing data. Further, local ecosystem modelling has been conducted by Pasetto et al. (2018). In the same context, Gray et al. (2018) investigated estuarine environments, but contrary to previous studies that were primarily based on single-source data, a multi-source approach has been chosen for this study implementing drone and satellite imagery.

In the context of mining, the previously observed tendencies of data fusion and broad application of remote sensing were found as well. Applications range from resource exploration to mine feature extraction up to the monitoring of re-cultivated mining sites by implementing single-source or multi-source remote sensing datasets.

At the turn of the millennium, Sabins (1999) already presented applications of remote sensing for mineral exploration by having a closer look at hydrothermally altered rocks, which are recognizable in remote sensing data. That investigations in this domain are still of interest has been confirmed by Pour and Hashim (2012), who investigated epithermal gold deposits and porphyry copper deposits (Figure 2-1) using Aster imagery. Therefore, minerals that belong to a porphyry-copper deposit have first been analyzed by spectroscopy regarding their spectral reflectance characteristics, and then spectral signals have been resampled to Aster bands (Figure 2-2). Multi-source approaches for the exploration of porphyry copper and for the exploration and monitoring of mines have been conducted by Safari et al. (2018), who integrated two optical sensors in their investigation and Kirsch et al. (2018), who performed terrestrial and airborne hyperspectral analysis and photogrammetry. In the domain of exploration, a particular focus was on lithium exploration, as this raw material is of significant importance for future energy storages, applied e.g. in electric vehicles (Cardoso-Fernandes et al. 2019). Even though the majority of studies were based on the availability of optical sensor imagery, some studies have applied terrestrial laser scanning (TLS) in the exploratory phase when it comes to volume

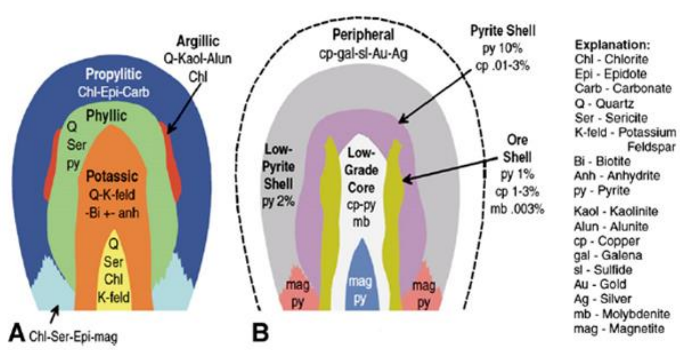

Figure 2-1: Schematic cross-section through a porphyry copper deposit with related mineral zones (left) and ore zones (right); Source: Pour and Hashim (2012).

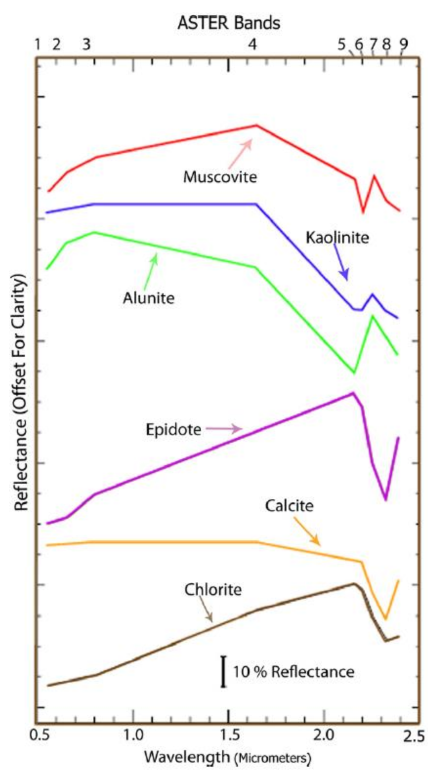

Figure 2-2: Spectral signals of minerals associated with porphyry copper deposits that have been resampled to Aster bands; Source: Pour and Hashim (2012).

computation (Xu et al. 2019). Besides pure exploration for raw material depletion, mineral detection has proven to support the analysis of toxic substances in wastes, which are considered a primary by-product of mining activities (Lozano-Cotrina et al. 2018). While earlier studies that had a clear focus on mineral detection for future exploration, several other studies have been conducted in order to map and monitor mines under operation. Yu et al. (2018) applied multi-source datasets for monitoring significant surface mining belts. In order to map existing mines and analyze their expansion, Vassena and Clerici (2018) conducted 3D open-pit mapping, while LaJeunesse Connette et al. (2016) developed indicators to identify potential mines, which have been considered when building up a Landsat based raster layer of potential mines. Subsequently, the latter has supported a guided digitization process to detect open-pit mines on a national scale in Myanmar. Within this novel model, mine expansion has been detected by albedo and brightness change between two points in time. This study provided a nationwide database of mining areas. In order to cover the entire range of applications from exploration, active mine monitoring and depleted mine detection, Raval (2018) proposed a review on advances in sensing systems.

Recent studies in the domain of remote sensing and mining have demonstrated that remote sensing analyses are not only restricted to the exploration of new resources, but they have also been applied for the assessment of potential and occurred consequences of mining activities. In the context of potential and occurred impacts, slope instability (Carlà et al. 2018; Sengupta et al. 2018), topographic modelling and monitoring (Beretta et al. 2018; Wasowski et al. 2018; Xiang et al. 2018) have been investigated closely to mitigate impacts as effectively as possible. Regarding land disturbance of tropical rainforests, Asner et al. (2013) detected gold mining sites in the Amazon by remote sensing, thereby emphasizing the importance of high resolution imagery for such objectives. Particular interest in monitoring mine waste dump sites and dams and dikes is demonstrated in the studies of Wei et al. (2018) and Mura et al. (2018). Given the fact that dam breaks have already happened several times, their monitoring is crucial in order to avoid the reoccurrence of such events. Further monitoring of acid mine drainage was carried out by Jackisch et al. (2018). An entire ecological risk assessment of a mining area based on remote sensing was proposed by Li et al. (2018a), who introduce an ecological risk index. An overview of potential remote sensing analyses for the assessment of social and environmental impacts of mining activities can be found in the studies of Banks et al. (2005) and Paull et al. (2006). Besides the impacts of current mining on the environment, several studies have recently been conducted in order to assess the recovery in the post-mining phase. Yang et al. (2018b) integrate the LandTrendr algorithm, which is based on NDVI computation, for the detection of vegetation disturbance on the one hand, but also in order to assess vegetation recovery in former mines. In a similar way, Wu et al. (2018) detect vegetation and landscape changes in mines by implementing the BFAST1-module, a time series analysis algorithm. While previous studies used primarily satellite remote sensing imagery, Johansen et al. (2019) investigated the rehabilitation performance of vegetation in former mines using unmanned aerial vehicles (UAV). Similarly, Beretta et al. (2018) compared the implementation of UAV and subsequent photogrammetry to laser scanning for the topographic modelling of mining sites.

2.3 Classifications and crowdsourcing

2.3.1 Classifications

In the domain of classifications, two main objectives of current research were observed. A large number of studies have a clear focus upon machine learning for classification purposes (Cheng et al. 2018; Han et al. 2018; Maxwell et al. 2018). Thereby, a mathematical algorithm is trained for prediction and decision-making. A clear dominance of the application of machine learning based classifications in the domain of cropland analysis has been observed, as demonstrated in the study of Ji et al. (2018), who applied 3D convolutional neural networks for the classification of crop types.

The second main focus of current research in the domain of classifications is a methodological comparison between pixel-based and object-based classifications. Given the fact that applications of these two types of classifications increase strongly, many studies have been conducted in order to compare the potential of object-based to pixel-based classifications. Similar to machine learning approaches, comparisons between pixel-based and object-based classifications are primarily conducted to analyze cropland features (Belgiu and Csillik 2018; Roy et al. 2018; Xiong et al. 2017). Remote sensing data ranges thereby from single-source (Belgiu and Csillik 2018) up to multi-source approaches (Xiong et al. 2017). In addition to these tendencies, methodological comparisons have been conducted in the domain of mangrove mapping (Wang et al. 2018a), coal fire classification (Yan et al. 2006), landslide detection (Keyport et al. 2018) and invasive species mapping (Sampedro and Mena 2018). The outcome of the majority of these studies was that object-based classification is mostly favored over pixel-based classifications, given the absence of the salt & pepper effect, the higher accuracy of soil and vegetation classification and in general better performance regarding accuracy. A detailed comparison has been conducted by Prudente et al. (2017), who outlined strengths of object-based classifications as well as potential limitations. Given the advantages of object-based classifications, many current studies investigated only object-based classifications and their optimizations for various application fields such as urban applications (Georganos et al. 2018) and land cover and grass land mapping (Li and Shao 2014; Ma et al. 2017a; Melville et al. 2018), thereby performing on single-source and multi-source level. A closer look upon segmentation and training has been observed in the study of Costa et al. (2017), who investigated the suitability of mixed objects for object-based classifications. An overview about emerging trends and future applications regarding Geographic Object-based Image Analysis (GEOBIA) has been given by Chen et al. (2018b).

Besides these two main focusses of current research, some studies on the implementation of spectral indices for classification and mapping have recently been conducted. Contrary to multi-source investigations, these approaches are considered to be single-source, by applying several bands of the same sensor for the computation of spectral indices. Frequently, the NDVI has been investigated, as it has been the case in Sonobe et al. (2018), who classified crops by deriving vegetation indices from Sentinel-2 imagery or Valderrama-Landeros et al. (2018), who conducted a NDVI-based classification of mangrove areas. Other than previous studies investigating or classifying only for a given timestamp, Palchowdhuri et al. (2018) classified crop types by spectral indices on a multi-temporal scale. In order to face the difficulty of threshold setting, Zhang et al. (2018) developed an automated dynamic model for threshold extraction for the classification of water bodies. A detailed discussion about NDVI applications, as well as an introduction to further spectral indices for Aster data, such as mineral indices, has been presented by Ninomiya (2003). By analyzing and comparing reflectance spectra of minerals in the laboratory, they derived spectral indices, among them the calcite index, the OH-bearing altered minerals index, the kaolinite index and the alunite index. In a case study, these mineral indices were applied using Aster data and confirmed the presence of cuprite at the study site.

The current trends in the domain of classifications have been partly observed in the context of mining as well. Especially spectral indices, pixel-based and object-based classifications have recently been used in order to map and monitor mines, to analyze change detection or to conduct impact assessment. Regarding spectral indices, NDVI has frequently been applied for analyzing vegetation dynamics in mining regions (Prakash and Gupta 1998; Jia et al. 2018) for land use mapping and change detection in coal fields (Prakash and Gupta 1998), or for mapping mine extent, as demonstrated by Pericak et al. (2018), who developed an open source model for NDVI-based mine mapping. Mine detection has been investigated by Castellanos-Quiroz et al. (2017) using data fusion and spectral indices classification. Besides NDVI, they included the Ferrous Mineral Index (FM), the Clay Mineral Index (CM) and the Iron Oxide Index (IO) for the subsequent extraction of mine features by specified thresholds. Mineral indices have further been applied in the spectroscopic detection of heavy metal substances in mine soils (Sawut et al. 2018). A novel index, the Ultra-Low-grade Iron-related Objects Index (ULIOI) has been developed by Ma et al. (2018a) for extracting tailing features from remote sensing imagery. This index is based on different spectral characteristics of mine objects (Figure 2-3). Mukherjee et al. (2019) did not only focus on tailings, but developed a novel mine detection index for Landsat imagery by computing the ratio between Short Wavelength Infrared (SWIR-I) (1.566-1.651 µm) and SWIR-II (2.107-2.294 µm) bands of Landsat 8.

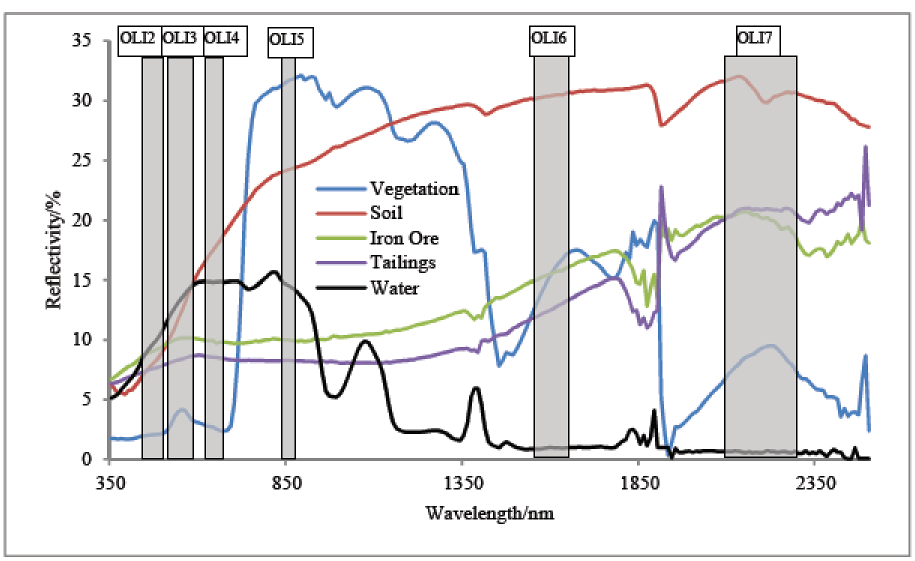

Figure 2-3: Spectral signatures of different features of open-pit mines and their surroundings within Landsat bands (OLI2-7); Source: Ma et al. (2018).

For the purpose of mine mapping, pixel-based classification approaches have been applied as demonstrated within the study of Lobo et al. (2018), who mapped mines in the Brazilian Amazon by conducting supervised classification. With a stronger focus on land change detection of mining areas, Garai and Narayana (2018) performed an unsupervised classification on pixel-level. Further land use and land cover change detection of mining areas has been investigated by implementing pixel-based classifications as shown in Basommi et al. (2015) and Karan and Samadder (2018a). The latter classified by applying a pixel-based Support Vector Machine (SVM) algorithm. Basommi et al. (2015) developed a pixel-based classification and complemented the land use and land cover change assessment of mining areas by NDVI analysis. Similar to Garai and Narayana (2018), Charou et al. (2010) conducted an unsupervised classification in order to assess the impact of mining upon land and water resources.

In the same context of impact assessment, object-based classification has been applied by Qian et al. (2018), who analyzed the impact of mining activity upon surrounding land and ecosystems services. It has been demonstrated by Bona et al. (2018) and Zhang et al. (2017) that object-based classification is also suitable for the classification of mining sites and change detection in mine areas. Bona et al. (2018) conducted a multi-source object-based classification of mining sites by the integration of Spot and Sentinel-1 imagery. For information extraction of a Nickel mine, Chen et al. (2018c) conducted object-based classification with hierarchical multi-scale segmentation.

As far as machine-learning based classifications in the domain of mining are concerned, Karan and Samadder (2018a), developed a model composed of a two wavelet-based image enhancement and subsequent SVM classification for accurate long-term change assessment of a coal mining area. Additionally, Karan and Samadder (2018b) performed dual-tree complex wavelet transform-based image enhancement first and applied then neural net supervised classification for the classification of a coal mine.

2.3.2 Crowdsourcing

As a recent development, crowdsourcing has been considered an additional option to generate geospatial data from remote sensing imagery. An overview of developments in crowdsourcing geospatial data has been given by Heipke (2010). A topology of tasks for deriving geographic information from crowdsourcing has been developed by Albuquerque et al. (2016). Different types of crowdsourcing tasks, such as classification, digitization and conflation have been discussed. By presenting a case study about a crowdsourced classification in the domain of humanitarian aid, Albuquerque et al. (2016) demonstrated that a high level of quality could have been achieved and thereby confirmed that crowdsourcing classification is a promising method for deriving spatial information on human settlements. Current crowdsourcing implementations are divers and range from novel GEO-reCAPTCHA developments, where the security reCAPTCHA prompts users to perform a digitization (Hillen and Höfle 2015), to global estimations about agricultural field size (Lesiv et al. 2019) up to 3D micro mapping, involving the crowd in 3D point cloud analysis (Herfort et al. 2018). Panteras and Cervone (2018) and Wang et al. (2018b) integrated crowdsourcing for flood extent computation and urban flood monitoring. Volunteers are either asked to perform a specific task on the screen, in the field or passively by carrying sensors. Most of the previously mentioned studies focus on task performance on the screen. An example in this context has been the study of Johnson et al. (2017), where volunteers contributed to the creation of an Open-Street Map (OSM) by digitization. Subsequently, this OSM data is applied as training data in a multi-source classification of land cover change. Concerning in-situ measurements, (Fritz et al. 2012) developed a crowdsourcing tool in order to enhance in-situ land cover data, which can be used in order to assess land cover products and in order to generated a hybrid global map.

The distribution of sensors among volunteers, passively generating geographic data, is considered as human sensing. In this case, Yang et al. (2018a) investigated the extraction of road boundaries by providing volunteers vehicles with GPS instruments and analyzing their registered trajectories. As already mentioned in regard to the study of Johnson et al. (2017), crowdsourcing can support classification by providing training data. Such potential support for classification by crowdsourcing has further been discussed by Li et al. (2018b). Besides the support during the classification process, Saralioglu and Gungor (2019) proposed that crowdsourcing can be implemented in the post-classification phase by collecting control points for accuracy assessments.

In the domain of mining, no studies have been found involving crowdsourcing as a method. Digitization tasks, performed by groups have been conducted within the study of Paull et al. (2006), who performed environmental impact monitoring of an open-pit mine, but this task has not been outsourced to a crowd. The only study in the domain of mining being slightly related to crowdsourcing is the study of Carabassa et al. (2019), who developed a methodology for self-evaluation of ecological restauration of a quarry by a non-scientific group.

2.4 Research gap and research question

To summarize the presented overview of current studies related to open-pit mining, remote sensing and classifications and crowdsourcing, the conclusion can be drawn that open-pit mines have been closely investigated in their production optimization and impact assessment. Regarding current developments in remote sensing, a clear focus on data fusion and multiple applicability has been determined, the latter being observed in the domain of mining as well. For classifications, a strong tendency towards machine learning approaches and comparatives studies between pixel-based and object-based classifications has been observed. In the domain of mining, primary pixel-based or object-based classifications have been applied. Even though index-based feature extraction has not been applied frequently with respect to mining, its importance is increasing. Crowdsourcing as a method – to my current knowledge – has not yet been applied within the context of open-pit mining.

As the overall motivation of this study is to provide spatial information for EHP analysis, this study fits in the current research regarding open-pit mines, which focuses, among others, on impact assessment. The objective of the study, which is the comparison of remote sensing analyses that can be applied for the computation of the spatial extent of mining areas, is closely related to several studies in the domain of classifications, as one main focus of current research is the comparison between pixel-based and object-based classifications. Thus, this study fits into the current state of the art.

Especially the study conducted by LaJeunesse Connette et al. (2016), who proposed a remote sensing methodology for the identification of mining areas in Myanmar, is thematically closely related to the objective of this study, as the issue of mining area detection is addressed. But methodologically considered, LaJeunesse Connette et al. (2016) conducted no comparative study for the assessment of strengths and weaknesses of different remote sensing analyses that can be applied for the area computation of different open-pit mines. In addition, the study from LaJeunesse Connette et al. (2016) has a clear focus on Myanmar, other than the objective of this study. Another investigation that is closely linked to the objective of this study is Castellanos-Quiroz et al. (2017), who detected mines in Colombia by data fusion and the integration of spectral indices. This study proposed one potential methodology, but did not compare further remote sensing analyses for area computation of different open-pit mines. That means thematically considered, some studies already focused on mine detection, but methodologically considered, no comparative study that assesses strengths and weaknesses of different remote sensing analyses in the context of mine area computation, has been conducted to this date. Furthermore, no such comparative study has been undertaken for the investigation of open-pit mines in different geographic regions.

This study will thus present a comparison that investigates pixel-based and object-based classification for the computation of mining area due to their initially presented advantages (chapter 1) and due to the fact that their suitability for the analysis of various mine features has currently been confirmed by Charou et al. (2010), Lobo et al. (2018) and Qian et al. (2018). Besides, index-based approaches will be compared, given the fact that a wide range of spectral indices has recently proven to be appropriate for mine feature detection (Castellanos-Quiroz et al. 2017). Furthermore, crowdsourcing that has not yet been applied in the domain of mining by purpose, appears to be a suitable remote sensing analysis for providing geographical information (Albuquerque et al. 2016). Therefore, it will be included in order to compute the spatial extent of open-pit mines. The broad range of available remote sensing data (Lillesand et al. 2008) will be integrated by performing classifications on single-source and multi-source level as well. Regarding the research object, the open-pit mine, this study will consider the features indicating a potential mine from LaJeunesse Connette et al. (2016) as key elements in the definition of an open-pit mine. The initial objective presented in the introduction will thus be refined to a clear research question as follows:

What are the strengths and weaknesses of remote sensing analyses, among them index-based, pixel-based and object-based classifications on single- and multi-source level, and crowdsourcing that can be applied in order to determine the delineation of the area that is subject to open-pit mining at earth surface in different geographic regions?

The answer to this question will close the previously mentioned research gap by providing a comparison of remote sensing analyses that can be applied in order to compute the spatial extent of open-pit mines in different geographic regions. Thereby, this study makes a clear contribution towards EHP analysis of open-pit mines by providing strengths and weaknesses of potential remote sensing methods that can be applied for the determination of the missing parameter "mine area at earth surface". The study is thus aiming to support decision-making in terms of selecting appropriate remote sensing analyses.

3 Study sites and materials

This chapter outlines the selection of the study sites and characterizes each study site according to its geographic location, its climatic and vegetation pattern as well as its geological context. Embedding the study into the climatic context is significant, as this correlates with the vegetation pattern of the study sites, respectively. For this reason it is crucial to consider the surroundings of mines when classifying or digitizing mines. The integration in geological dimensions is considered essential, as this is the origin of today's mining activities. Materials of this study comprise the remote sensing data for analyses, the reference data and mine indicators. In the following, the selection of remote sensing datasets and relevant pre-processing of the data is described. Furthermore, information about the reference data and the mine indicators will be provided at the end of this chapter.

3.1 Study site

When aiming for sustainable use and conservation of natural resources, as it is intended by the resource efficiency strategy (Bundesministerium für Umwelt, Naturschutz, Bau und Reaktorsicherheit (BMUB) 2016), iron ore, copper ore and bauxite need to be considered, since these three raw materials are primary used for industrial purposes (Neukirchen and Ries 2014). Considering the appearance of open-pit mines of these three raw materials at earth surface, bauxite open-pit mines differ due to their extensive dispersion from copper and iron ore open-pit mines. The reason for this difference of appearance at earth surface is related to different deposit styles of iron ore, copper ore and bauxite (Neukirchen and Ries 2014). For this study, iron and copper ore open-pit mines will be considered, because bauxite mines differ too strongly from copper and iron ore mining regarding their visual appearance at earth surface. Bauxite mines thus, need further detailed investigations.

The Federal Environment Agency (UBA) will investigate 100 globally distributed open-pit mines of iron ore, copper ore and bauxite. Out of this frame, a randomly chosen amount of 50 iron-ore and open-pit mines has been revised for this study. First, open-pit mines have been clustered into ecozones according to Schultz's ecozones (Schultz 2016). For the ecozones Tropical and Subtropical Dry Areas, Summer Humid Tropics, Wet Tropics, Winter Humid Subtropics and Dry Mid Latitudes, mines have been determined. Natural surroundings of these mines range from dense forest, sparse vegetation to sparse alpine vegetation and up to bare area. One mine of each ecozone has been chosen for this study. As soon as natural surroundings of two mines from different ecozones were considered to be similar, only one out of these two was chosen.

For further analysis the following four open-pit mines, among them two copper ore and two iron ore mines, have been selected as study sites:

a. Grasberg/Ertsberg Copper/Gold Mine (Indonesia)

b. Hamersley Iron Ore Mines (Australia)

c. Highland Valley Copper Mine (Canada)

d. Mariana Iron Ore Complex (Brazil)

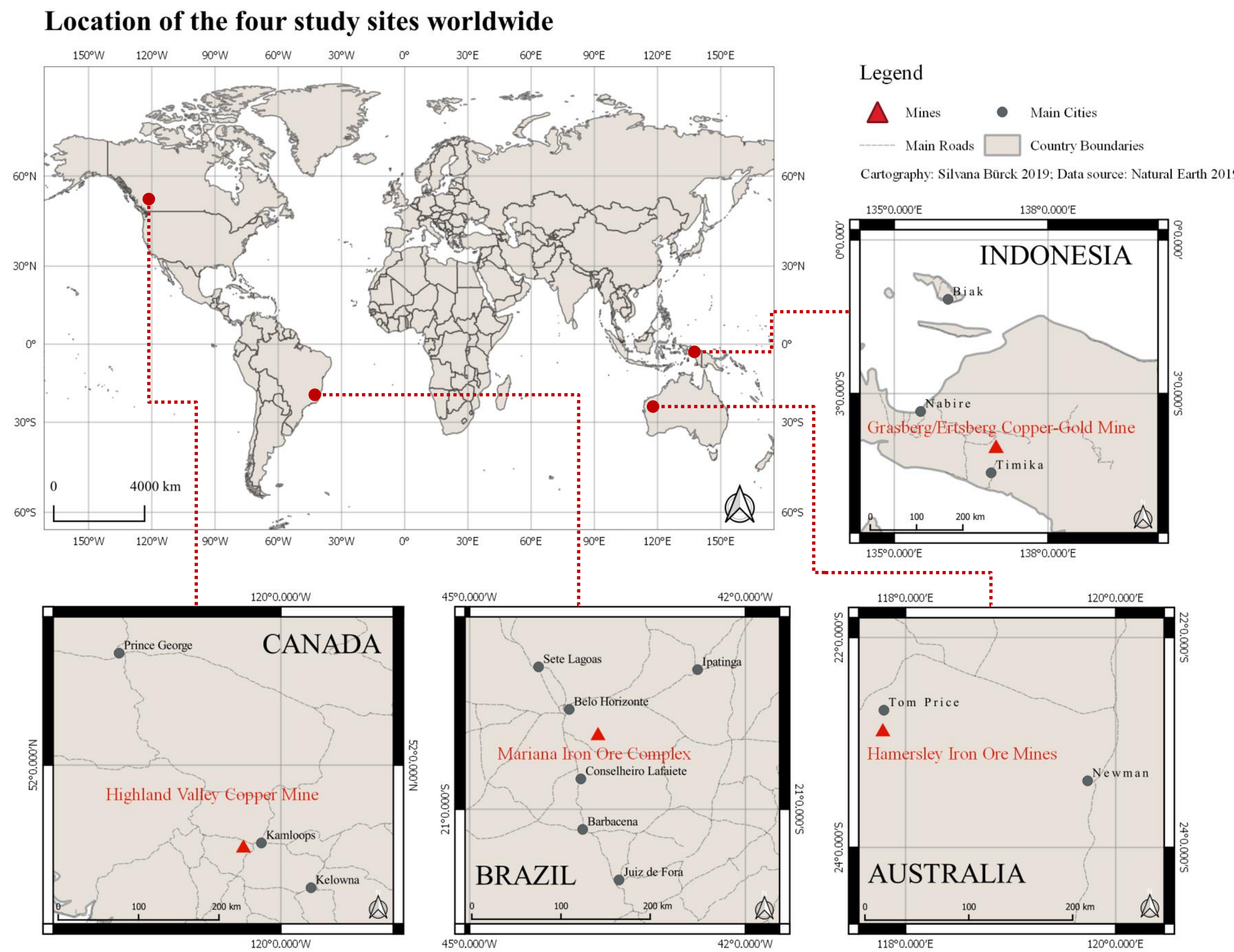

Figure 3-1: Location of the four open-pit mines of this study on small and large scale.

Figure 3-1 shows that they cover different geographic regions as they are located in Canada, Brazil, Australia and Indonesia. For simplification in the further course of this thesis, the entire names of the mines will be abbreviated to Grasberg mine, Hamersley mine, Highland mine and Mariana mine.

a. Grasberg mine

Grasberg-Ertsberg Copper-Gold Mine (Figure 3-2) is located in Indonesia within Papua province at 4°3'21.48"S and 137°6'35.61"E, which is 60 km northeast of the city of Timika. At an altitude of 3799 m above sea level, the mine is situated within the alpine zone.

For Timika, the city which is closest to the study site, the average annual air temperature is 26.1 °C; annual precipitation value averages around 3366 mm. According to Köppen and Geiger’s climate zones, this study site is thus considered to be an Af climate, which refers to tropical climate with monthly mean air temperatures of 18 °C and continuous precipitation (Figure 3-3) (Glawion 2012). Concerning Schultz’s ecozones, this study site belongs therefore to the Wet Tropics, where acid soils, leaching and evergreen deciduous forest is dominant (Schultz 2016). Image inspections of Google Earth Pro confirm that dense vegetation cover extents south of the mine. Nevertheless, as the open-pit mine is located in high altitude, direct surroundings are primary dominated by rocky bare area within a steep relief (Figure 3-2). Thus, this study sites appears to be a homogeneous study site with the mine embedded in rocky surroundings.

The mine belongs to the Grasberg Igneous Complex (GIC), which is characterized by sedimentary rocks such as shale, siltstone, sandstone, limestone and dolomite from Trias-Miocene. Several phases of intrusion, among them the Dalam Diatreme and the Main Grasberg Intrusion (MGI) have induced porphyry ore bodies. This Cu-Au deposit has been mined since 1989 and is primarily owned by Freeport McMoran Copper & Gold Inc. and some further shareholders. Mining is operated in an open-pit mine and underground. The open-pit mine forms a mile-wide crater at the surface, which is recognizable in satellite imagery. The Grasberg mine is considered to be one of the most extraordinary mineral systems worldwide, as it provides 6 % of the world supply of copper ore and holds large quantities of gold. It is the largest gold and the second largest copper ore mine worldwide. Annual ore extraction of the open-pit is approximately 67 million tons. Nevertheless the mine is expected to be exploited in less than 50 years (Bensaman et al. 2015). Environmental issues regarding Grasberg mine are already present, as reported by Kumah (2006), who explains that tailings have been deposed into the Ajkwa River, exposing environment and community to serious health risks.

Figure 3-2: View in the pit of Grasberg mine.
© iStock.com/joster69.

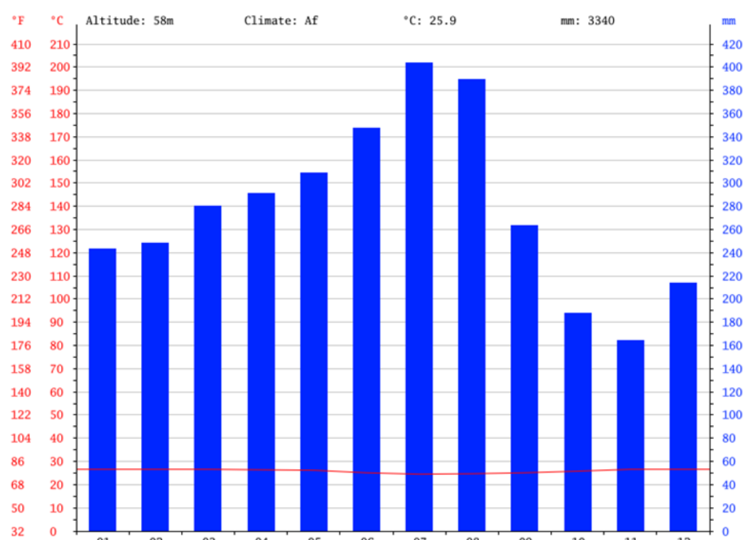

Figure 3-3: Climate chart of Timika, the closest city to the study site;
Source: Climate-data.

b. Hamersley mine

Hamersley Iron Ore Mines (Figure 3-4) are located in Australia, in the northwest of the state Western Australia. More precisely, Hamersley Iron Ore Mines comprise a total of 10 single open-pit mines, the mine investigated within this study is located 10 km southwest of the city Tom Price at 22°45'50.43"S and 117°47'4.65"E on an altitude of 772 m above sea level.

The Köppen-Geiger climate of Tom Price is BSh, which refers to a dry-hot steppe climate with annual air temperature above 18 °C (Glawion 2012). The climate chart in Figure 3-5 demonstrates that monthly air temperatures have only in June, July and August mean air temperatures below 18 °C, whereas during the other months mean air temperatures exceed 20 °C. Precipitation is about 38 mm a year, with higher precipitation values from December to March and very low precipitation values < 20 mm from July to November. Given its location and climatic characteristics, Hamersley mine belongs to the Tropical and Subtropical Dry Areas with subtropical deserts and semi-deserts according to Schultz's ecozones (Schultz 2016). This ecozone comprises dry deserts, where precipitation occurs, but only sufficient enough for sparse desert vegetation on leached soils. Satellite imagery confirms that the surroundings of Hamersley mine appear to be very bare, which makes it therefore difficult to distinguish the mine from its surroundings. Therefore, this study site is also considered to be homogeneous.

Hamersley Iron Ore Mines are Banded Iron Formations (BIF), belonging to the Mount Bruce Megasequence Set, which are Precambrian sedimentary and volcanic rocks overlying the Pilbara Craton (Barley et al. 1999). The mine investigated in this study is located close to Mount Tom Price, therefore sometimes called Tom Price mine. Mount Tom Price belongs to the Brockman Iron Formation, which is subject to open-pit mining at Hamersley mine (Thorne et al. 2004) with an annual volume of 28 million tons of iron ore. The mine is owned by Rio Tinto. Hamersley Iron Ore Mines are considered to hold one of the largest iron ore mine deposits of the world. According to Vogel (2014), environmental risk of these mines is primarily related to mine-pit lakes, because they might contaminate nearby ground water and ecosystems.

Figure 3-4: View on mining facilities of Hamersley mine. © 169169 / Adobe Stock.

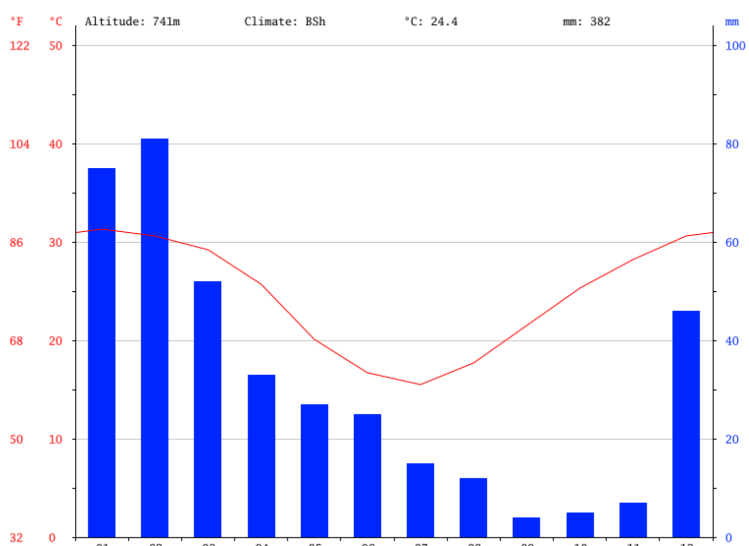

Figure 3-5: Climate chart of Tom Price, the city being closest to Hamersley mine; Source: Climate-data.

c. Highland mine

The Highland Valley copper mine is situated in the province of British Columbia of Canada. Located at 50°32'6.25"N and 121°4'18.62"W, the mine is 50 km southwest of the city of Kamloops at 1221 m above sea level (Figure 3-6).

Considering the climate, Kamloops belongs to the BSk climate type, a dry cold steppe climate with annual air temperatures < 18 °C (Glawion 2012). Figure 3-7 confirms that the monthly mean air temperature exceeds the 18 °C limit only in month June, July and August. Precipitations are generally low with an annual amount of 305 mm. Given its low amount of precipitation and its strong difference between winter and summer air temperatures, this study site belongs to the Dry Mid-Latitudes by Schultz's ecozones (Schultz 2016). This zone constitutes the transition of forest steppe to desert with corresponding soils such as Chernozems, Kastanozems and Phaeozems. Imagery inspection reveals moderate vegetation cover with sparse and dense vegetation around the open-pit mine.

Geologically considered, this open-pit mine belongs to the calc-alkaline composite Guichon Creek batholith, an intrusion from Triassic age. According to Olade (1977) and Olade and Fletcher (1976), the composition of this intrusion ranges from diorite to quartz monzonite, with porphyry copper deposits in the center of the intrusion. The mine is owned by Tech Resources Ltd. and operated through two pits with an annual volume of 116,300 tons of copper ore and 10 million pounds of molybdenum. Rehabilitation projects have been realized after impacts upon the environment, especially lakes, have been noticed (McAllister et al. 2014). On a global scale, this mine is considered to be among the largest open-pit mines worldwide.

Figure 3-6: Tailings pond of Highland mine.
© hpbfotos / Adobe Stock.

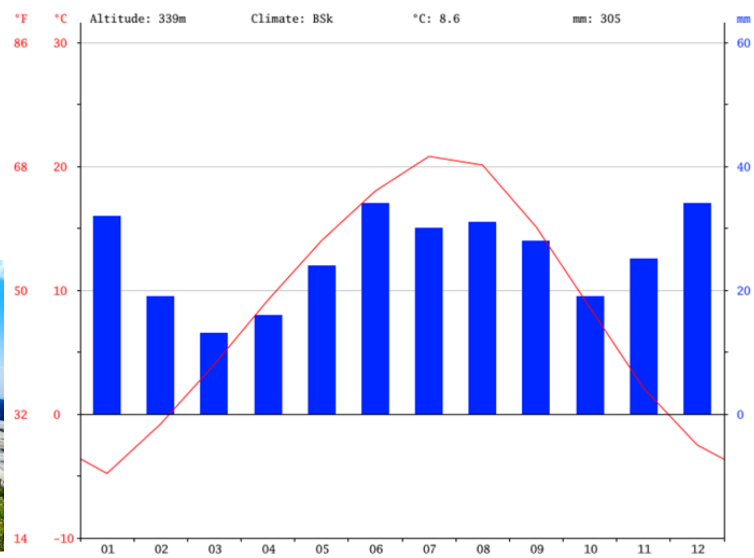

Figure 3-7: Climate chart of Kamloops, the closest city to Highland mine; Source: Climate-data.

d. Mariana mine

The open-pit mine of Mariana Iron Ore Complex is located in Brazil, in the state of Minas Gerais. At 60 km southeast of Belo Horizonte, the mine is situated at 20°10'59.13"S and 43°29'48.45"W at an approximate altitude of 990 m above sea level.

According to Köppen and Geiger's climate zones, this study site is considered to belong to the Cwa climate. This climate zone represents a warm temperate climate with drought in the winter of the southern hemisphere and a minimum of one month exceeding 22 °C air temperature (Glawion 2012). These characteristics are confirmed by Figure 3-9 that shows the annual mean air temperature of 20.5 °C. Precipitation reaches about 1430 mm with a maximum in the summer of the southern hemisphere, respectively. Considering its ecozone, this study site belongs to the Humid Savannah of the Summer Humid Tropics (Schultz 2016). Vegetation cover ranges from deciduous forest up to dense savannah, accordingly. Even though soils, such as Lixisoils, are prone to high levels of leaching, biodiversity is considered to be high and increases further with humidity.

Mariana mine belongs to the Quadrilátero Ferrífero (QM), an extensive iron ore deposit from Precambrian age covering an area of 7,000 km^2 (Selmi et al. 2009). Two iron formations that are quarzitic and dolomitic itabirite are dominant within QM. Mariana mine, which is owned by Vale S.A., is operated within three pits. The dam failure at Mariana of 2015 has raised awareness recently (Figure 3-8). This hazard was considered a humanitarian crisis, due to the fact that cities were flooded and aquatic systems such as the rio Doce and parts of the Atlantic ocean were polluted (Fernandes et al. 2016).

Figure 3-8: Mud flow after the dam burst in Minas Gerais. © Christyam / Adobe Stock.

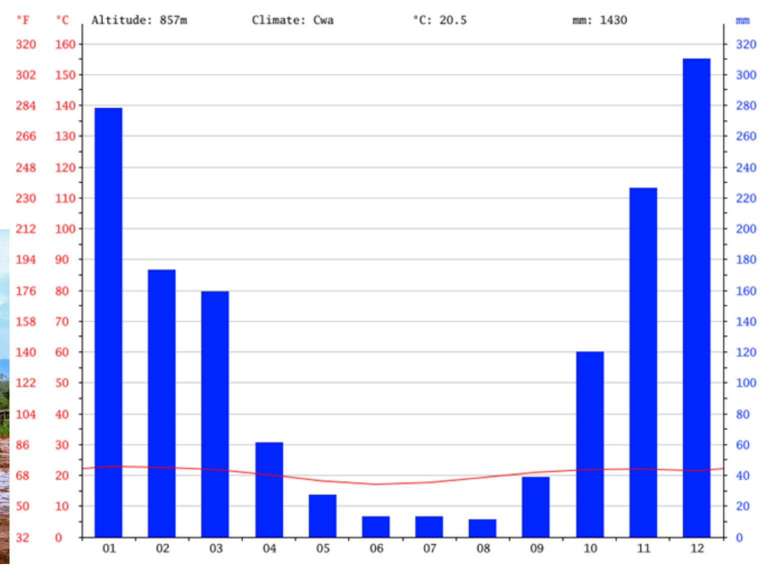

Figure 3-9: Climate chart of Belo Horizonte (closest city to the study site); Source: Climate-data.

3.2 Materials

This chapter presents the three types of datasets used within the study and relevant pre-processing. First optical satellite imagery will be outlined, followed by Digital Elevation Models (DEMs) and subsequently radar imagery.

3.2.1 Datasets and Acquisition

The objective of the study is to compare remote sensing analyses, among them classifications such as index-based, pixel-based and object-based classifications on single- and multi-source level and crowdsourcing that can be applied for the computation of the spatial extent of mining areas. Mines are expected to be distinguished by two factors, namely their spectral signal and their elevation. When distinguishing mines from their surroundings, their spectral signal will be considered because mines reflect solar radiation in a different wavelength than vegetation, soil, water or other surroundings (Figure 2-3) (Ma et al. 2018a). Information about the elevation will serve as additional information, due to the fact that mines are likely to differ from their surroundings as the pit itself has lower elevation values. For Grasberg mine as an example, the deepest explored part of the open-pit is around 2.5 km below the pre-mining surface (Bensaman et al. 2015). This implies that in this study multi-spectral imagery as well as DEMs will be used. Taking into account that some of the study sites are located within the Subtropics or Tropics, the occurrence of cloud issues is expected. Radar imagery is supposed to meet this difficulty due to the fact that this is an active sensor, thereby being able to penetrate clouds (Lillesand et al. 2008). Thus, three types of materials will be required for this study and applied within the classifications and crowdsourcing.

In the last years, many satellite missions such as Landsat, SPOT, Sentinel-2, Digital Globe and others have been carried out. They are either launched by public or commercial operators and vary among their purpose and by their instruments on the platform. For this study three dataset criteria had to be considered when choosing the appropriate optical sensor:

Dataset criterion:

a. Spatial and temporal availability of imagery for the study sites

b. Sufficient spatial resolution < 30 m

c. Free access to imagery

All three criteria are considered to be of equivalent importance. The first criterion is referring to the fact that imagery must be available for the exact location of the four selected open-pit mines. In addition, imagery has to be up-to date, which means that data acquisition has taken place during the year 2018. This is especially important when considering that mining often comes along with land use change. For this reason, mines might vary in extent when comparing current imagery to imagery from the last decade. As far as temporal availability is concerned, the factor season needs to be considered as well. When mines are located in high latitudes, imagery of winter time is not suitable for analyses as large parts of the mine might be covered by snow.

Sufficient spatial resolution < 30 m is a crucial criterion for the detection of mine features. The higher the spatial resolution, the better small objects can be detected. Especially roads, buildings and small tailings require a high resolution as they might in some cases cover an area < 90 m^2.

The last criterion is related to the open access to imagery. As previously mentioned, satellite missions originate either from public or from the commercial sector. Commercial satellite products do sometimes provide imagery with highest spatial accuracy, nevertheless free imagery with sufficient spatial resolution < 30 m is also available by a large number of operators.

All three criteria are fulfilled by Sentinel-2 products from the European Space Agency (ESA), given the fact that Sentinel-2 imagery is available for all four study sites that spatial resolution is between 10 and 60 m, that temporal resolution is 5 days and that all imagery is freely accessible. Data is hold in three different levels of data pre-processing that is Level-1A, Level-1C and Level-2A. Level-1C data are atmospheric reflectance values within a cartographic geometry, thus being radiometric and geometric corrected. Data has been accessed through the online platform from ESA Copernicus Open Access Hub (ESA 2014). For each study site a imagery has been downloaded that covers the open-pit mine, that has been acquisitioned within the vegetation period from 2018 and that has a cloud cover index < 10 % (Table 3-1). These three criteria are selection criteria for the imagery itself. The acquisition within the vegetation period is crucial, since this will facilitate the distinction between vegetation and the open-pit mine. Cloud cover is also highly important as the presence of clouds limits the visibility of the mine.

Regarding Digital Elevation Models (DEMs), there is a large variety of data sets such as SRTM, Aster, ALOS and others available. They are generated by stereoscopic pairing methods such as interferometric SAR or digital image correlation. Similar to optical sensors, when choosing the appropriate DEM, the previously mentioned criteria a., b. and c. need to be considered. Detailed information about the three criteria has been given in the previous section. Among the large variety of DEMs, ASTER Global DEM (GDEM) fulfills the determined criteria. All study sites are covered within the latest version of Aster's DEM at a spatial resolution of 30 m. Data is provided by the National Aeronautics and Space Administration (NASA) and freely available on their online platform Earth data (NASA 2019). For each study site a DEM of the second generation, i.e. version 2, was downloaded (Table 3-1).

As far as SAR imagery is concerned, data of Sentinel-1, ENVISAT, PALSAR and others are available. In this context, the previously mentioned criteria are also of high importance. Sentinel-1 data, provided by the ESA, is considered suitable because of the fact that imagery is available for all four study sites at a spatial resolution of 5 x 20 m and a temporal resolution of 12 days. Through the same platform as for Sentinel-2 imagery, data was freely downloaded (ESA 2014). Thereby, data acquisitioned during vegetation period had to be considered, in line with Sentinel-2 imagery selection criteria. Available data products are Level-0, Level-1 Single Look Complex (SLC), Level-1 Ground Range Detected (GRD) and Level-2 L2 Ocean Product (OCN). As Level-1 GRD data is focused SAR data that has been detected, multi-looked and projected to ground range using an earth ellipsoid model, Level-1 GRD from Interferometric Wide Swath Mode (IW) with Vertical Polarization (VV) and Vertical Horizontal Polarization (VH) has been downloaded.

Table 3-1: Overview of the three datasets of each study site.

		Grasberg mine	Hamersley mine	Highland mine	Mariana mine
Sentinel-2	Scene Identifier	S2A_MSIL1C_20180514T011731_N0206_R088_T53MQR_20180514T025012	S2B_MSIL1C_20180805T021339_N0206_R060_T50KNV_20180805T062858	S2A_MSIL1C_20180617T185921_N0206_R013_T10UFA_20180617T224132; S2A_MSIL1C_20180617T185921_N0206_R013_T10UFB_20180617T224132	S2A_MSIL1C_20180623T130251_N0206_R095_T23KPT_20180623T162223
	Sensor type	Optical	Optical	Optical	Optical
	Acquisition date	2018/05/14	2018/08/05	2018/06/17	2018/06/23
	Band info	13 multi-spectral bands	13 multi-spectral bands	13 multi-spectral bands	13 multi-spectral bands
	Resolution (m)	10-20	10-20	10-20	10-20
	Cloud Cover (%)	17.13	0.25	2.0; 3.64	0.97
Aster GDEM	Scene Identifier	ASTGTM2_S05E137	ASTGTM2_S23E117	ASTGTM2_N50W121; ASTGTM2_N50W122	ASTGTM2_S21W044
	Sensor type	Optical	Optical	Optical	Optical
	Release date	2011	2011	2011	2011
	Band info	DEM	DEM	DEM	DEM
	Resolution (m)	30	30	30	30
	Cloud Cover (%)	-	-	-	-
Sentinel-1	Scene Identifier	S1A_IW_GRDH_1SDV_20180918T091217_20180918T091242_023750_02970B_D677	S1B_IW_GRDH_1SDV_20180814T213152_20180814T213217_012264_016993_4946	S1B_IW_GRDH_1SDV_20180715T015404_20180715T015429_011815_015BE0_A7B0	S1B_IW_GRDH_1SDV_20180522T082104_20180522T082129_011031_014365_FA04
	Sensor type	C-Band Radar	C-Band Radar	C-Band Radar	C-Band Radar
	Acquisition date	2018/09/18	2018/08/14	2018/07/15	2018/05/22
	Band info	VV & VH	VV & VH	VV & VH	VV & VH
	Resolution (m)	5 x 20	5 x 20	5 x 20	5 x 20
	Cloud Cover (%)	-	-	-	-

3.2.2 Pre-processing

Each of the downloaded datasets that are shown in Table 3-1 need to be pre-processed in order to generate data ready-to-use for the subsequent classification and crowdsourcing.

The entire process of pre-processing for all three types of datasets is shown in Figure 3-10.

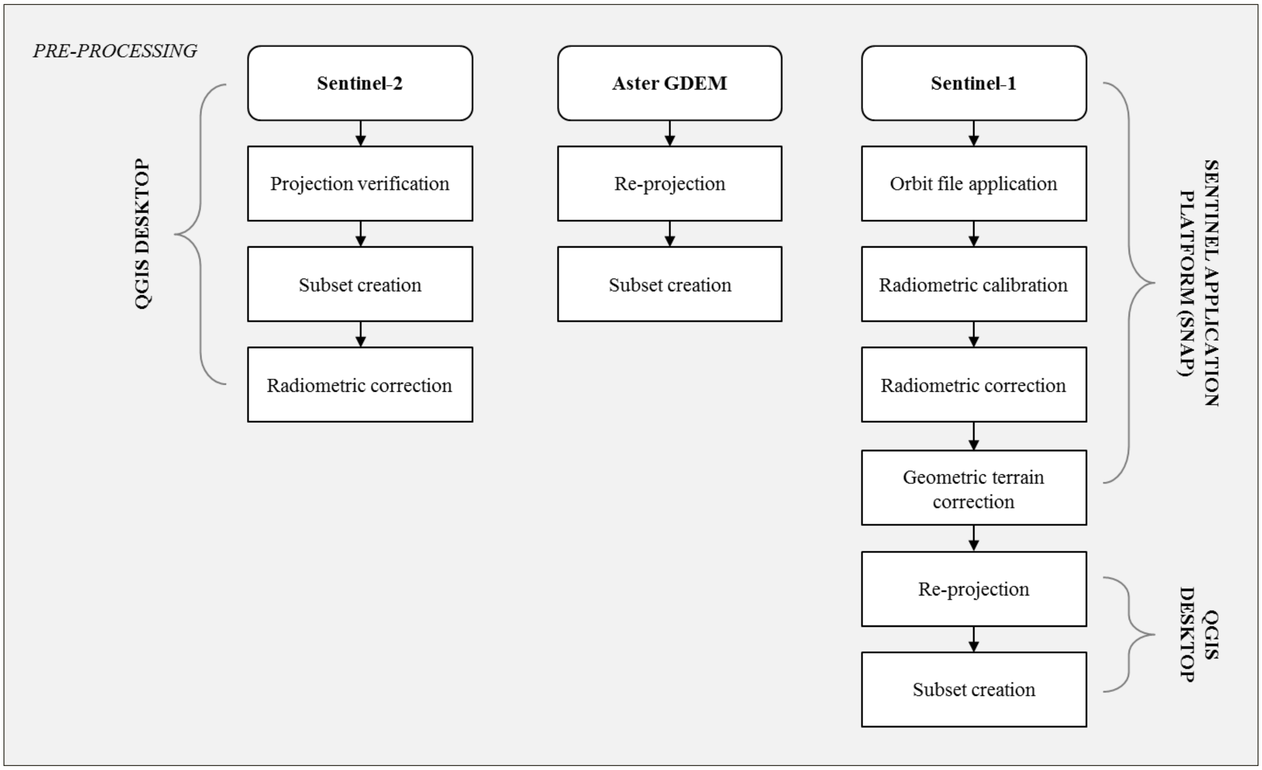

Figure 3-10: Pre-processing steps for Sentinel-2, Aster GDEM and Sentinel- 1 data and corresponding software.

Pre-processing of Sentinel-2 imagery has been performed within the Geographic Information System (GIS) software QGIS Desktop 3.4.5 (QGIS Development Team 2019), by means of the Semi-Automatic-Classification Plugin (SCP) (Congedo 2018). Given the fact that all images are already provided in the correct projected coordinate system, i.e. Universal Transverse Mercator (UTM), no further re-projection needs to be undertaken. Nevertheless, verification of the correct projection is crucial for all types of remote sensing imagery pre-processing, therefore being mentioned.

The following EPSG codes contain the projection corresponding to the study site:

a. Grasberg mine: 32753

b. Hamersley mine: 32750

c. Highland mine: 32610

d. Mariana mine: 32723

All multi-spectral bands except for band 1, 9 and 10 have been stacked together to a band set. The three bands mentioned are excluded from analysis, as they are dedicated to aerosol, water vapor and cirrus cloud detection, which is not in line with the objective of this study. Subsequently, a subset has been created in order to clip the entire imagery to the Area of Interest (AOI) that contains the open-pit mine. The following UTM extents of Upper-Left (UL) and Lower-Right (LR) coordinates have been chosen:

a. Grasberg mine extent:

UL: 728234.9999999982537702, 9544045.0000000000000000

LR: 741224.9999999982537702, 9556285.0000000000000000

b. Hammersley mine extent:

UL: 559332.4840105901239440, 7474585.2672052076086402

LR: 591774.0723712206818163, 7497593.0664593977853656

c. Mariana mine extent:

UL: 649354.6810842915438116, 7753633.9922552965581417

LR: 678563.1302923100301996, 7782902.4793856339529157

d. Highland mine extent:

UL: 622089.8850756828906015, 5586652.3008707538247108

LR: 652422.4318524983245879, 5611726.5938905468210578

Taking into account that Level-1C data are atmospheric reflectance values, data needs to be radiometric corrected in order to obtain surface reflectance values, as for this study the solar radiation reflected at earth surface is of interest. Surface reflectance values can be derived by applying DOS1 atmospheric correction within the SCP plugin to all clipped bands. Required metadata for this conversion is obtained from the MTD file that comes together with the imagery.

Aster Pre-processing has been performed within the QGIS environment as well. As this data is not projected into the same coordinate system like Sentinel-2 imagery, all images need to be re-projected by means of the previously mentioned EPSG Codes. Re-projected images further need to be clipped to the AOI by setting the UTM coordinate values presented previously. For visual impression, raster symbology can be adjusted. For classification this is, however, not required.

Pre-processing of Sentinel-1 imagery has been performed with the Sentinel Application Platform (SNAP) (SNAP 2019). First, the orbit file had to be applied to enable further pre-processing. Further radiometric calibration is required in order to obtain calibrated backscatter coefficient values. Subsequent radiometric correction removes the sometimes misleading influence of topography upon backscatter values of the imagery. Therefore, radiometric terrain flattening is performed. A SRTM 1sec HGT elevation model is automatically downloaded within the execution of terrain flattening and is required in order to remove the influence of the terrain. Due to spatial distortions within the data, which were induced by the fact that data has not been acquired from a nadir position, additional geometric terrain correction was performed. During acquisition time, imagery has been captured from two different perspectives, which is a horizontal and a vertical perspective. Imagery of both polarizations is available and has been used within this study. One image of each perspective has been exported into QGIS Desktop for further pre-processing. Each image has been re-projected into the same coordinate system as the Sentinel-2 imagery and the Aster GDEM by means of the previously presented EPSG. With the previous mentioned UTM coordinate values, a spatial subset of each imagery has been created. Similar to the Aster GDEM, symbology modifications are recommended, but only required for visual impression.

3.2.3 Reference data

For all four study sites no reference data such as in-situ GPS measurements exists. Nevertheless, reference is crucial in order to conduct an accuracy assessment of the classifications. Therefore, reference datasets have been created upon expert knowledge. For each study site, two reference datasets have been created upon pre-processed Sentinel-2 Red Green Blue (RGB) imagery within ENVI 5.5 (Harris Geospatial 2019a). Hence, a total of 50 samples for each class have been collected. Because index-based classification and crowdsourcing digitizations will contain two classes − that is the class mine and non-mine − a binary reference dataset has been created for these two methods. Given the fact that for pixel-based and object-based classifications several land-use classes will be trained, a reference dataset with 6 land use classes including the class mine has been created for these two classification methods. Thus, a total of 8 reference datasets has been created. Table 3-2 and Table 3-3 give an overview of the two reference datasets for each study site.

Table 3-2: Overview of the reference datasets for index-based classifications. For each study site one NDVI reference dataset has been created.

	Reference datasets for index-based classifications			
	Grasberg mine	**Hamersley mine**	**Highland mine**	**Mariana mine**
Amount of pixels	15084	17008	23991	19599
Area [km^2]	1.50	1.70	2.40	1.96
Area relative to entire study site [%]	0.99	0.41	0.37	0.26

Table 3-3: Overview of the reference datasets for pixel-based and object-based classification. For each study site one reference dataset has been created.

	Reference datasets for pixel-based and object-based classifications			
	Grasberg mine	**Hamersley mine**	**Highland mine**	**Mariana mine**
Amount of pixels	11031	12298	23674	33006
Area [km^2]	1.10	1.23	2.37	3.30
Area relative to entire study site [%]	0.99	0.30	0.37	0.44

3.2.4 Mine indicators

LaJeunesse Connette et al. (2016) developed a methodology in order to assess the extent and expansion of open-pit mines in Myanmar. For the identification of current mining sites they created a list of features indicating a potential mine (Table 3-4). This study will directly incorporate these indicators, while defining that for classifications and crowdsourcing, the class mine needs to contain the features indicating a potential mine from LaJeunesse Connette et al. (2016).

Table 3-4: Features indicating potential mining areas from LaJeunesse Connette et al. (2016). Source: LaJeunesse Connette et al. (2016), modified; contains modified Copernicus Sentinel data (2018).

Features indicating a potential mine	
Bare ground (particularly irregular shaped patches)	
Piles of rock or soil	
Pools of water with unusual or varying colors (Changes in river color)	
Ruts or pits in the earth	
Roads	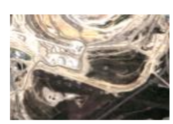
Industrial buildings, processing facilities or large equipment	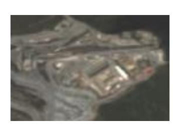

4 Methodology

The objective of this study is to compare different remote sensing analyses that can be applied to compute the spatial extent of open-pit mines in different geographic regions. Remote sensing analyses comprise classifications, including index-based, pixel-based and object-based classification, as well as crowdsourcing. This chapter explains in detail the classifications and crowdsourcing process. The methodological concept of this study will be presented first in order to give a general overview of the procedure. A detailed explanation of each method will be given subsequently. In order to compare both methods, the application of a comparison metric will be further introduced. When no specific information about parameter choice has been given, the default settings were accepted.

4.1 Research design

The entire study is composed of three parts, the data acquisition & pre-processing, the analyses and the comparison. A simplified overview of the entire procedure is given in Figure 4-1. All three steps of the initial part data acquisition & pre-processing, which are related to the choice of the study sites and datasets, the dataset acquisition and pre-processing, have been explained previously in chapter 3.

The analyses are subdivided into two parts, the classifications and the crowdsourcing. First, different classifications will be performed. Index-based, pixel-based and object-based classifications will be applied to the datasets of each study site. Thereby, index-based and pixel-based classifications will be performed on single-source-multi-band level, whereas object-based classifications will be conducted on multi-source-multi-band level. Subsequently, the classifications will be post-processed. Area values will be derived by calculating class statistics. In a final step, an accuracy assessment will be conducted in order to evaluate the classifications.

Crowdsourcing constitutes the second part of the analyses. Therefore, a crowdsourcing project was launched, where volunteers were invited to digitize the delineation of the four study sites based on Sentinel-2 RBG imagery. Subsequent post-processing of the received digitizations included the conversion of the digitization from a vector model to a raster model. Following, the smallest (Min polygon) and largest polygon (Max polygon) will be chosen. Additionally, a frequency distribution raster layer will be generated that demonstrates the frequency of selection of each pixel. Further, a majority polygon, which represents the mine according to the majority, will be derived. Computing area values by class statistics and computing a confusion matrix of the majority polygon, will constitute the final step of this method.

In order to compare both methods, a comparison metric, which is the Intersection over Union (IoU), will be applied. This requires the calculation of the area of spatial intersection and the area of spatial union for each combination of classifications and majority polygons. Comparison between the two methods will then be conducted by comparing them by IoU, area and accuracy values as well as their visual interpretation. Taking the main findings regarding the results and the implementation of the two methods into account, strengths and weaknesses of each method will be determined.

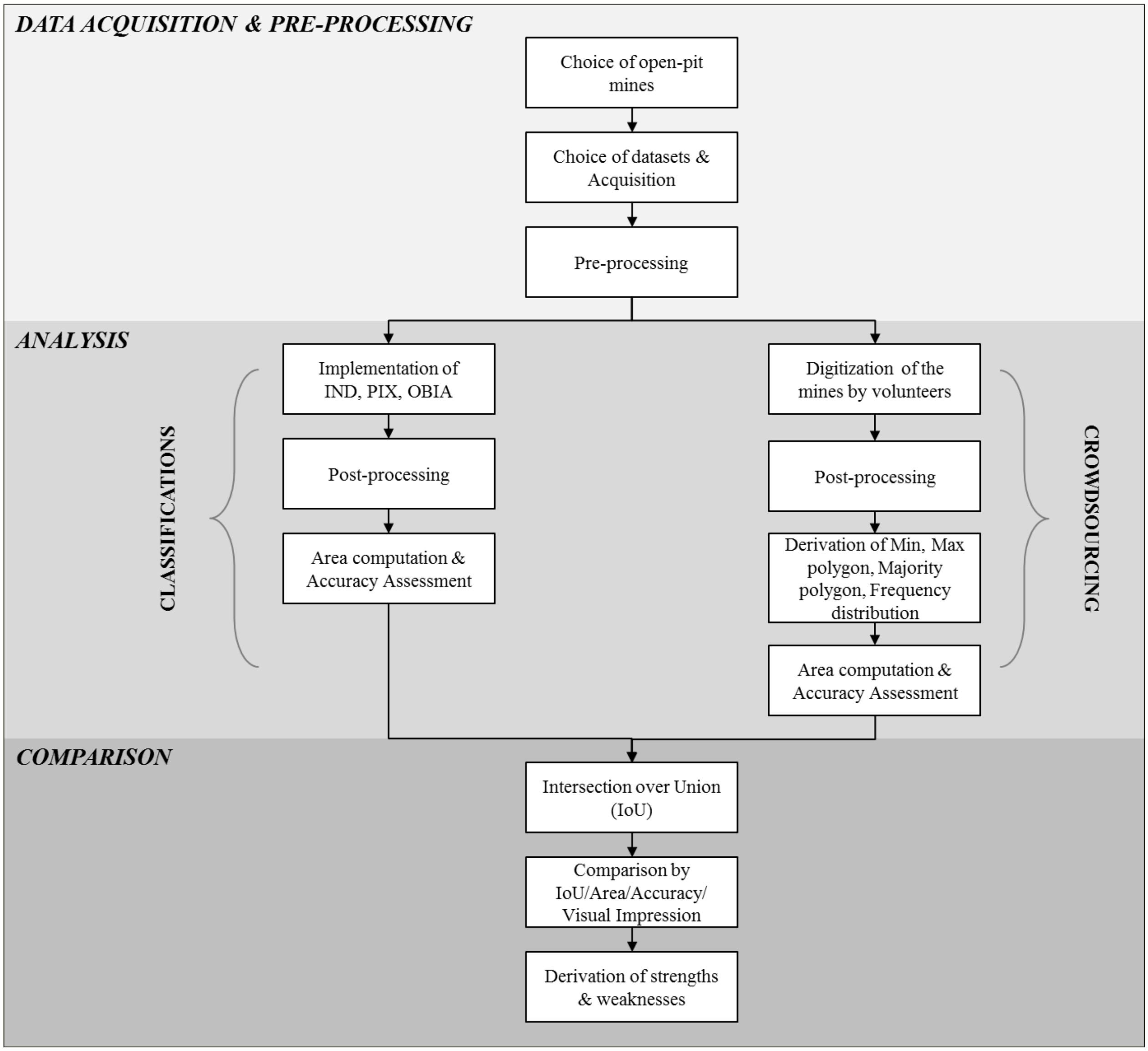

Figure 4-1: Overview of the methodology. The abbreviations IND, PIX and OBIA refer to the index-based, pixel-based and object-based classifications.

4.2 Classifications

The following section is dedicated to detailed explanations of the classes, as well as the classifications. All three types of classifications are multi-spectral classifications. For simplification in the further course of this thesis, the name multi-spectral classifications will be abbreviated to classifications.

4.2.1 Classes

All classifications contain the class mine, which is defined as the class containing all features indicating a potential mine from LaJeunesse Connette et al. (2016). Therefore, this class contains the open-pit, piles of rock, bare ground, buildings and roads dedicated to mining activity as well as pools of water. Detailed information about these features has been given in the previous chapter 3.2.4.

The amount of further classes being considered within the classifications varies among classification methods. For index-based classifications, only two classes, which are the mine and the class non-mine, were created. The class non-mine represents the surroundings of the mine.

For pixel-based and object-based classifications, additional land use classes were integrated, as this might provide further information of spectral similarities and discrepancy between the mine and its surroundings. Besides the class mine, the class bare area, sparse vegetation, dense vegetation, shadows and clouds will be part of the classifications (Table 4-1). The distinction between sparse vegetation and dense vegetation was achieved by defining that dense vegetation is referred to a closed canopy such as forest, whereas sparse vegetation is related to grassland. The class bare area represents areas without vegetation, such as rocky areas. The class shadows comprise shadows of clouds as well as shadows from mountains or other relief that – according to the illumination conditions – is either exposed to sunlight or shadow. Only for Hamersley mine a further land use class called humid areas has been assigned, as it is not clear if these areas constitute sparse vegetation areas or ephemeral water run-offs.

Table 4-1: Overview of the land use classes for pixel-based and object-based classifications.

Land use classes for pixel-based and object-based classifications
Mine
Bare area
Sparse vegetation
Dense vegetation
Clouds
Shadow
Humid areas

4.2.2 Index-based classification

Index-based classifications (IND) are based on single-source-multi-band level. Sentinel-2 constitutes the single source, Sentinel-2 bands 4, 8A, 11, 12 represent the multi-spectral bands. Ratio images will be calculated for subsequent mine extraction. Thereby, each pixel value of one band is divided by the pixel value of another band. Given the fact that ratio images or index bands show the spectral characteristics of investigates features irrespective of distinct illumination, ratio images are effective in highlighting spectral differences in a given scene. In a single band, these features are frequently less recognizable than in a ratio band. The following three indices were considered to be of interest for the index-based classification:

1. Normalized Difference Vegetation Index (NDVI)
2. Ferrous Mineral Index (FMI)
3. Clay Mineral Index (CMI)

NDVI is applied for vegetation detection as it is an indicator for the vitality of vegetation. The background of this index is that vegetation absorbs solar radiation within the red wavelengths (RED) of the electromagnetic spectrum (0.6-0.7 µm), whereas it reflects radiation in the Near Infrared (NIR) wavelengths of the electromagnetic spectrum (0.7-1.3 µm) (Albertz 2009). The absorption in the visible part of the electromagnetic spectrum is due to the presence of chlorophyll that strongly absorbs energy in the electromagnetic spectrum ≤ 0.7 µm. The increase in reflection in the NIR part is due to cell structures in the leaves that reflect solar radiation ≥ 0.7 µm. An increase in vitality of vegetation is thus accompanied by an increase in reflection within the NIR of the electromagnetic spectrum (Lillesand et al. 2008). Consequently, the index can serve in detecting vital vegetation, but also to discriminate between vegetation and non-vegetation, which is the reason for its application within the study. The NDVI is computed by applying the following formula I). The derived ratio band is composed of coded color values for each pixel that indicate vegetation vitality. Given the normalization, NDVI values range from -1 to 1, whereas higher values indicate a dominance of vegetation.

$$\text{I) } NDVI \equiv \frac{NIR - RED}{NIR + RED}$$

The FMI is an indicator for iron-bearing minerals (Castellanos-Quiroz et al. 2017; Drury 1993). As iron-ore open-pits will be investigated within this study, this index has been applied in order to discriminate between the mine, - where iron-bearing minerals might by more dominant - , and its surroundings. This index is a ratio between the Short Wavelength Infrared (SWIR1) (1.55-1.75 µm) and the NIR of the electromagnetic spectrum (0.706-0.9 µm) and is computed by the following formula II). Similar to the NDVI, high values correlate with a high amount of iron-bearing minerals.

$$\text{II) } FMI \equiv \frac{SWIR1}{NIR}$$

The CMI indicates hydrothermally altered rocks containing clay and alunite (Castellanos-Quiroz et al. 2017; Drury 1993). Taking into account that open-pit mining in tropical regions might result in an accumulation of hydrothermally altered rocks, this index is expected to indicate areas of current mining, thus being suitable for this study. The ratio is derived by dividing the Short Wavelength Infrared (SWIR1) (1.55-1.75 µm) by the Short Wavelength Infrared (SWIR2) (2.08-2.35 µm), shown in formula III). Similar to previous indices, the higher the value, the more clay bearing material is present.

$$\text{III) } CMI \equiv \frac{SWIR1}{SWIR2}$$

Index-based classifications have first been conducted script-based with the software Python 3.7 (Python Software Foundation 2019). Based on pre-processed multi-spectral bands of Sentinel-2, NDVI, FMI and CMI were calculated for each study site and constitute thus the integral part of index-based classifications (Figure 4-2). Given the fact that the red band is represented by band 4 and the NIR band by band 8A among Sentinel-2 multi-spectral bands, NDVI has been calculated in a first script with the following formula I.I):

$$\text{I.I)} \quad NDVI \equiv \frac{Band\,8A - Band\,4}{Band\,8A + Band\,4}$$

For Sentinel-2, SWIR1 corresponds to Band 11 and NIR to Band 8A. The following formula II.I) was applied in a second script in order to compute FMI:

$$\text{II.I)} \quad FMI \equiv \frac{Band\,11}{Band\,8A}$$

In a third script, CMI was computed by the following formula III.I):

$$\text{III.I)} \quad CMI \equiv \frac{Band\,11}{Band\,12},$$

Where Band 11 and Band 12 represent SWIR1 and SWIR2, respectively.

In an iterative process, the index-range covering all features of a potential mine from LaJeunesse Connette et al. (2016) was set manually by defining an upper and lower threshold of NDVI values. This second step was performed script-based as well. Subsequently, all pixels within this range were extracted and stored in a separate raster layer. This step of setting the mine thresholds was repeated for all three indices and for all study sites. A corresponding table with spectral ranges (Table 8-1) and exemplary figures of the NDVI, the FMI and the CMI calculation for Grasberg mine are attached in the appendix (Figure 8-1). Contrary to the FMI and the CMI, only for the NDVI a clear range covering the mine features could be found, the index-based classification is thus based upon the NDVI only.

Table 4-2 includes the NDVI ranges for each study site. As the study sites differ in vegetation type, the NDVI range had to be determined individually for each mine.

Table 4-2: NDVI range for each study site that defines the mine within the NDVI imagery.

	Grasberg mine	**Hamersley mine**	**Highland mine**	**Mariana mine**
NDVI range	-0.85-0.08	-1-0.1	-0.795-0.14	-0.651-0.2

Taking into account that the NDVI range of mines includes the NDVI range of clouds, further cloud masking has been required, which was performed in QGIS Desktop 3.4. The implemented SCP Plugin provides cloud masking. The cloud mask (MSK_Clouds) that comes together with the downloaded multi-spectral files was first converted to a shapefile and then rasterized in order to enable its application upon the raster images. Value 1 has been selected as the pixel value representing clouds when rasterizing. Given the fact that this raster cloud mask does not contain all clouds of the multi-spectral bands of Sentinel-2, the cloud mask was edited by integrating further clouds into the cloud mask through cloud digitization. Finally, cloud masking was performed on the NDVI raster image, resulting in a new raster layer representing the NDVI values of the mine only.

Subsequent calculation of class statistics and accuracy assessment was carried out in ENVI 5.3. Class statistics were derived by counting the pixels of each class. In this case, two classes were determined, namely the mine (being represented by the set NDVI range) and non-mine (referring to the surroundings of the mine). The amount of pixels of the class mine was multiplied by the spatial resolution of Sentinel-2 imagery, which is 10 m, to obtain area values in m^2 and km^2.

In order to evaluate the classifications, a classification error matrix was derived for each classification. Thereby, the reference data was compared to the corresponding classification, in this case to the index-based classification. The matrix is composed of columns representing the amount of pixels of each class within the reference versus rows, which represent the amount of pixels of each class within the classification. Calculated accuracy metrics that were derived from the confusion matrix comprise overall accuracy, the Kappa coefficient value, producer's and user's accuracy and the omission and commission error. Overall accuracy represents the total amount of correctly classified pixels divided by the total amount of all reference pixels. The higher the value, the more accurate the classification. The Kappa coefficient value is a further accuracy metric that includes the factor chance agreement, in order to avoid that accuracy is only due to chance. According to Lillesand et al. (2008), the Kappa coefficient value k is defined as the difference of observed agreement between the reference dataset and the classification and the chance agreement between both datasets. In order to compute the Kappa coefficient, the following formula IV) from Lillesand et al. (2008) is applied within the accuracy assessment:

$$\text{IV)}\quad k = \frac{N \sum_{i=1}^{r} x_{ii} - \sum_{i=1}^{r} (x_{i+} * x_{+i})}{N^2 - \sum_{i=1}^{r} (x_{i+} * x_{+i})}$$

Where

r = number of rows in the error matrix

x_{ii} = number of observations in row i and column i (major diagonal)

x_{i+} = total amount of observations in row i

x_{+i} = total of observations in column i

N = total number of observations included in matrix

Kappa coefficient values range from 0 to 1, whereas 0 represents chance agreement and 1 observed agreement.

The producer's accuracy was obtained by dividing the amount of correctly classified pixels of each class by the amount of all reference pixels of the same class and indicates how well the reference is classified. The user's accuracy is a metric of reliability and indicates the probability that a classified pixel represents this class in reality. It is calculated by dividing the amount of correctly classified pixels of each class by the amount of all classified pixels of the same class. Besides these accuracy metrics, omission and commission errors can be derived from the confusion matrix. The omission error represents the false negatives that means the amount of pixels that were excluded from a class, even though they would belong to this class. The commission error is a metric of the amount of false positives, which refers to pixels being falsely included in a class. Producer's and user's accuracy, as well as omission and commission errors range from 0 to 100 %.

Figure 4-2 shows the entire process of index-based classifications.

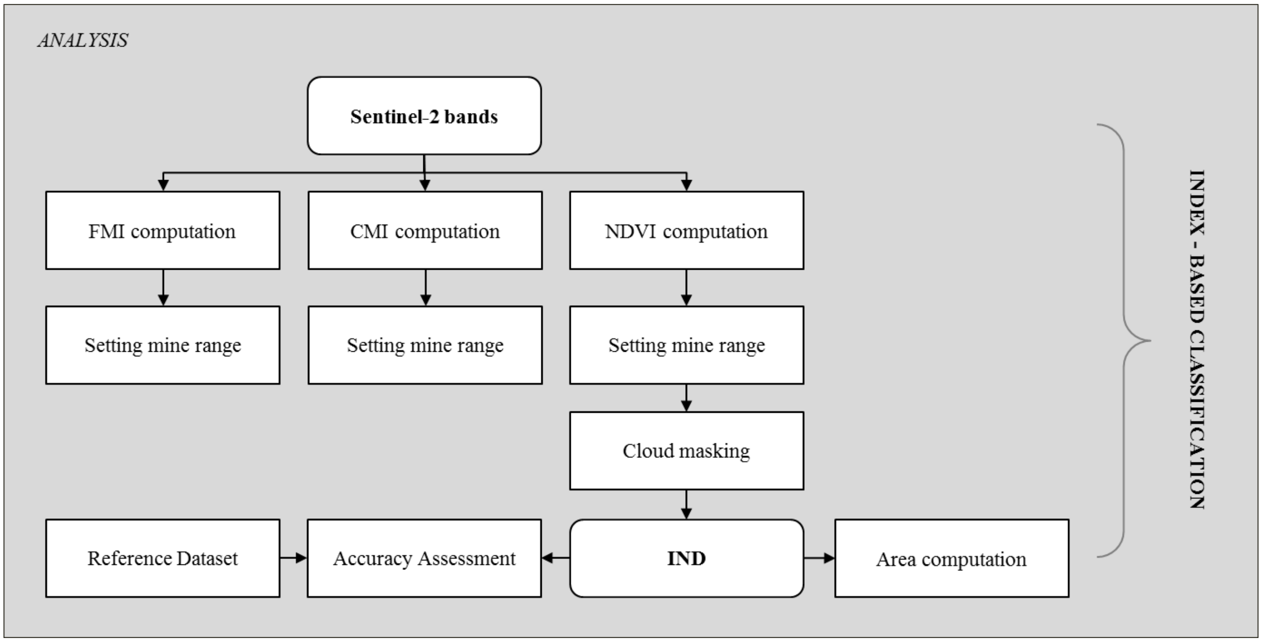

Figure 4-2: Overview of all steps in the index-based classification. Input and Output are shown in rounded cells. IND refers to the index-based classification output.

4.2.3 Pixel-based classification

Pixel-based classification (PIX) is considered to be a single-source-multi-band classification. Similar to the index-based classification, Sentinel-2 constitutes the single source, Sentinel-2 bands 2, 3, 4, 5, 6, 7, 8, 8A, 11, 12 represent the multi-spectral bands. Different bands can partially contain the same information, which means that multi-spectral analysis faces sometimes the problem of inter-band correlation. In order to reduce redundancy within the data and to improve computation performance (Lillesand et al. 2008), preliminary Principal Component Analysis (PCA) has been performed within QGIS Desktop 3.4. As the PCA calculation requires stacked multi-spectral bands, a raster stack of the bands was created at first. PCA, with 10 principal components was carried out with the raster stack. All components are hold in one band as a PCA stack. The PCA analysis reveals that the first three components cover already > 96 % of the entire variance among 10 multi-spectral bands. Therefore, the three components are extracted from the PCA stack and stored in separate raster layers for further analysis.

Subsequent classification was performed within ENVI 5.3. For the pixel-based classifications, the first three principal components as well as the three ratio bands (NDVI, CMI, FMI) were included in the classification process (Figure 4-4). Preliminary, these 6 raster images were stacked together. Semi-automatic classification requires training samples. Within the ENVI environment, training is performed by creating Regions of Interest (ROI), which represent a training set composed of polygons assigned to a specific class. At first, polygon geometries were collected that represent the ROIs. For all 6 land use classes, which refer to 6 ROIs, a minimum of 20 training samples were created. Detailed information about the training samples can be found in the appendix (Table 8-4). Increased training was performed for land use classes, which were considered to be more dominant within the imagery. For Hamersley mine, only 5 land use classes could be detected within the satellite imagery. Specific band combinations were set in order to support the training process by displaying either the principal components or the ratio images. The machine-learning algorithm Support Vector Machine (SVM), which outperforms other algorithms, appears to be suitable for a large variety of application fields and sensors and requires only a small amount of training samples (Whyte et al. 2018). Therefore, the SVM algorithm was chosen as classifier. The base of this algorithm is a particular training dataset, in this case the ROIs that contain all the training polygons, which were assigned to the corresponding classes. Training samples are separated by fitting a hyperplane between the training samples in a way that the samples are separate most accurately that means the margin in between the samples is largest (Figure 4-3). The samples being closest to the hyperplane are considered to be the support vectors. Classification that means deciding to which class pixels belong, depends thus on the side of the hyperplane where pixels are located (Ma et al. 2017b).

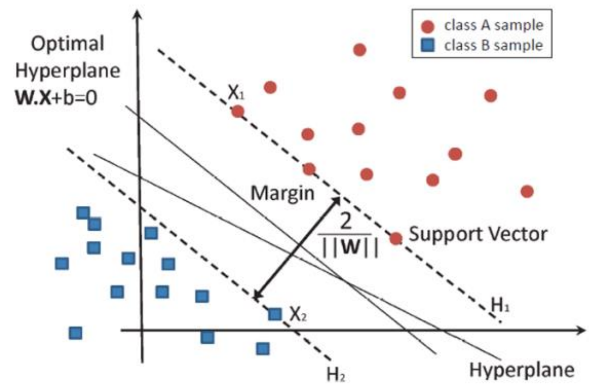

*Figure 4-3: Concept of Support Vector Machine algorithm. x_1 and x_2 are referred to training samples of class A and class B respectively. H_1 and H_2 represent the marginal hyperplanes delimiting class A and B. The margin in between H_1 and H_2 is defined as $\frac{2}{IIwII}$, where w represents the weight vector. The optimal hyperplane in between H_1 and H_2 is defined as w*x+b=0, where b is referred to the bias; source: García-Gonzalo (2016).*

Training and subsequent supervised classification was carried out for all four study sites. Subsequent post-processing was conducted by sieving and majority analysis. Sieving was performed on the classified image in order to face the problem of isolated pixels. Thereby, isolated pixels are integrated to the class unclassified as soon as the surrounding pixels all have the same class. The amount of surrounding pixels being considered in this sieving process can be either 4 or 8. For this study, a consideration of 8 surrounding pixels has been chosen. In this case, the central pixel is assigned to the class unclassified as soon as the 8 surrounding pixels belong to the same class.

Subsequently, a majority analysis was performed for the class unclassified in order to assign these unclassified pixels to the majority class of the pixels given in a specific kernel. For this study, majority analysis was conducted with a 3 x 3 kernel size window.

In order to compute the area of each mine in m^2 and km^2, class statistics were calculated by deriving the pixel amount of each class. Multiplied by the spatial resolution of the classification image, which is 10 m, the area of each class and thus the area of the mine in m^2 and km^2 were computed.

For evaluation, a confusion matrix was generated in the same way as explained before in chapter 4.2.3. Thereby, the classification is compared to the reference dataset for pixel-based and object-based classifications that was presented in chapter 3.2.3.

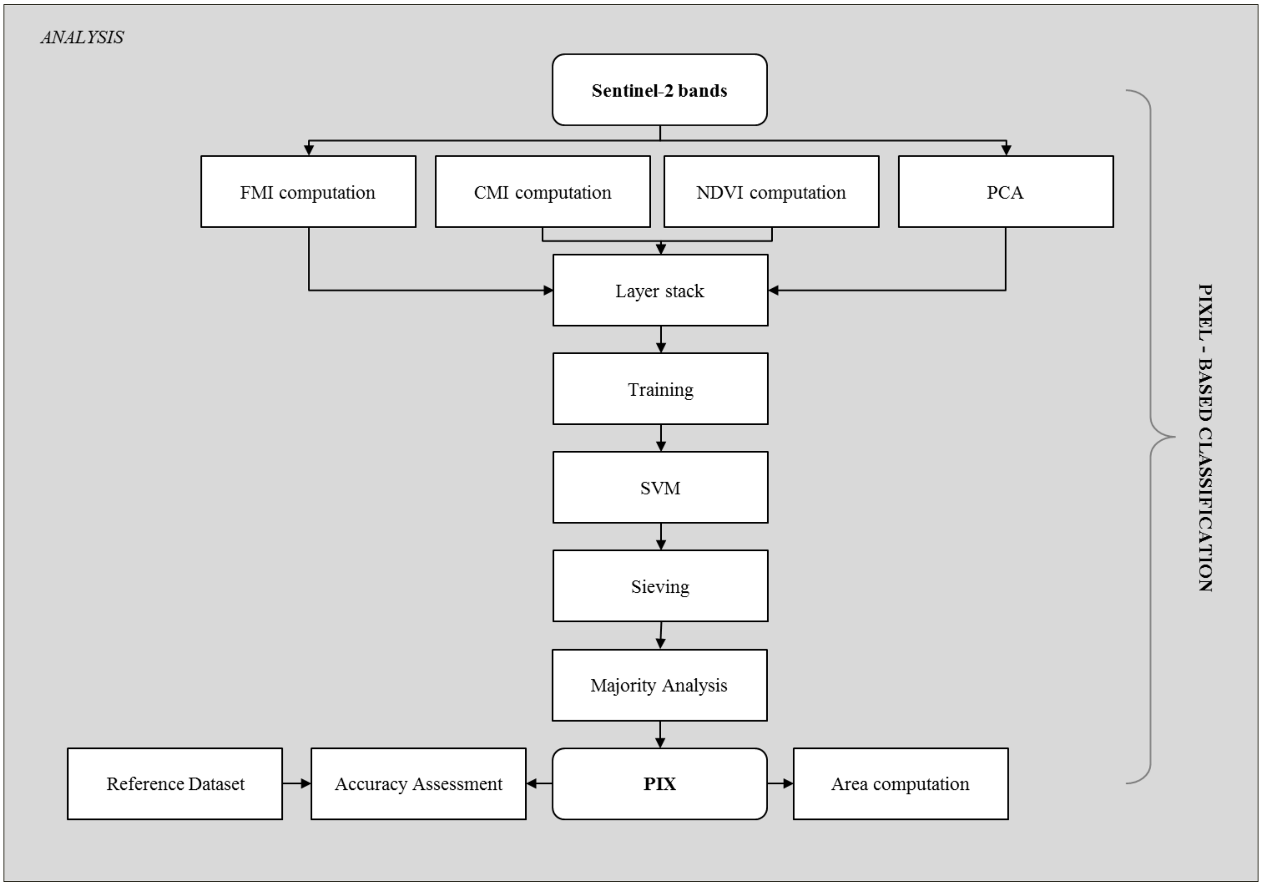

Figure 4-4: Overview of all steps of pixel-based classifications. Input and Output are shown in rounded cells. PCA refers to principal component analysis, SVM refers to support vector machine algorithm and PIX refers to the pixel-based classification output.

4.2.4 Object-based classification

Object-based classifications (OBIA) are considered to be the multi-source-multi-band classifications within this study, as several datasets from different sources and accordingly several bands are used within this classification.

Similar to pixel-based classifications, the analysis of object-based classifications was performed within the software ENVI 5.3. First of all, a layer stack of the bands the classification shall be performed on is required. The three principal components that are already stacked together were loaded as input image. Example-based feature extraction in ENVI enables the integration of additional datasets that support segmentation, training and classification. In order to make use of this potential, the three ratio images (NDVI, FMI, and CMI), the pre-processed Aster GDEM and the preprocessed two SAR images from Sentinel-1 were loaded as ancillary data (Figure 4-5). Contrary to pixel-based classification, where classification is based on pixel-level only, object-based classification derives segments first and then classifies the segments (Lillesand et al. 2008). Segmentation is the first step in the example-based feature extraction workflow. Segmentation partitions the input image into segments, which ideally represent real world objects. By grouping neighboring pixels that have the same spectral, textural and spatial attributes, pixels were aggregated to segments. A detailed list of the attributes is given in the appendix (Table 8-6; Table 8-7; Table 8-8). Segmentation is performed on the three principal component bands with the edge algorithm and a scale factor of 10. The scale parameter is a decisive factor within segmentation, because it defines the amount of segments being created. The higher the scale factor, the more segments are created, resulting thus in smaller segments. As for this case mine features might vary in extent and might even contain small features, a scale factor of 10 was chosen. Contrary to the intensity algorithm, the edge algorithm is suitable for segmenting objects that have sharp edges instead of gradual transitions, as it is the case for example for elevation. As mines are expected to have rather sharp edges than gradual transitions, the edge algorithm was selected for this study. Subsequent merging was performed with the full Lambda Schedule algorithm on a merge level of 60 in order to merge adjacent segments together that contain the same spectral characteristics. Full lambda schedule is a merge algorithm, merging small segments within over-segmented areas, such as clouds, together. The high scale factor has been chosen in order to aggregate segments in over segmented areas, such as vegetated areas, clouds, shadow etc. Texture attributes are calculated within a kernel, which is a moving window. This window of specific size moves all over the image thereby computing the texture attributes such as texture range, texture mean, texture variance and texture entropy. A detailed list of all texture attributes is given in the appendix (Table 8-7). For this study, the texture kernel size was set to 3, because a small moving window size is required for the segmentation of small areas with higher variance, such as mine areas. A moving box of 3 x 3 pixels is centered over each pixel, computes the texture attributes and moves further over the image.

Once segmentation was performed, training data was collected as for the pixel-based classification. Similar to the previous classification method, a minimum amount of 20 training sets for each class was collected by creating polygons and assigning them to the corresponding land use classes. Detailed information about the training samples is given in the appendix (Table 8-5). The option of previewing the temporary classification was considered helpful in order to find out if the amount of training samples for each class is sufficient. Band combinations were used in order to recognize the mine features in a better way, e.g. by displaying only the ratio images or the elevation model. Subsequently, attributes being considered in the classification process and the bands they should be derived from were chosen. The three principal components as well as all additional data, which are the ratio images, the elevation model and the SAR images, were chosen as selected bands from which all attributes are derived from. A total of 4 spectral attributes, 4 texture attributes and 14 spatial attributes are the attributes the classification is based on. Detailed information about these attributes can be found in the appendix (Table 8-6; Table 8-7; Table 8-8). As for the pixel-based classification, the SVM algorithm is chosen for the classification of the input image with all default settings.

As for the other classification methods, post-processing was conducted by sieving and majority analysis, whereas all parameter settings of the pixel-based classification post-processing were adopted. In order to derive area values, class statistics were computed. The amount of pixels of each class was multiplied by the spatial size of the dataset, which is 10 m, for obtaining area values in m^2 and km^2.

For evaluation, classifications were cross-checked with the reference dataset for pixel-based and object-based classifications (chapter 3.2.3) in a confusion matrix. Accuracy metrics were computed in the same way as in chapter 4.2.3.

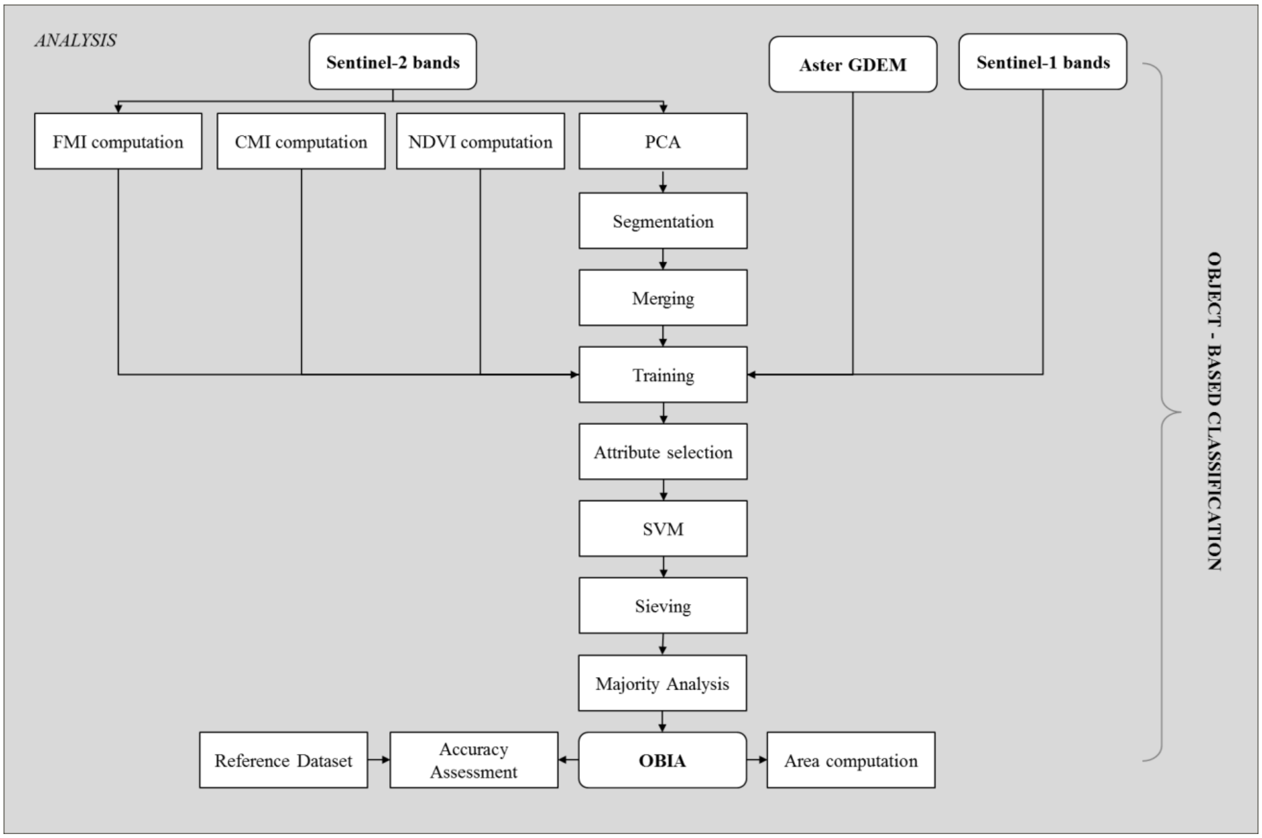

Figure 4-5: All steps of object-based classifications. Input and Output (OBIA represents the object-based classification output) are shown in rounded cells. PCA refers to principal component analysis, SVM refers to support vector machine algorithm.

4.3 Crowdsourcing

A crowdsourcing project was launched, where volunteers were asked to digitize the delineation of the four open-pit mines manually. For the crowdsourcing project, a heterogeneous group of people was included with different professional backgrounds, such as environmental scientists, geo-information scientists and volunteers not familiar with environmental research or geo-informatics. Volunteers received detailed instructions (Figure 8-2; Figure 8-3), including information about this study, the scope of digitization, features indicating a potential mine from LaJeunesse Connette et al. (2016) which should be included into the digitization and a precise explanation of the digitization process. Together with the instructions, volunteers received a Sentinel-2 RGB and an empty Shapefile of each study site, ready for digitization. Digitization was performed within QGIS software. Volunteers had to start an edit session and draw a polygon, which represents the delineation of the open-pit mine. Thereby, volunteers were asked to create only one polygon for each open-pit mine and assign the value 1 as id when saving. Finally, volunteers were asked to upload their final product, which is the digitized feature, upon a platform. The project was run for 10 days.

A total of 18 volunteers digitized the four mines, thus resulting in a total of 72 delineations. Subsequent post-processing was required. All following steps were performed within QGIS Desktop 3.4. At first, data integrity was verified in order to guarantee that all delineations were saved correctly, that the amount of digitized polygons was uniform and that polygons were assigned the similar id. This step was essential for the further analysis.

All post-processed polygons of each study site were overlaid. With the field calculator, a new area field was added to the attribute table of each polygon. The field calculator holds a function $area, which was subsequently applied to calculate the area in m^2 of the polygon and to store this value within the new column. This enabled the selection of the smallest (Min polygon) and the largest polygon (Max polygon).

Following, all delineations which are hold in a vector model, had to be converted into a raster model for subsequent comparison (Figure 4-6). Rasterization was conducted by converting the vectorized polygon into a rasterized polygon based on the id. All pixels being covered by the previous vectorized polygons were assigned the value 1, as this is the id representing mine for all digitized polygons. For the rasterization process, georeferenced units were chosen as output raster size units, a horizontal and vertical resolution of 10 m and the extent values of each study site, presented in chapter 3.2. The obtained raster layers were used for subsequent analyses.

Further raster computations required that no no-data values are contained in the data. Therefore, the function r.null of Grass GIS was applied in order to assign the value 0 to all pixels that have a no-data value. This step resulted in a raster layer containing the mine, which is represented by pixels holding the value 1, and the surroundings of the mine, which are represented by pixels holding the value 0.

With the raster calculator, a frequency distribution was calculated by adding up all raster layers. The frequency distribution raster layer represents thus the frequency count, which is the amount of pixels being included into the digitization by volunteers. This means a pixel value of 8 indicates that 8 volunteers included this pixel into their mine digitization.

For further comparison with the classifications, the pixels being assigned to the mine by the majority of the volunteers were extracted. All pixels that were selected by ≥ 9 volunteers are referred to represent the majority. Pixels were extracted by saving all pixels of the frequency distribution layer that have a value ≥ 9 into a new raster layer. This new polygon dataset is considered to be the majority polygon (MAJ)

The area of the majority polygon was derived by computing class statistics within ENVI as previously described. Similar to the classifications, the amount of pixels of each class was calculated. In this case there are two classes, the mine, represented by class 1 and the surroundings represented by class 0.

For evaluation, an accuracy assessment was conducted whereby the majority polygon of each study site was compared to the reference dataset. Similar to previous accuracy assessments carried out within this study, accuracy metrics were derived such as overall accuracy, Kappa coefficient, and producer's and user's accuracy and omission and commission errors.

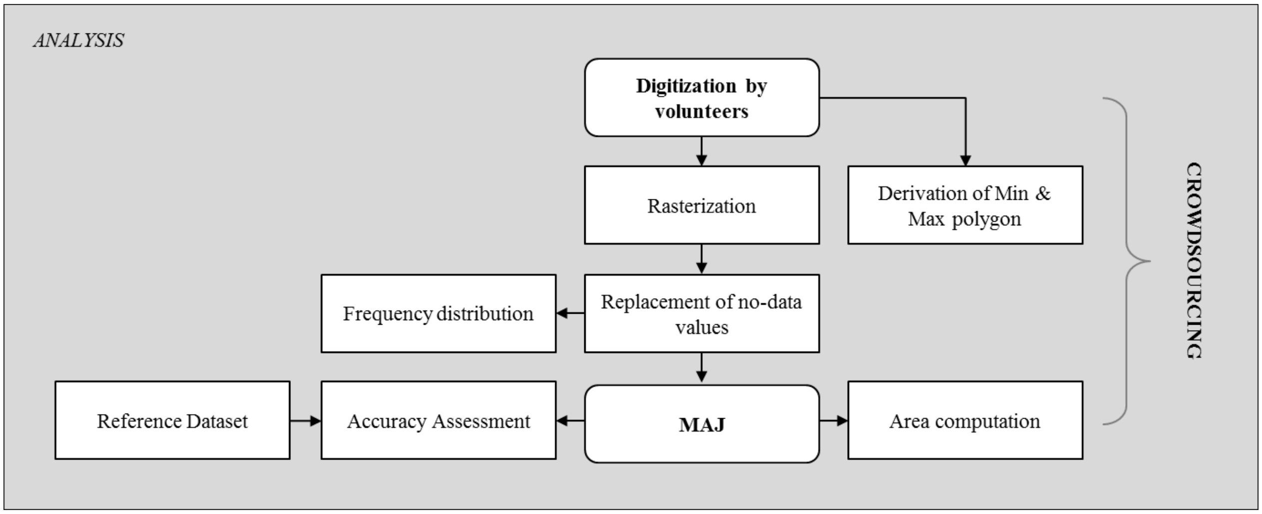

Figure 4-6: Overview of the crowdsourcing process. MAJ refers here to the majority polygon.

4.4 Comparison metric

In order to compare the classifications to crowdsourcing, the comparison metric Intersection over Union (IoU) was chosen. IoU is a ratio describing how similar two objects, in this case two mine polygons are. This comparison metric is suitable for this study, as it provides information about similarities and discrepancies between classifications and crowdsourcing. It is calculated by dividing the area of spatial intersection/overlap by the area of spatial union of the two polygons being compared (Figure 4-7) (Everingham and Winn 2012; Everingham et al. 2010; Jaccard 1901). IoU ranges from 0 to 1. The higher the value, the more similar the two objects are to one other.

For this study, the polygon of the class mine of each classification was compared to the corresponding majority polygon, which was generated by crowdsourcing. As classification results comprise all classes in a raster image, but only the class mine is required for IoU computation, all pixels being classified as mine needed to be extracted and stored in a separate raster layer. This extraction was done within QGIS. An overview of the 12 conducted comparisons is given in Table 4-3.

As previously mentioned, IoU requires the area of spatial intersection and the area of spatial union of the two polygons being compared. The area of spatial intersection was calculated by extracting all pixels that have the value 1 in the classification and the majority polygon, and storing them in a new raster layer. The area, which has been assigned to a mine by the classification and the majority polygon, is therefore represented by the intersection layer. For the area of spatial union, all pixels that have the value 1 in the classification or the majority polygon were extracted and stored in a new raster layer. Contrary to the intersection layer, the union layer is thus a representation of the area which has been assigned to a mine by the classification or the majority polygon.

For each of the 12 comparisons, the area of spatial intersection and the area of spatial union were computed.

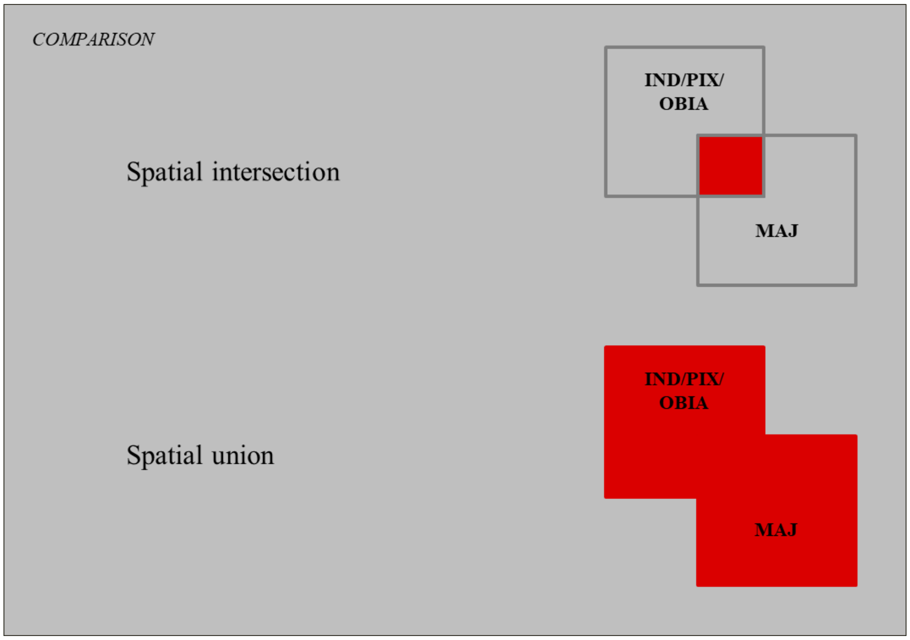

Figure 4-7: Concept of Intersection over Union (IoU). For calculating IoU, the area of spatial intersection and union between MAJ (majority polygon) and IND (Index-based classification), PIX (Pixel-based classification and OBIA (Object-based classification) has been computed.

In order to get the amount of intersection and union pixels of the intersection and union layers, the amount of pixels that were assigned the value 1 was derived. This amount was multiplied by the spatial resolution of the imagery, which is 10 m, in order to get spatial area values in m^2 and km^2.

IoU for each of the 12 comparisons (Table 4-3) was computed by the following formula V):

$$\text{V)}\quad \text{Intersection over Union} \equiv \frac{\text{Area of spatial intersection (km}^2\text{)}}{\text{Area of spatial union (km}^2\text{)}}$$

Table 4-3: Classification-Majority polygon comparison. For each study site, each classification is compared to the majority polygon.

	Conducted Comparisons
Grasberg mine	Index-based classification & majority polygon Pixel-based classification & majority polygon Object-based classification & majority polygon
Hamersley mine	Index-based classification & majority polygon Pixel-based classification & majority polygon Object-based classification & majority polygon
Highland mine	Index-based classification & majority polygon Pixel-based classification & majority polygon Object-based classification & majority polygon
Mariana mine	Index-based classification & majority polygon Pixel-based classification & majority polygon Object-based classification & majority polygon

5 Results

In this study, the area being subject to open-pit mining was derived using three different classification methods and by digitizing within a crowdsourcing project. In the following, results of the different classification approaches and the crowdsourcing project are presented individually (chapters 5.1 and 5.2). In chapter 5.3, results of each method are compared to one another in terms of visual interpretation, area calculation and accuracy.

5.1 Classifications

The following figures (Figure 5-1; Figure 5-2; Figure 5-3 and Figure 5-4) show the results of all classifications of each study site, which will be explained subsequently.

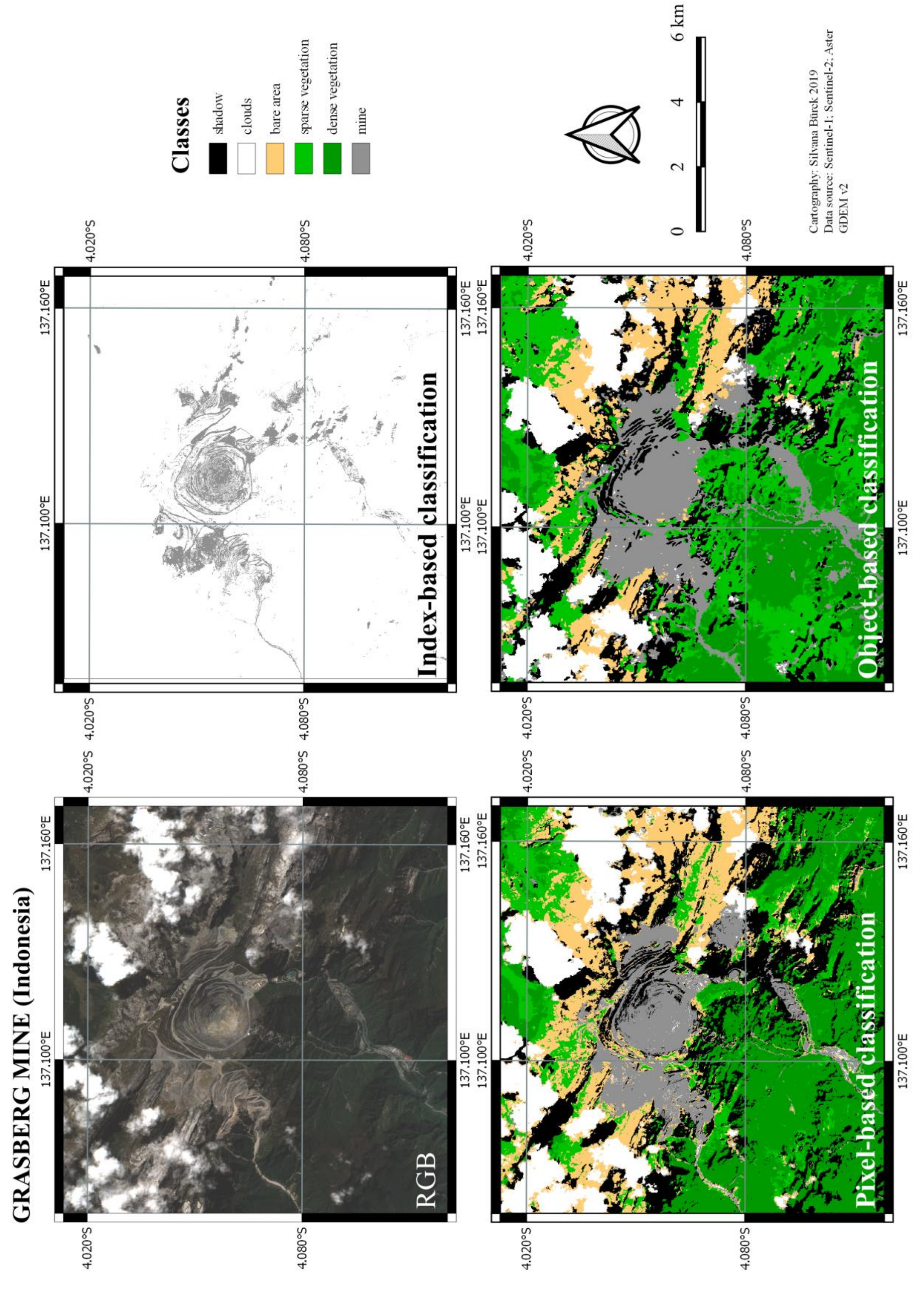

Figure 5-1: Sentinel-2 RGB and index-based (IND), pixel-based (PIX) and object-based (OBIA) classification of Grasberg mine. Visual interpretation reveals that the class mine covers the same area within all three classifications; contains modified Copernicus Sentinel data (2018) and modified Aster GDEM v2 (2011).

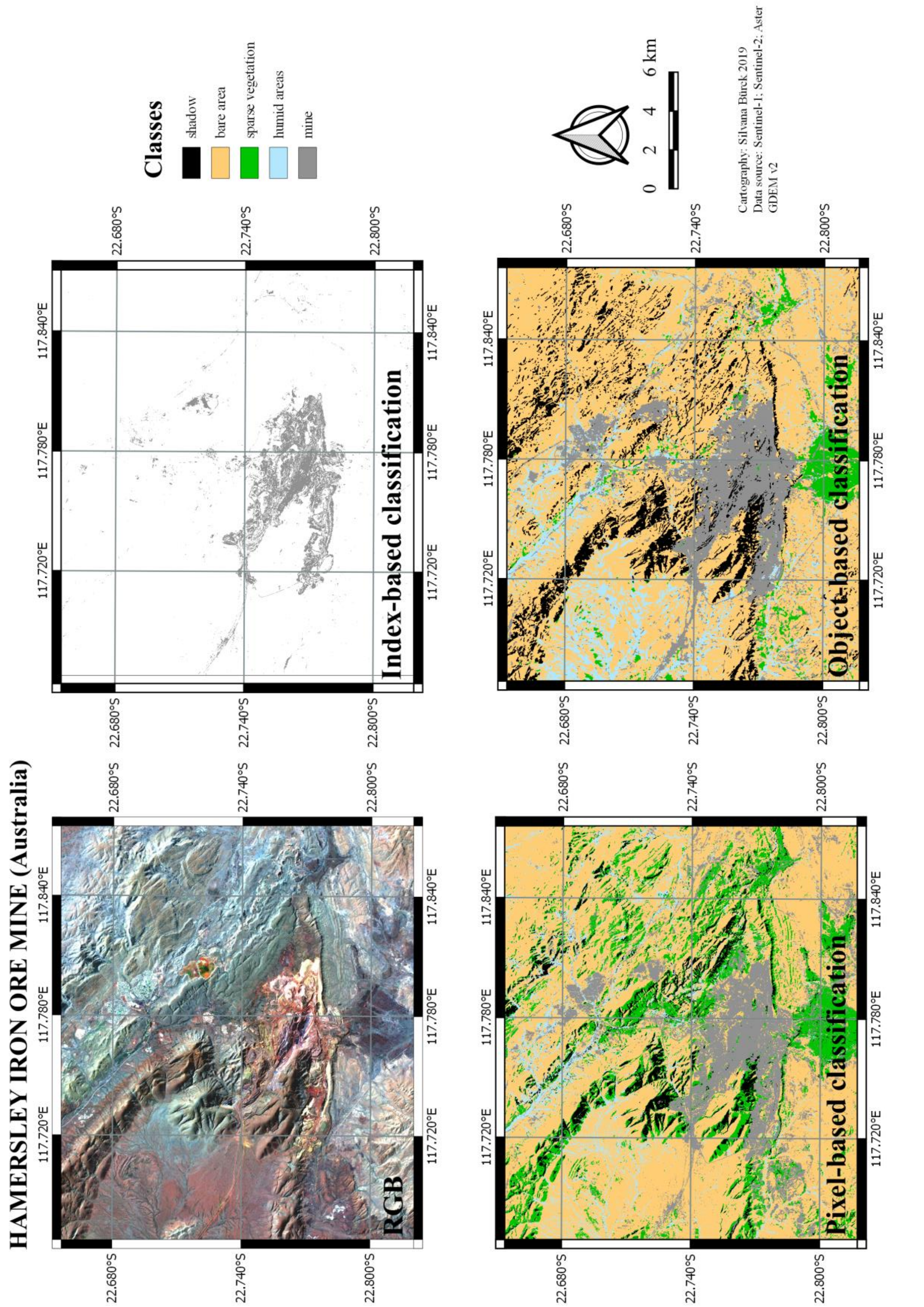

Figure 5-2: Sentinel-2 RGB and index-based (IND), pixel-based (PIX) and object-based (OBIA) classification of Hamersley mine. In the pixel-based classification, a clear dominance of the class sparse vegetation compared to the other classifications is visible; contains modified Copernicus Sentinel data (2018) and modified Aster GDEM v2 (2011).

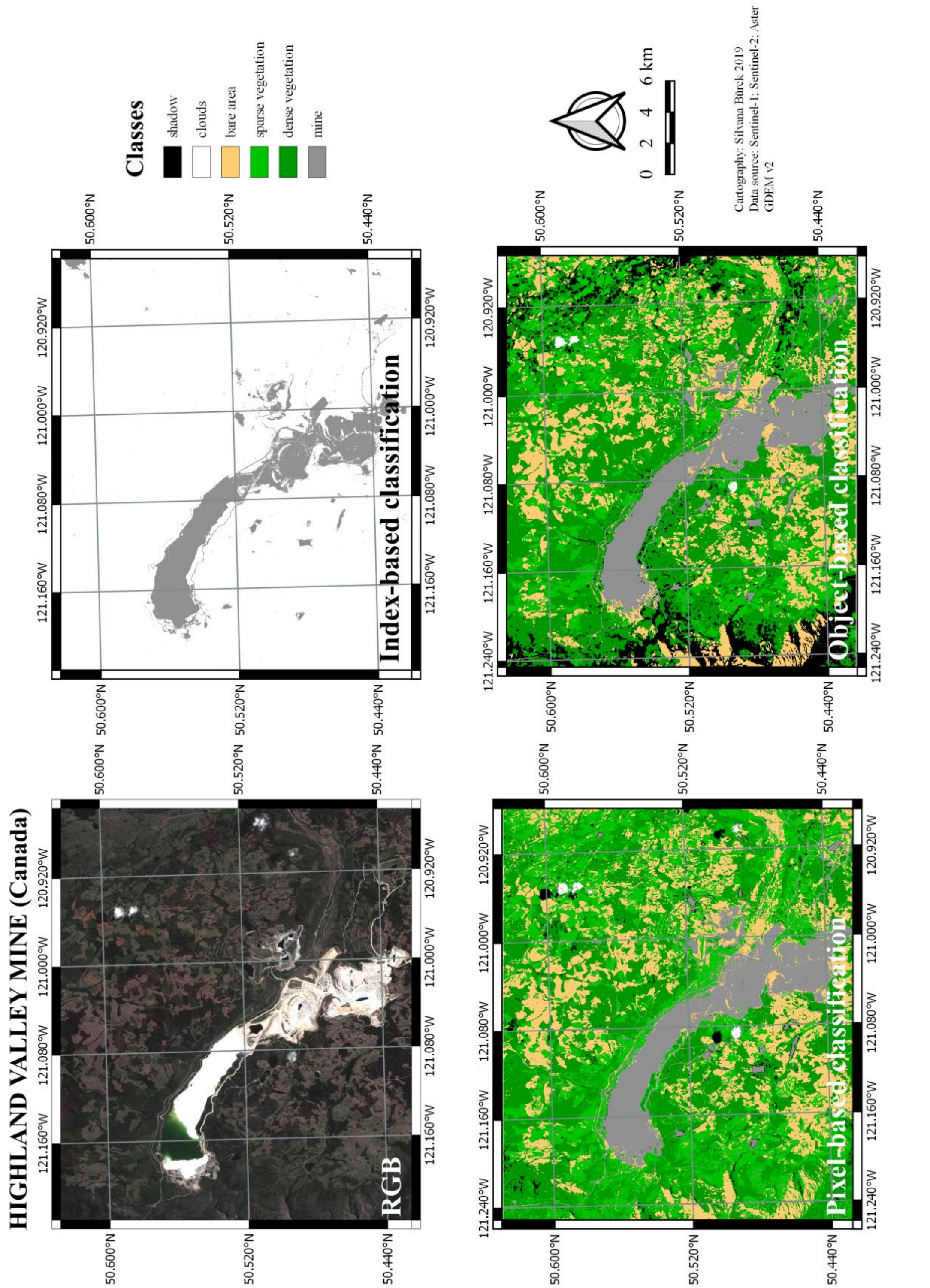

Figure 5-3: Sentinel-2 RGB and index-based (IND), pixel-based (PIX) and object-based (OBIA) classification of Highland mine. In the object-based classification, a clear dominance of the class shadow compared to the other classifications is visible; contains modified Copernicus Sentinel data (2018) and modified Aster GDEM v2 (2011).

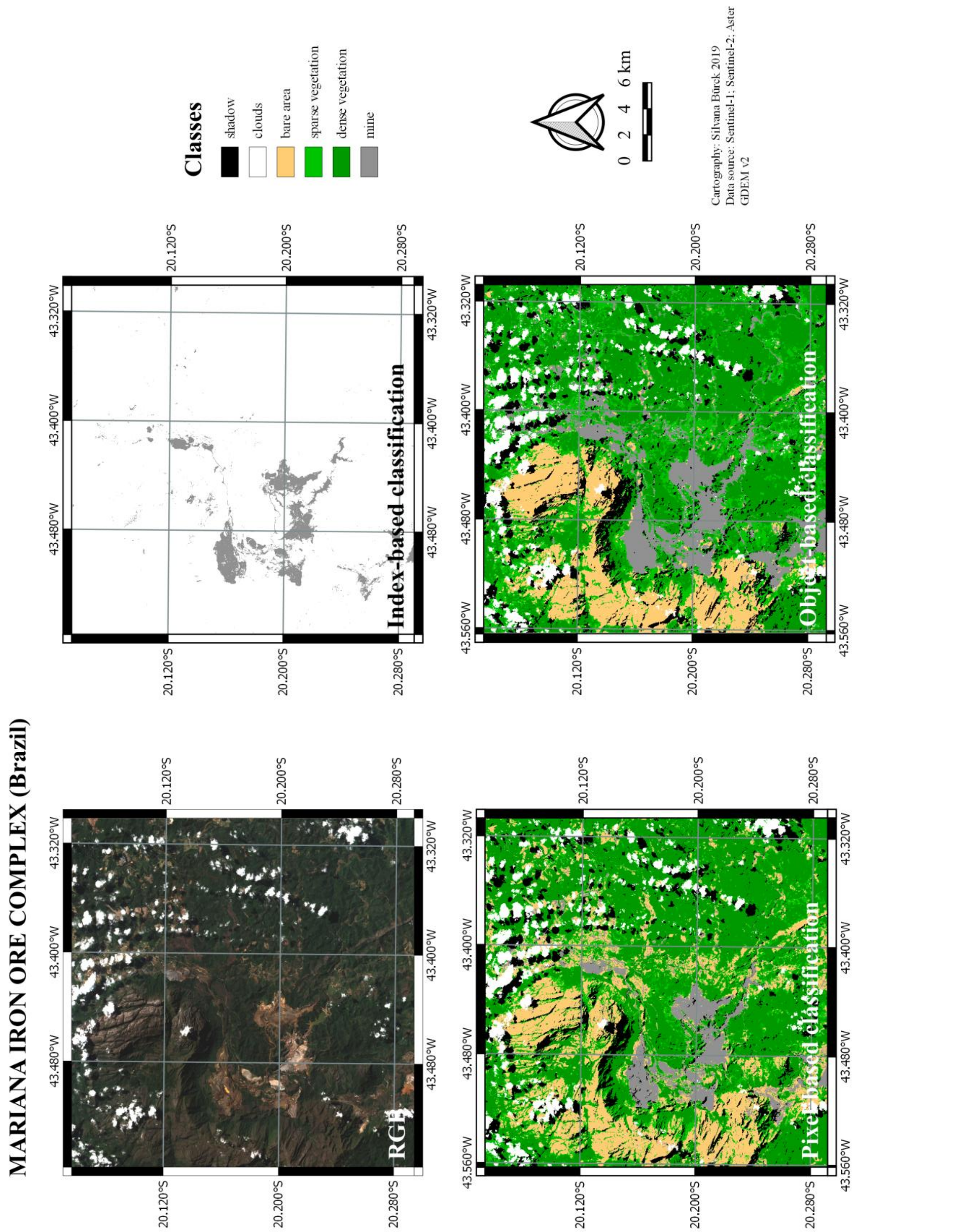

Figure 5-4: Sentinel-2 RGB and index-based (IND), pixel-based (PIX) and object-based (OBIA) classification of Mariana mine. In the pixel-based classification, bare area is more abundant than in the other classifications; contains modified Copernicus Sentinel data (2018) and modified Aster GDEM v2 (2011).

5.1.1 Visual interpretation

Figure 5-1 to Figure 5-4 show the results of the three classification methods – index-based, pixel-based an object-based – for each study site. When visually comparing all three classifications of each study site, the classifications of Grasberg mine appear to be very similar (Figure 5-1), whereas for the other study sites differences between the pixel-based and the object-based classifications occur. For Hamersley mine (Figure 5-3), a dominance of sparse vegetation within the pixel-based classification and an abundance of shadow in the object-based classification are observable. Regarding Highland mine, for the object-based classification (Figure 5-2), a dominance of shadow and for Mariana mine (Figure 5-4), a dominance of bare area for the pixel-based classification was identified. This first visual impression includes the consideration of all classes.

Focusing only on the class mine itself, a similar impression among all classifications of each study site was found. Meaning, when comparing the classifications among each other, which is referred to the intra-mine comparison, mine appears to cover the same area within each classification. This phenomenon of same spatial extent of the class mine can be observed in Figure 5-1, where mine is represented similarly within each classification. This second visual impression is especially true for Grasberg mine and Highland mine. For Hamersley mine (Figure 5-3), a slight extension of the class mine in the northern part of the AOI is visible in the pixel-based and object-based classification. Regarding Mariana mine, an extension of the class mine within the object-based classification was detected, as shown in Figure 5-4, where mine extents further north, east and south in the object-based classification.

With respect to an inter-mine comparison, which means comparing study sites between each other, the largest variations among classifications were observed for Hamersley mine. For this study site, the class mine, as well as other land use classes, vary stronger in extent among the three classifications.

Furthermore, it has been observed that in accordance with LaJeunesse Connette et al. (2016), all features indicating a potential mine such as bare ground, artificial pools, piles of rock, roads, buildings and pits are comprised within the class mine. In the RGB of Grasberg mine (Figure 5-5) numbers from 1 to 6 exemplify the features indicating a potential mine from LaJeunesse Connette et al. (2016). The same features are all covered by the class mine within the pixel-based classification. This observation is valid for all classification methods.

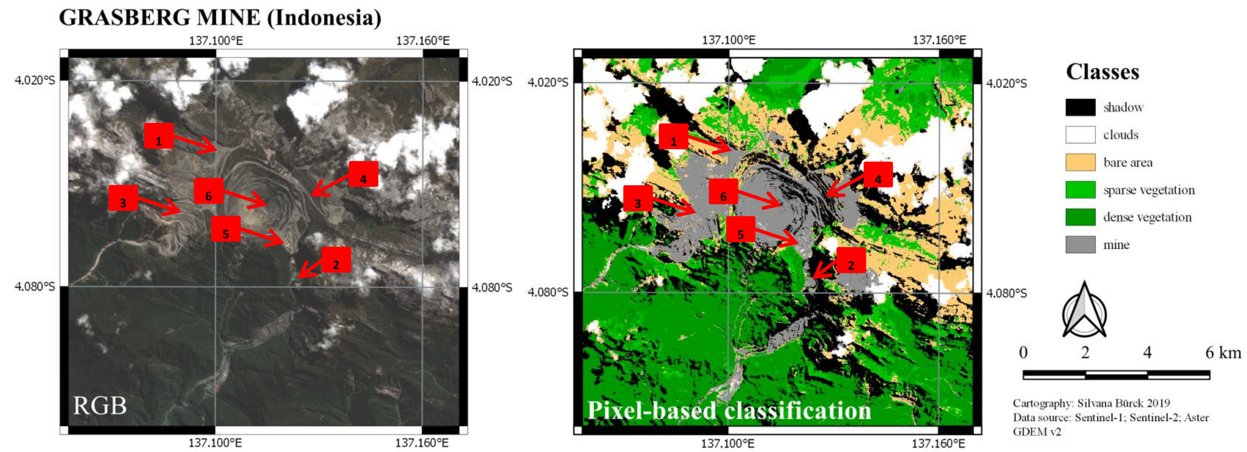

Figure 5-5: Features indicating a potential mine within the RGB (left) and pixel-based classification (right) of Grasberg mine. [1]-Bare Area; [2]-Artificial Pools; [3]-Piles of rock; [4]-Roads; [5] Buildings; [6]-Pit; contains modified Copernicus Sentinel data (2018).

Thus, the class mine comprises a wide range of mine features, but some roads, buildings and some water bodies were included in the class mine even though they do not belong to this class. For Highland mine, some lakes west and east of the mine were classified as a mine, even though their irregular shape indicates that these water bodies represent natural lakes instead of artificial pools (Figure 5-6). The same difficulty regarding the assignment of lakes to the class mine occurs within Mariana mine.

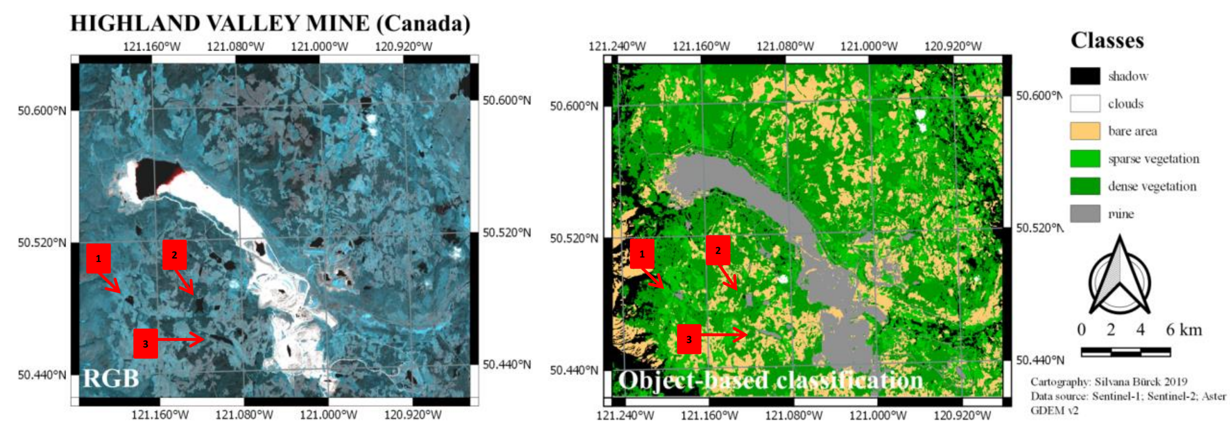

Figure 5-6: False color image (4-5-6) and object-based classification of Highland mine. Numbers from 1-3 indicate water bodies that represent natural lakes, but have been classified as mine; contains modified Copernicus Sentinel data (2018) and modified Aster GDEM v2 (2011).

Another visual difference between the three classifications of each study site is that when having a closer look into the index-based and pixel-based classifications the so-called salt & pepper effect becomes visible (Figure 5-7). Isolated pixels all over the AOI were classified as mine. On the contrary, when zooming into the object-based classification, more homogeneous entities and thus less isolated classified pixels are visible.

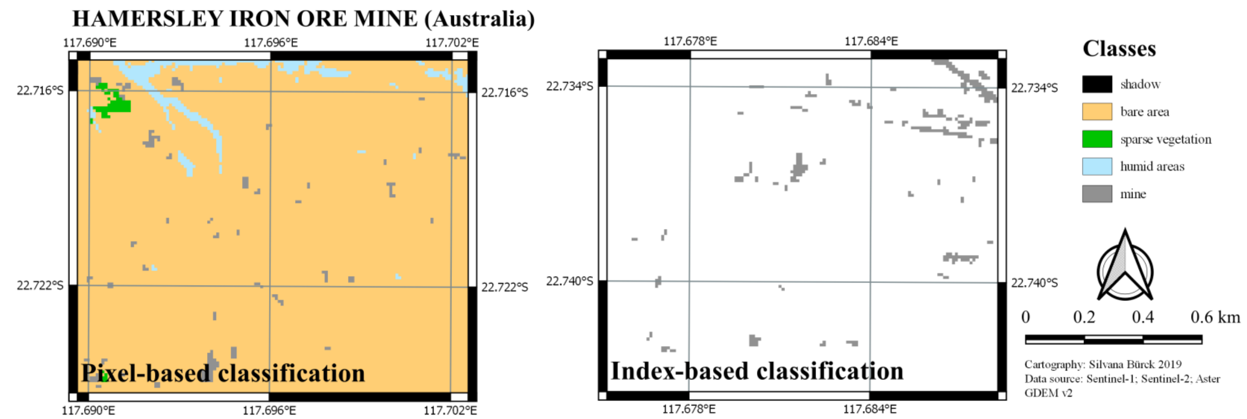

Figure 5-7: Evidence of salt & pepper effect within the index-based and pixel-based classifications as indicated by grey isolated mine pixels; contains modified Copernicus Sentinel data (2018) and modified Aster GDEM v2 (2011).

5.1.2 Area calculation

When computing class statistics for all classifications, the amount of pixels of each class can be derived. The pixel amount was multiplied with the pixel size (10 x 10 m) in order to derive area values in m^2 and subsequently divided by the factor 100,000 in order to obtain area values in km^2. Contrary to the previously presented visual impression, strong differences in area values between the classifications were found. Figure 5-8 (left) shows that the index-based classifications result in the smallest area being classified as mine, whereas in most cases object-based classification results in the largest mine area. With 8.59 km^2, the index-based classification of Grasberg mine has a smaller extent of the class mine than the object-based classification with 22.78 km^2 (Table 5-1). Especially for Mariana mine there are strong differences between the index-based classification with 29.33 km^2 and the object-based classification with 82.01 km^2. The same pattern is also true when comparing differences between classifications and study sites in terms of the relative area (Figure 5-8, right). Differences between the study sites were determined when comparing the mean area values of each study site (Table 5-1). Highland valley mine represents the largest mine with 65.97 km^2, followed by Mariana mine with 54.08 km^2 and Hamersley mine with 43.15 km^2. Grasberg mine is the smallest mine covering a mean area of 14.92 km^2.

Table 5-1: Overview of the area of the mine polygon of each classification and the mean area of each study site.

	Grasberg mine			Hamersley mine			Highland mine			Mariana mine		
	IND	PIX	OBIA	IND	PIX	OBIA	IND	PIX	OBIA	IND	PIX	OBIA
Area of mine [km^2]	8.59	13.39	22.78	19.4	54.78	55.25	51.17	78.57	68.17	29.33	50.88	82.01
Area of mine relative to the entire study site [%]	5.67	8.84	15.04	4.72	13.34	13.47	7.93	12.18	10.58	3.93	6.82	11.00
Mean area of mine of each study site [km^2]	14.92			43.15			65.97			54.08		

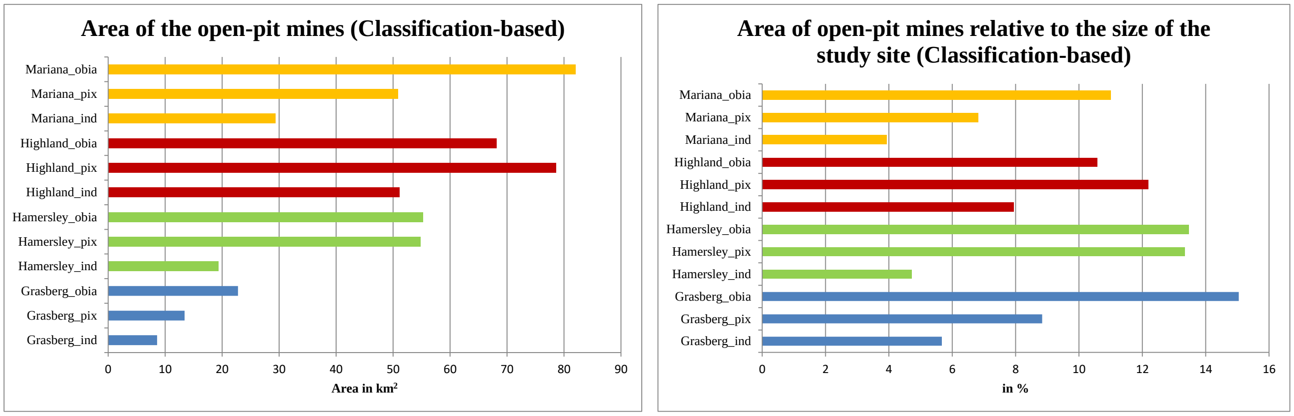

Figure 5-8: Total area calculation for all classifications (left) and relative area calculation for all classifications (right). Classifications of each mine are represented in a specific color.

5.1.3 Accuracy Assessment

Comparing classification results of the class mine on an intra-mine level with the reference dataset in a confusion matrix, an overall accuracy of ≥ 77.41 % was achieved for all classifications. Regardless of the classification results of Hamersley_pix (with the lowest accuracy), classification accuracy was overall high with ≥ 85.05 %. Overall accuracy ranges from 77.41 % (Hamersley_pix) up to 97.89 % (Mariana_obia), with slightly higher overall accuracy values for index-based classifications (Table 5-2). When comparing inter-mine accuracy, Hamersley mine achieved the lowest and Mariana mine the highest overall accuracy values (Figure 5-9).

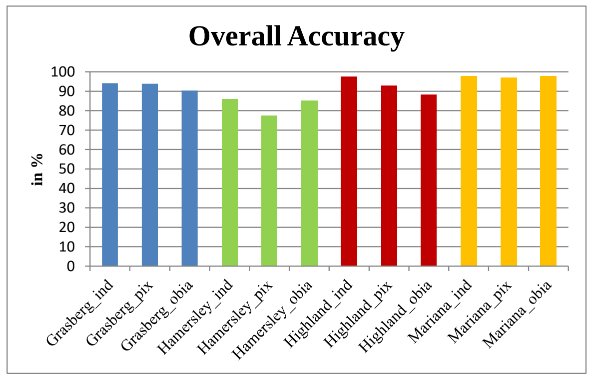

Figure 5-9: Overall accuracy of all classifications.

Similarly, a high Kappa coefficient of ≥ 0.54 for all classifications and a Kappa coefficient value ≥ 0.8 for all classifications except for Grasberg_ind (0.56), Hamersley_ind (0.54) and Hamersley_pix (0.68) demonstrates high observed agreement between classifications and reference (Table 5-2). According to the explanations of the Kappa coefficient value in chapter 4.2.2, this means that most classifications are 80 % better than random pixel assignment, given the fact that a Kappa coefficient value of 0.8 refers to 80 % accuracy. Highest Kappa coefficient values were found for Mariana_pix (0.96) and Mariana_obia (0.97). A correlation between Kappa values and classification methods was not observed. When comparing on an inter-mine level, Hamersley mine has, similar to the consideration of overall accuracy, the lowest Kappa coefficient values.

The producer's accuracy demonstrates how well the reference is classified, in other words which percentage of the reference has been covered by the classification. For all classifications, producer's accuracy ≥ 44.12 % (Figure 5-10, left) was calculated. Similar to previous results, a low producer's accuracy of 47.89 % for Grasberg_ind and 44.12 % for Hamersley_ind was determined, which means that for these classifications < 50 % of the mine in the reference dataset was classified as mine. Contrary to all other classifications, > 70 % of the class mine in the reference dataset was classified as mine within the classifications. Regarding intra-mine comparison, the lowest producer's accuracy values occur within index-based classifications. On an inter-mine level, especially Highland and Mariana mine achieve very high producer's accuracies of > 90 %, whereas producer's accuracy is lowest for Hamersley classifications.

The user's accuracy is a metric of reliability for the user and demonstrates how confident a user can be that a classified area represents this specific land use and land cover type in reality. For all classifications, user's accuracy is ≥ 77.47 % (Figure 5-10, right). The user can thus be sure that > 70 % of the classified mine represents mine in reality. As shown in Table 5-2, Grasberg _ind has the lowest user's accuracy values with 77.47 %. Regarding intra-mine comparison, no correlation between classification methods and user's accuracy can be detected, but on an inter-mine level Hamersley mine, Highland mine and Mariana mine have highest user's accuracies, contrary to Grasberg mine.

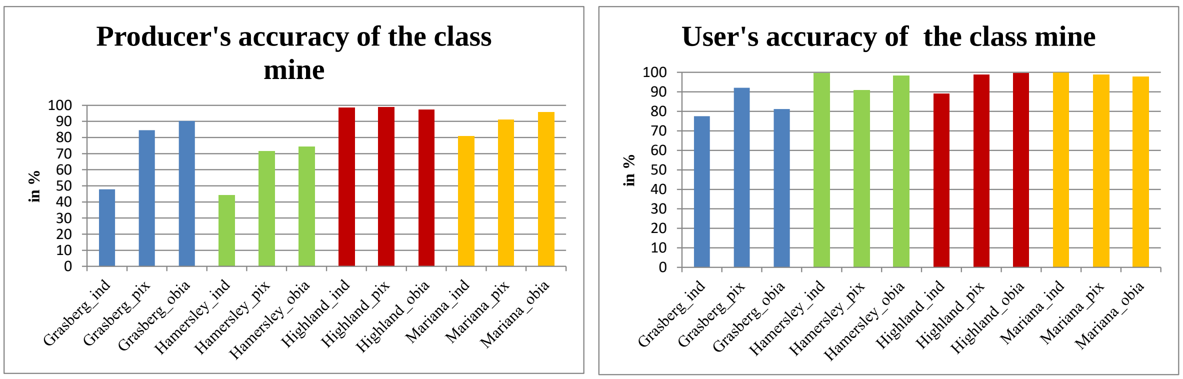

Figure 5-10: Producer's (left) and user's (right) accuracy for each classification.

Further accuracy metrics are the omission and commission errors, also referred to as the type 1 error and type 2 error, respectively. The omission error represents the percentage of excluded mine pixels, the false negatives. For all classifications, the omission error is ≤ 55.88 %. Considering the intra-mine level, the index-based classifications appear to have the highest amount of missing mine pixels among the classifications as shown in Figure 5-11 (left) and Table 5-2, where Grasberg_ind and Hamersley_ind have a type 1 error of 52.11 % and 55.88 %, respectively. On an inter-mine level, Highland mine and Mariana mine have the lowest omission error for all classifications, contrary to Grasberg and Hamersley mine (Figure 5-11, left). Further analysis of the confusion matrix of pixel-based and object-based classifications show into which class the false negatives were included as well as the percentage of these excluded pixels. Primarily, pixels of the class bare area should have been included into the class mine. Detailed information about this further investigation of false negatives is given in the appendix (Table 8-2). Using the classification Hamerley_pix as an example, another 22.12 % of the classified bare area should have been included into the class mine. Figure 5-12 shows evidence of this type 1 error because here classified bare area (left) represents mine in reality.

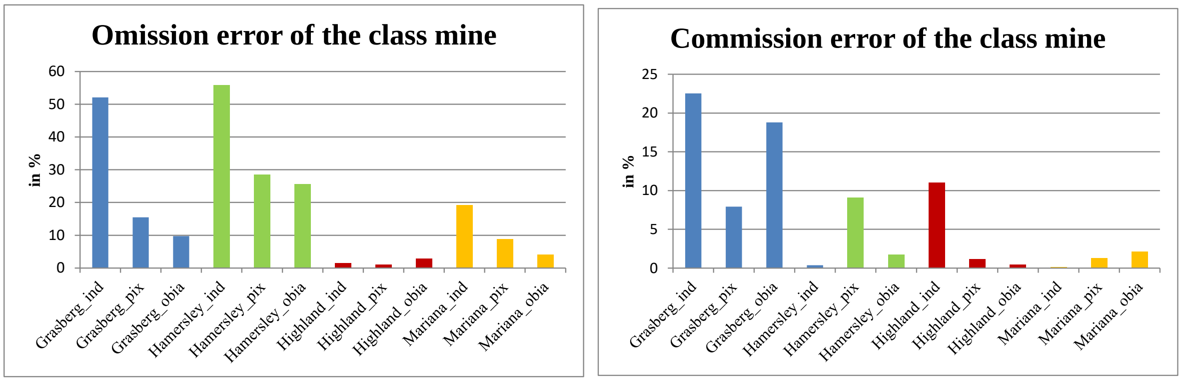

Figure 5-11: False negatives (left) and false positives (right) of the class mine within all classifications.

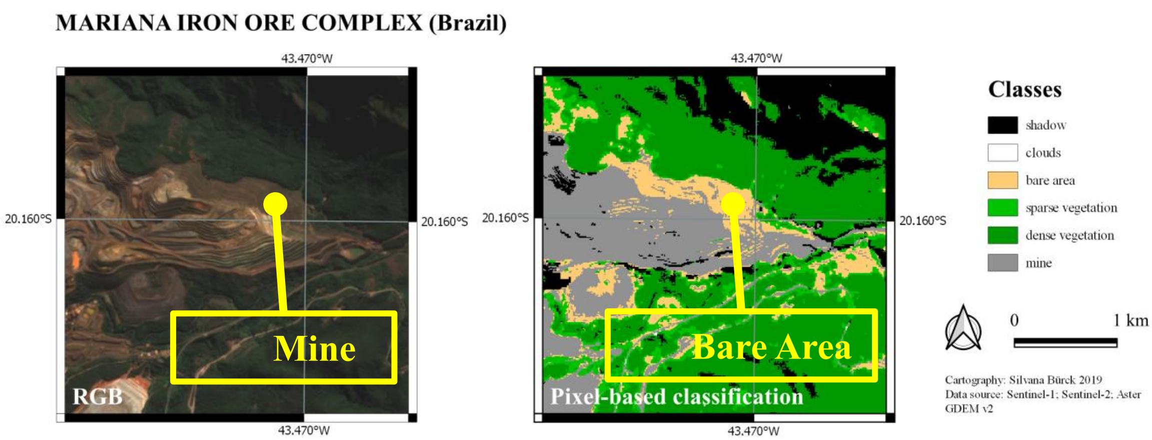

Figure 5-12: Classified bare area (right) of the object-based classification of Mariana mine represents mine in reality (left); contains modified Copernicus Sentinel data (2018).

For all classifications, the commission error is ≤ 22.53 %. Similar to the omission error, the commission error of the classifications is highest for the index-based classifications, when comparing on an intra-mine level. That means the amount of false positives, in other words the amount of pixels being falsely included into the class mine, is highest for index-based classifications (Figure 5-11, right). Grasberg_ind and Highland_ind have a type 2 error of 22.53 % and 11.04 %, respectively. Among study sites, Grasberg mine is the mine with the highest amount of falsely integrated pixels. Further investigation of the confusion matrix reveals that for Grasberg mine, in most cases pixels that belong to the class bare area were falsely included into the class mine. For Hamersley mine, pixels of the class bare area and sparse vegetation have been falsely included. Evidence is given in Figure 5-13. The sparse vegetation along humid areas (left) was classified as mine (right), as indicated by grey color in the classification (right). Similar to the error of omission, detailed information about the percentage of commission error is given in the appendix (Table 8-3).

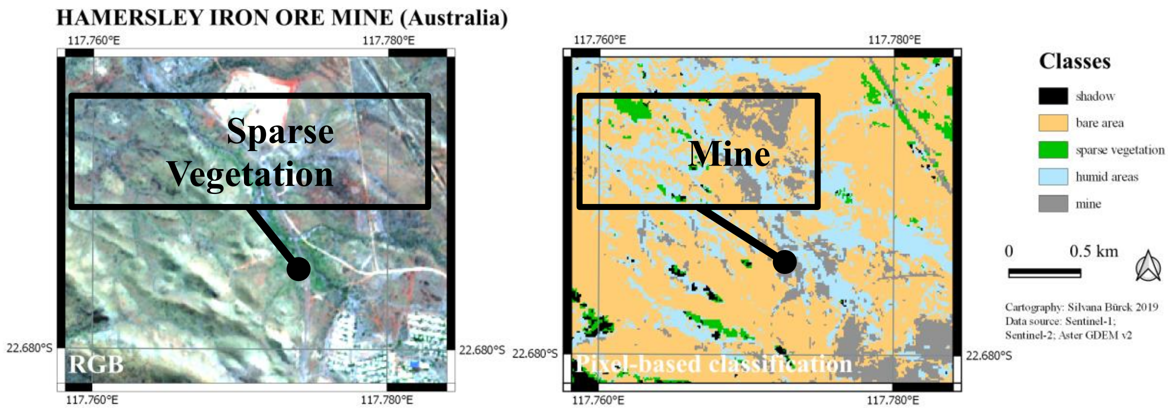

Figure 5-13: Sparse vegetation in the northern part of Hamersley mine (left) is classified as mine (right) within the pixel-based classification; contains modified Copernicus Sentinel data (2018).

With respect to correctly classified mine pixels, − the so-called true positives −, there are strong deviations between classifications (Figure 5-14). That means the amount of the correctly classified mine pixels is dependent on the classification method. For all mines, the index-based classifications have the lowest amount of true positives and object-based classification the highest. Grasberg_ind accounts for 636 true positives, whereas Grasberg_obia contains 2139 correctly classified mine pixels. When comparing the true positives to all pixels that have been classified as mine, − the so called totals −, within the area of the reference dataset, the same pattern becomes visible. The difference reveals that there is no tendency recognizable between all classified and correctly classified mine pixels. For some study sites, the strongest difference was detected within index-based classification, sometimes within the other classifications. Especially for Grasberg mine, differences between true positives and totals are significant for all classifications. When comparing on an inter-mine level, Highland mine seems to have the highest amount of correctly classified and total mine pixels, which leads to the assumption that this mine is the largest mine, contrary to Grasberg mine, which is referred to be the smallest mine.

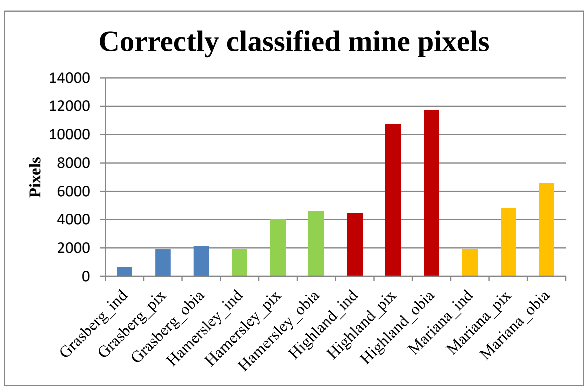

Figure 5-14: True positives of all classifications.

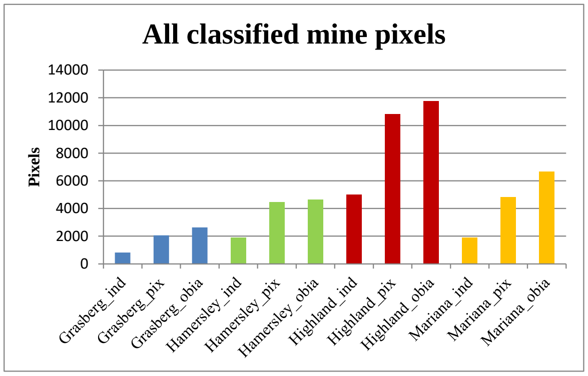

Figure 5-15: All classified mine pixels within the area of the reference dataset.

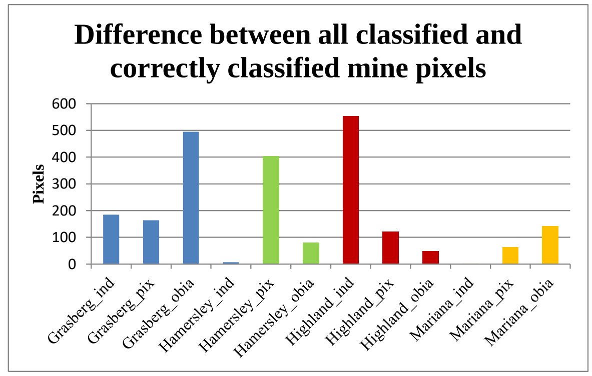

Figure 5-16: Difference between all classified mine pixels and true positives.

Table 5-2: Overview of accuracy metrics for the three classifications (IND refers to index-based classifications, PIX refers to pixel-based classifications and OBIA represents object-based classifications) of each study site.

	Grasberg mine			**Hamersley mine**			**Highland mine**			**Mariana mine**		
	IND	**PIX**	**OBIA**	**IND**	**PIX**	**OBIA**	**IND**	**PIX**	**OBIA**	**IND**	**PIX**	**OBIA**
Overall accuracy [%]	94.18	93.80	90.31	85.95	77.41	85.05	97.41	92.80	88.37	92.17	97.73	97.01
Kappa Coefficient	0.56	0.92	0.88	0.54	0.68	0.80	0.92	0.90	0.83	0.84	0.88	0.96
Producer's accuracy [%]	47.89	84.51	90.29	44.12	71.53	74.40	98.52	99.03	97.22	83.01	80.89	91.22
User's accuracy [%]	77.47	92.07	81.21	99.63	90.94	98.28	97.41	92.80	88.37	99.81	97.73	97.01
Omission Error [%]	52.11	15.49	9.71	55.88	28.47	25.60	1.48	0.97	2.78	19.11	8.78	4.07
Commission Error [%]	22.53	7.93	18.79	0.37	9.06	1.72	11.04	1.13	0.41	0.11	1.30	2.13
True positives [pixels]	636	1904	2139	1881	4046	4562	4457	10707	11700	1875	4770	6532
Totals [pixels]	821	2068	2634	1888	4449	4642	5010	10829	11748	1877	4833	6674
Difference between totals and true positives	185	164	495	7	403	80	553	122	48	2	63	142

5.2 Crowdsourcing

5.2.1 Visual interpretation

All 18 delineations of each mine were compared to each other and visually interpreted. The first impression is that all digitized polygons are in very close proximity to the mine and not in other parts of the satellite imagery. Nevertheless, differences regarding the extent of polygons occur, shown in Figure 5-17.

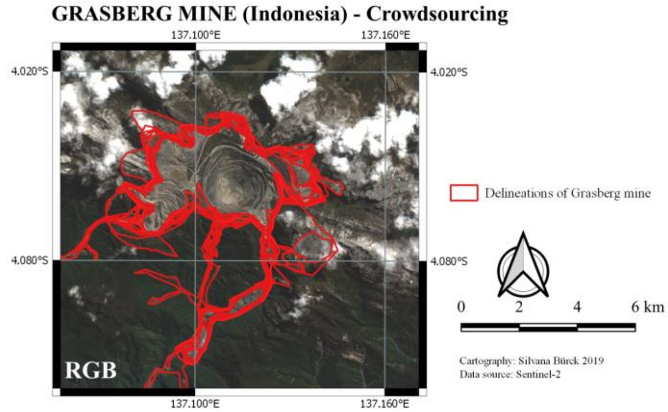

Figure 5-17: Overview of all digitizations of Grasberg mine. Digitized polygons are not entirely congruent; contains modified Copernicus Sentinel data (2018).

Comparing the smallest (Min polygon) and the largest (Max polygon) polygon of all study sites to each other, very strong differences were found for Grasberg mine and Hamersley mine. Evidence is given in Figure 5-18 and Figure 5-19, where a strong difference in extent between the Min polygon and the Max polygon was observed. For all study sites (Figure 5-18; Figure 5-19; Figure 5-20; Figure 5-21), the Min polygon always refers to the pit itself, whereas the Max polygon contains several mine features and is thus larger in extent.

In the following, the results of the crowdsourcing analyses including among others the Max and Min polygons, will be presented in Figure 5-18, Figure 5-19, Figure 5-20 and Figure 5-21.

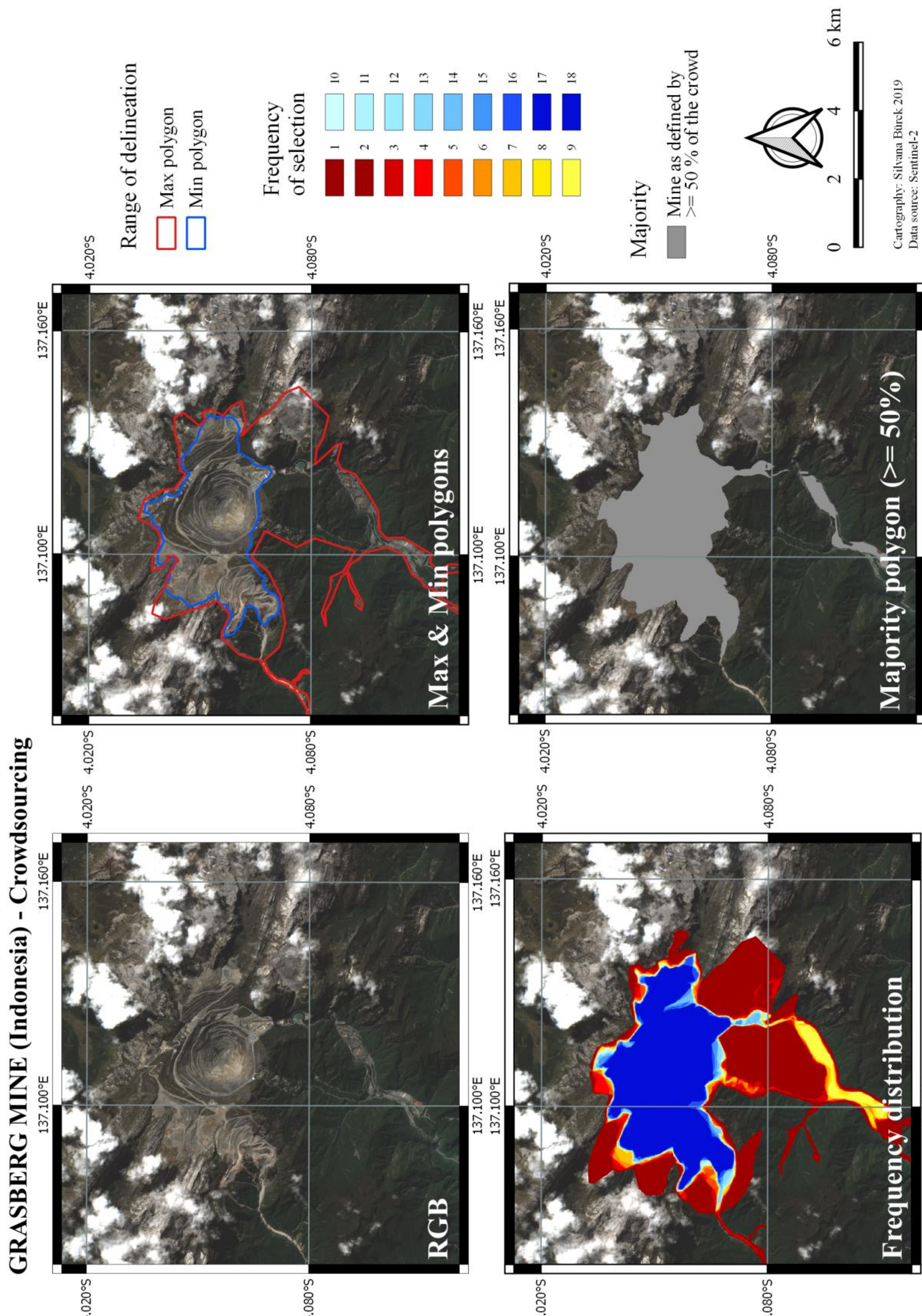

Figure 5-18: Sentinel-2 RGB, Maximum and Minimum polygon, frequency of selection and majority polygon for Grasberg mine; contains modified Copernicus Sentinel data (2018).

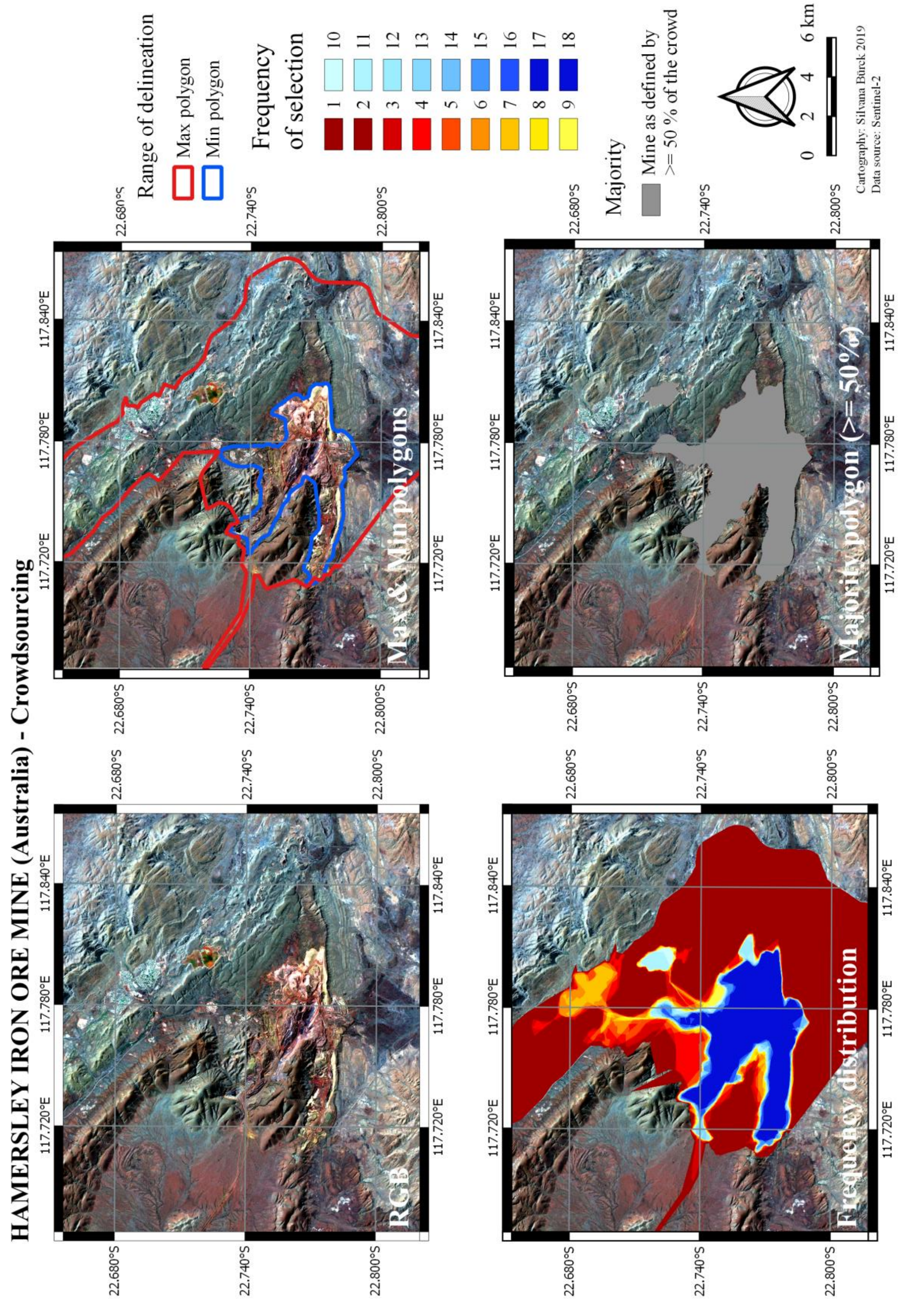

Figure 5-19: Sentinel-2 RGB, Maximum and Minimum polygon, frequency of selection and majority polygon for Hamersley mine; contains modified Copernicus Sentinel data (2018).

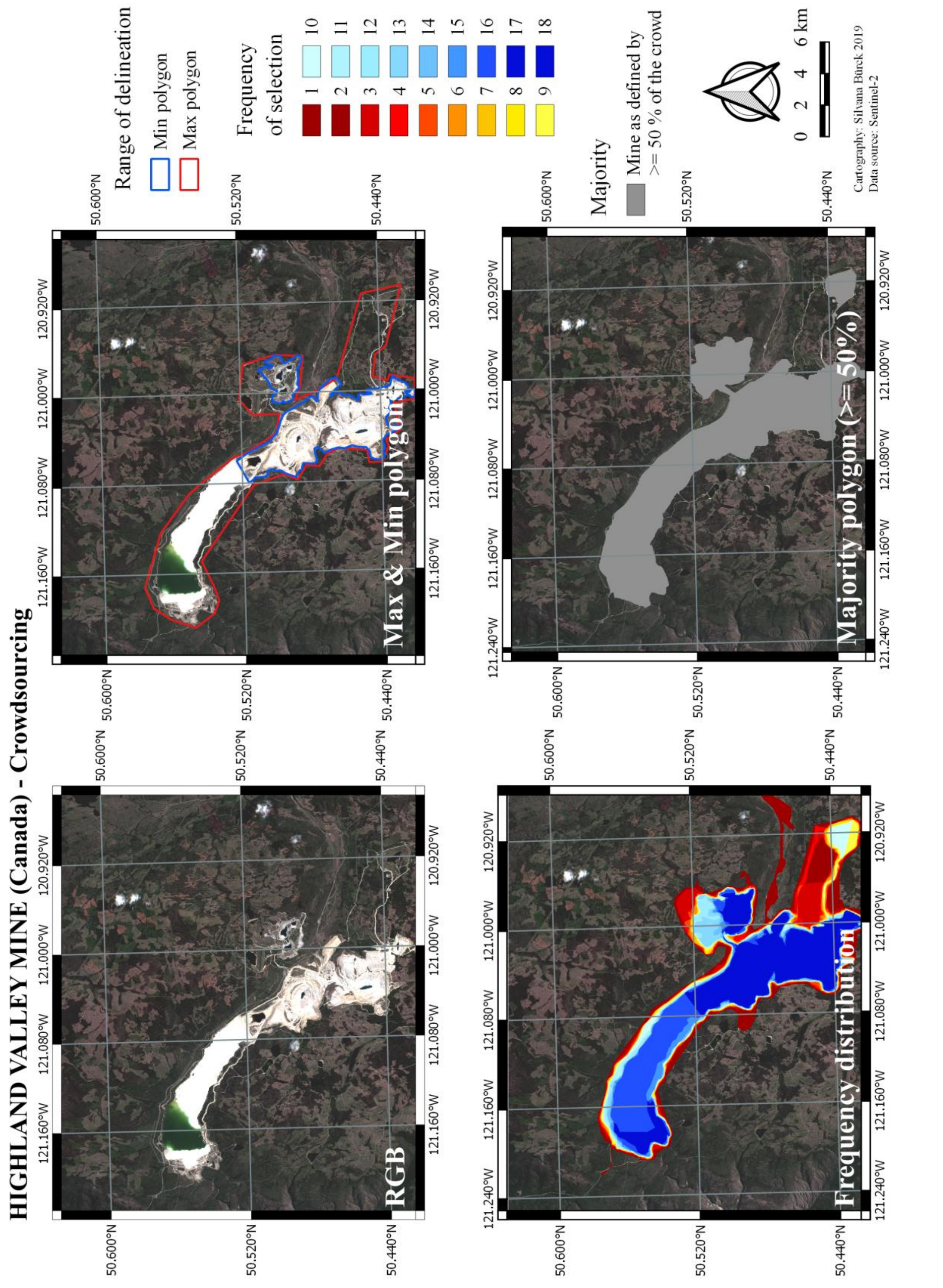

Figure 5-20: Sentinel-2 RGB, Maximum and Minimum polygon, frequency of selection and majority polygon for Highland mine; contains modified Copernicus Sentinel data (2018).

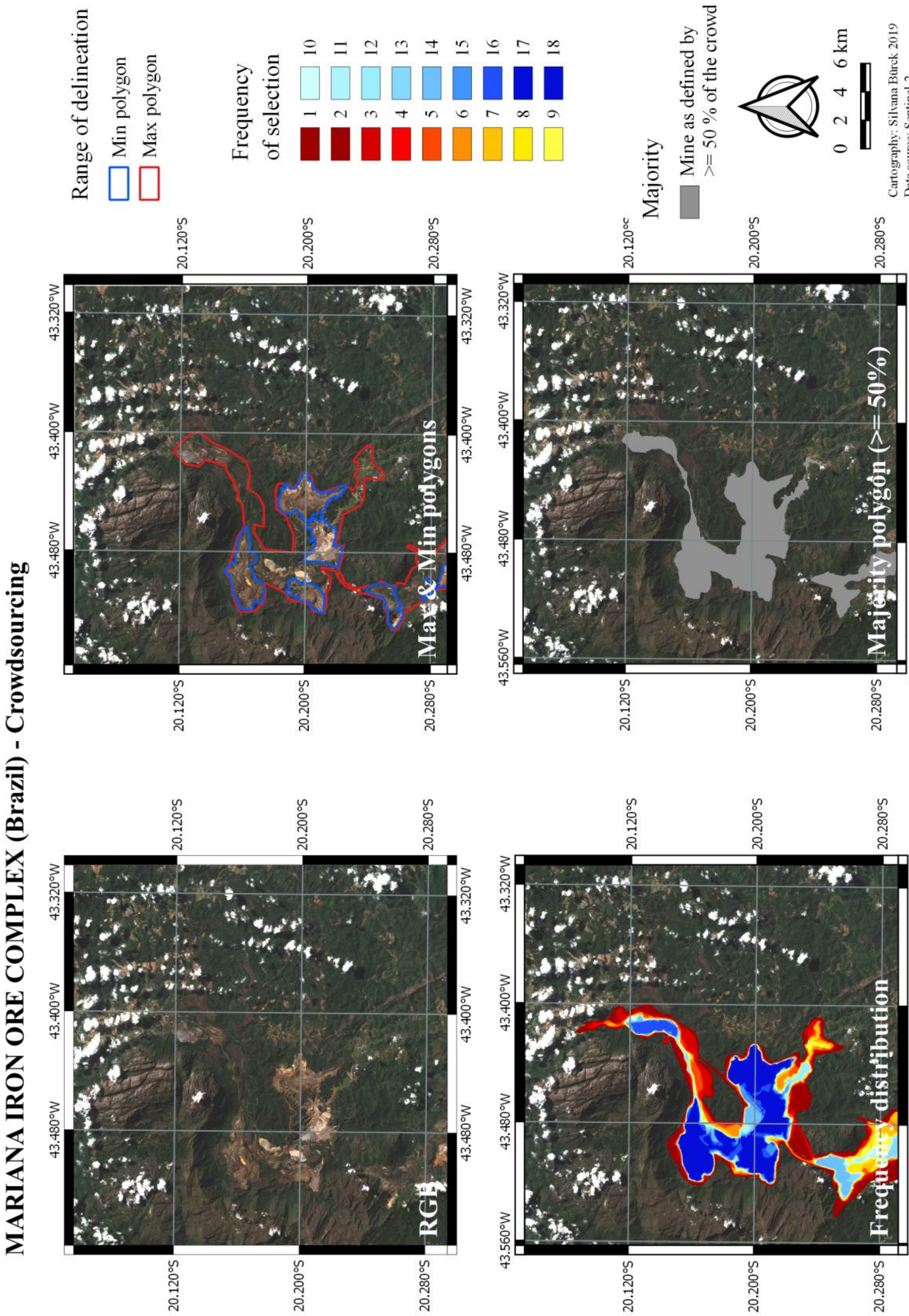

Figure 5-21: Sentinel-2 RGB, Maximum and Minimum polygon, frequency of selection and majority polygon for Mariana mine; contains modified Copernicus Sentinel data (2018).

The frequency distribution within Figure 5-18 to Figure 5-21 shows how often a pixel was considered to represent mine by the volunteers. Red color indicates pixels that were included in the digitized polygon only by a few volunteers, whereas blue color represents a high frequency of selection. Blue color always reflects the pit itself, indicating that for all study sites 18 people included the pit within their digitization. Regarding the red color and thus the low agreement, only < 4 volunteers digitized the mine in a progressive way. Comparing the frequency distributions on an inter-mine level, a dominance of red color for Grasberg mine (Figure 5-18) and Hamersley mine (Figure 5-19) is visible, in contrast to the other study sites. The red color indicates that only a few volunteers assigned this area to the mine, but the wide extent shows that these volunteers included a large area into the digitized polygon. For Highland mine (Figure 5-20) and Mariana mine (Figure 5-21), red color, indicating a low frequency of selection was recognized, but less dominant than for Grasberg mine and Hamersley mine, which indicates that agreement among volunteers was higher. Furthermore, regarding Mariana's frequency distribution, artefacts were observed, as indicated in Figure 5-22.

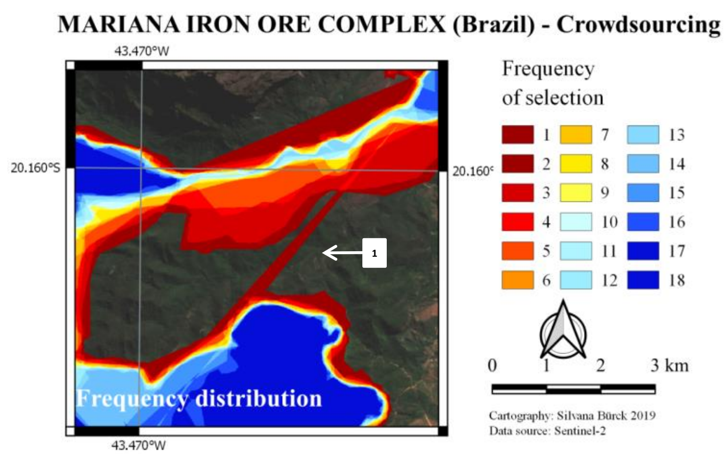

Figure 5-22: Artefact within the digitization of Mariana mine, indicated by [1]; contains modified Copernicus Sentinel data (2018).

For accuracy assessment and further comparison of classifications, the majority polygon (Figure 5-18 to Figure 5-21) was derived. It includes all pixels that were assigned to the mine by the majority of the crowd that means by ≥ 9 volunteers. For all study sites, the majority polygon is a multi-polygon as it is composed of several polygons. The area in between the polygons does thus not belong to the mine. The majority polygon represents the pit itself, but not in a conservative way as the Min polygon, because it contains further mine features.

With respect to the features indicating a potential mine from LaJeunesse Connette et al. (2016), all features such as bare ground, artificial pools, piles of rock, roads, buildings and pits are comprised within the majority polygon as Figure 5-23 demonstrates. Nevertheless, not all features indicating a potential mine within the entire imagery are covered by the majority polygon (Figure 5-24).

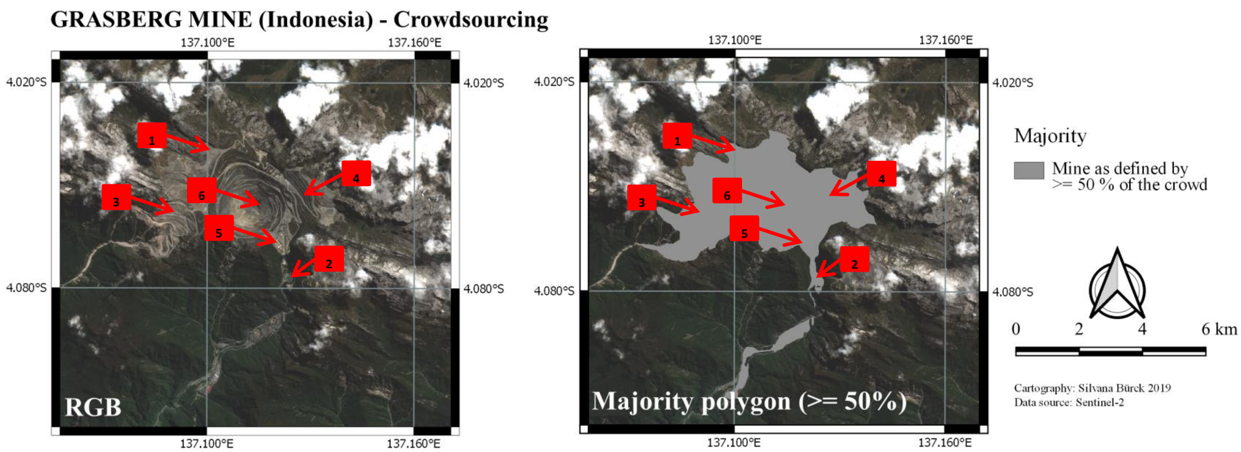

Figure 5-23: Features indicating a potential mine within the RGB (left) and majority polygon (right) of Grasberg mine. [1]-Bare Area; [2]-Artificial Pools; [3]-Piles of rock; [4]-Roads; [5] Buildings; [6]-Pit; contains modified Copernicus Sentinel data (2018).

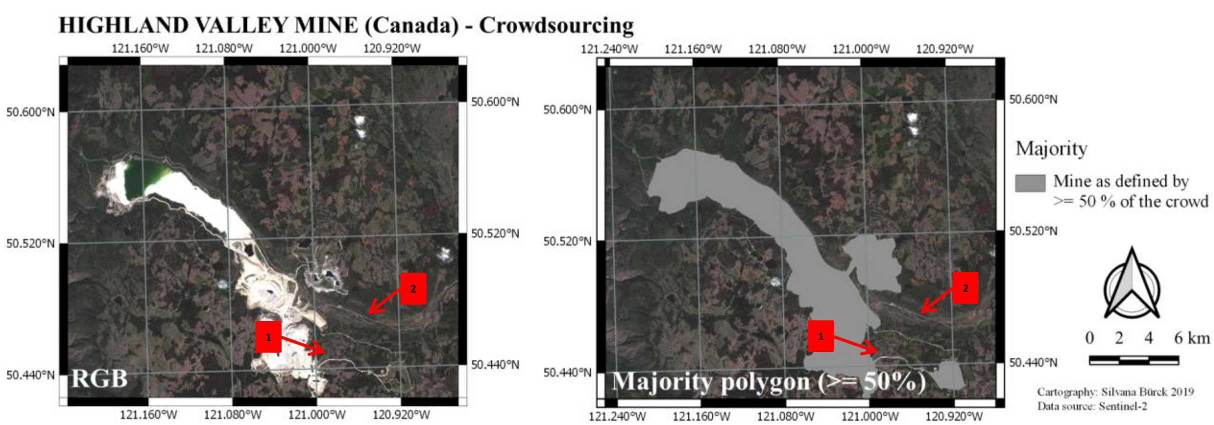

Figure 5-24: Sentinel-2 RGB (left) and majority polygon (right) of Highland mine. Numbers from 1-2 indicate roads. [1] points to a road that is covered by the majority polygon, whereas [2] indicates a road that has not been covered by the majority polygon; contains modified Copernicus Sentinel data (2018).

5.2.2 Area calculation

After computing class statistics for the majority polygons, the entire amount of pixels within the majority polygons was derived. This amount of pixels was further multiplied by the pixel size in order to obtain area values of the majority polygons. Area values of the class statistics represent the entire area of the majority polygons. Figure 5-25 (left) and Table 5-3 clearly show that Grasberg mine is the smallest mine covering an area of 17.34 km^2, followed by Hamersley mine with 37.67 km^2 and Mariana mine with a spatial extent of 56.4 km^2. Highland mine is the largest mine with 82.27 km^2. Figure 5-25 (right) shows further the percentage of mine relative to the entire study site, according to crowdsourcing. Grasberg mine and Highland mine appear to cover larger parts of the study site than it is the case for Hamersley mine and Mariana mine.

Table 5-3: Area values for all majority polygons.

	Grasberg mine	**Hamersley mine**	**Highland mine**	**Mariana mine**
	MAJ	**MAJ**	**MAJ**	**MAJ**
Area of mine [km^2]	17.34	37.67	82.27	56.42
Area of mine relative to the entire study site [%]	11.45	9.17	12.75	7.56

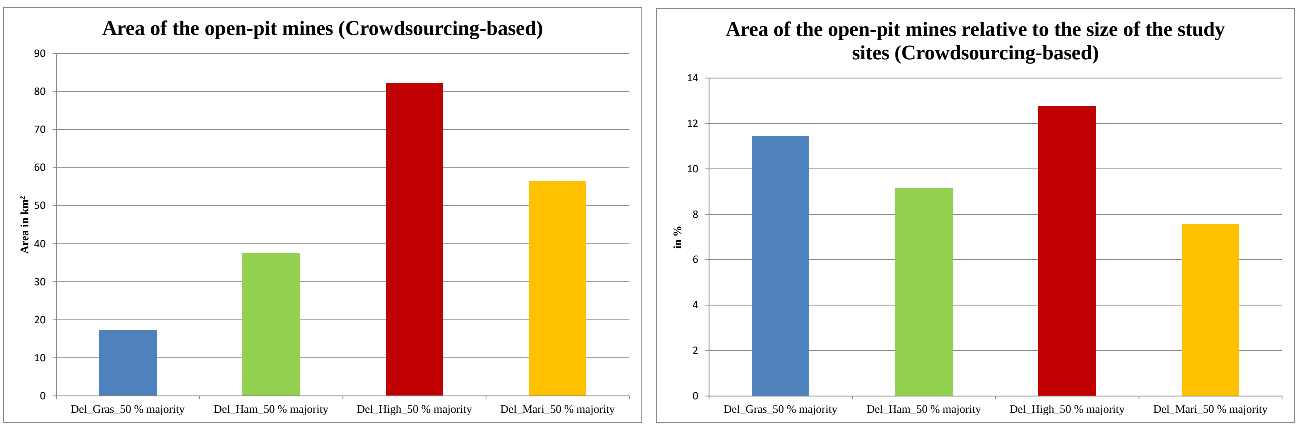

Figure 5-25: Area calculation of all majority polygon (left) and area value of each mine relative to the entire study site (right). Concerning the column labelling, the word delineation is abbreviated to Del, the following letters indicate the study site and 50 % majority refers to the majority polygon.

5.2.3 Accuracy assessment

Overall accuracy was computed when comparing the majority polygon of each study site with the reference dataset within a confusion matrix. For all majority polygons an overall accuracy of ≥ 92.17 % has been achieved, as shown in Figure 5-26. The majority polygon of Grasberg mine has the highest overall accuracy with 97.29 % (Table 5-4). Lowest overall accuracy was achieved for Highland mine with 92.17 %.

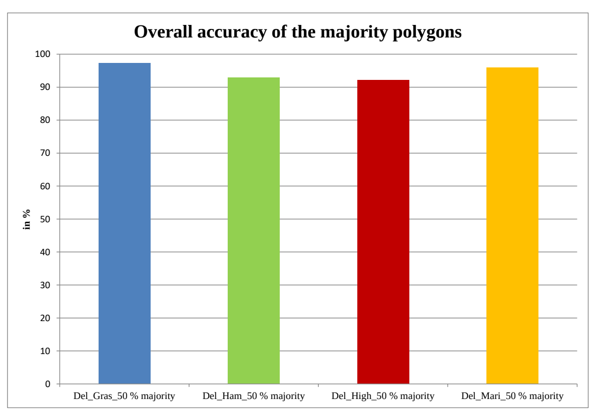

Figure 5-26: Overall accuracy for all majority polygons of each study site. Concerning the column labelling, the word delineation is abbreviated to Del, the following letters indicate the study site and 50 % majority refers to the majority polygon.

Similar to high overall accuracy, high Kappa coefficient values of ≥ 0.83 for all majority polygons indicate observed high agreement between the reference dataset and the majority polygons. Kappa coefficient values range from 0.83 for the majority polygon of Mariana mine up to 0.91 for Grasberg mine's majority polygon, which means that again Grasberg mine achieved highest accuracy values.

As for the different classifications, producer's and user's accuracy was calculated. All majority polygons have a producer's accuracy ≥ 74.56 %, which means that ≥ 74.56 % of the mine within the reference dataset is covered by the majority polygons (Figure 5-27, left). As for the previous accuracy metrics, the majority polygon of Grasberg mine achieved the highest producer's accuracy with 86.73 %, whereas Mariana mine had the lowest producer's accuracy with 74.56 % (Table 5-4).

Regarding reliability of the majority polygons, a user's accuracy ≥ 98.89 % was achieved for all majority polygons as shown in Figure 5-27 (right). Grasberg mine's majority polygon has the highest user's accuracy with 100 %, confirming that a user can be sure that the entire area being covered by the majority polygon represents mine in reality. Slightly lower values were obtained for the other study sites, with Hamersley mine having the lowest user's accuracy of 98.89 %.

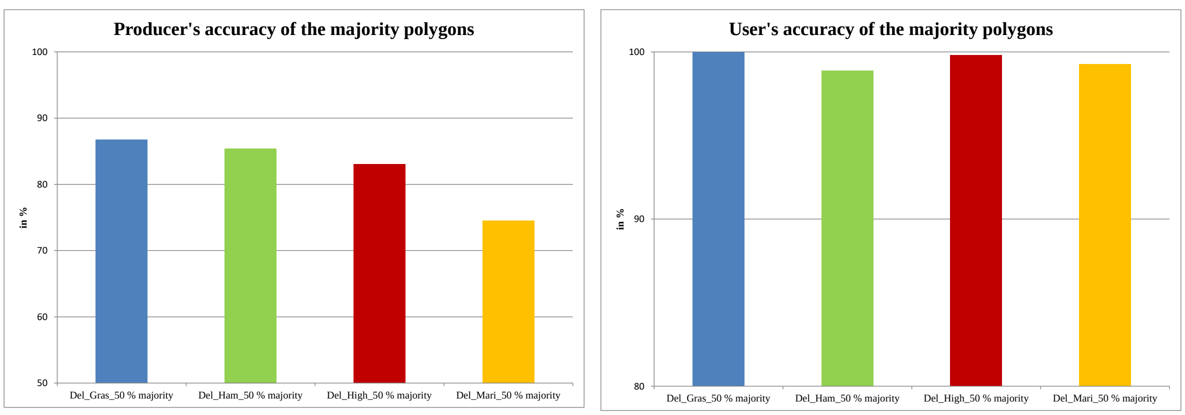

Figure 5-27: Producer's (left) and user's (right) accuracy for all majority polygons. Concerning the column labelling, the word delineation is abbreviated to Del, the following letters indicate the study site and 50 % majority refers to the majority polygon.

The omission error, representing false negatives, is ≤ 25.44 % (Figure 5-28, left) for all majority polygons. This type 1 error indicates that less than 25.44 % of the area being not covered by the majority polygon belongs to the majority polygon. Omission error values range from 13.27 % for Grasberg mine up to 25.44 % for Mariana mine, presented in Table 5-4.

False positives range from 0.00 % for Grasberg mine up to 1.11 % for Hamersley mine's majority polygon. The commission error is thus ≤ 1.11 % for all study sites indicating that ≤ 1.11 % of the majority polygon should not have been included into the majority polygon Figure 5-28 (right).

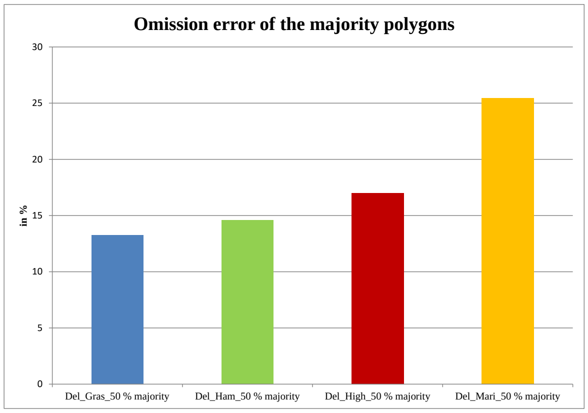

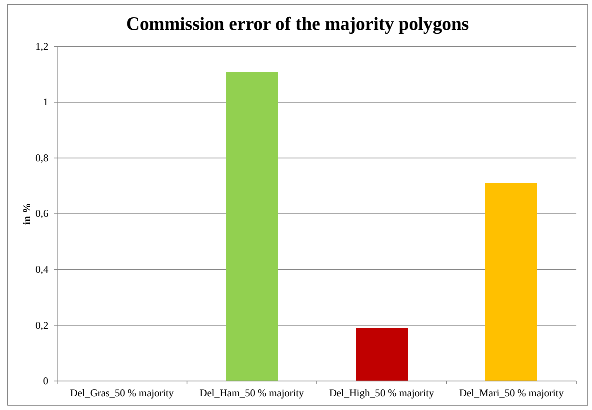

Figure 5-28: False negatives (left) and false positives (right) for all majority polygons. Concerning the column labelling, the word delineation is abbreviated to Del, the following letters indicate the study site and 50 % majority refers to the majority polygon.

Given the fact that for the confusion matrix only two classes were available, namely the majority polygon itself and the surroundings, no further investigations could be carried out in order to get information about the type and percentage of land use and land cover not being included into the majority polygon. The same applies for the commission error. Due to its binary character, no further analysis of the land use and land cover type and the percentage that was falsely included into the majority polygon, could have been deduced.

With respect to true positives that means correctly classified pixels, the pixel amount varies from 1954 pixels for the majority polygon of Grasberg mine to up to 8975 pixels for Highland mine, according to the study site. When comparing the amount of true positives to the amount of all pixels of the majority polygon, differences in pixel amount vary from 0 to 54 pixels (Table 5-4). That means for Hamersley mine, there is a difference of 54 pixels between the amounts of correctly included and all included pixels of the majority polygon. Regarding Grasberg mine, all pixels belonging to the majority polygon within the extent of the reference dataset represent true positives at the same time (Figure 5-29).

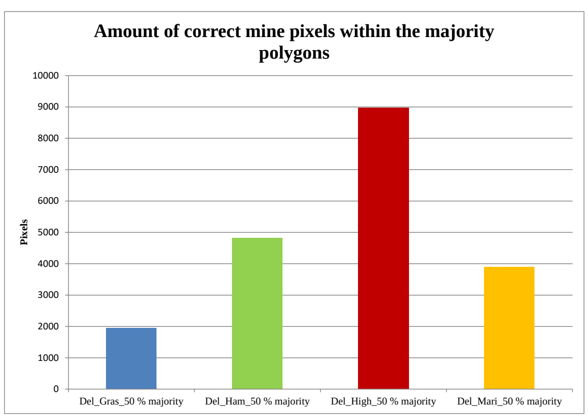

Figure 5-29: True positives of all classifications. Concerning the column labelling, the word delineation is abbreviated to Del, the following letters indicate the study site and 50 % majority refers to the majority polygon.

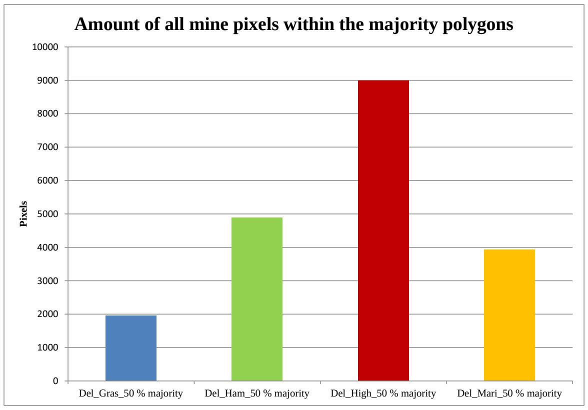

Figure 5-30: All classified mine pixels covering the reference dataset. Concerning the column labelling, the word delineation is abbreviated to Del, the following letters indicate the study site and 50 % majority refers to the majority polygon.

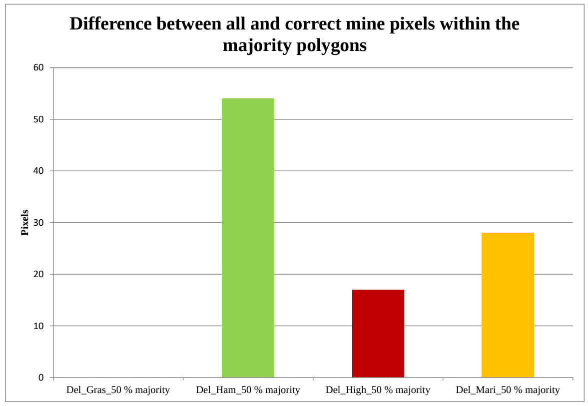

Figure 5-31: Difference between all classified and true positives. Concerning the column labelling, the word delineation is abbreviated to Del, the following letters indicate the study site and 50 % majority refers to the majority polygon.

Table 5-4: Overview of all accuracy metrics for the majority polygons (MAJ) derived within the confusion matrix.

	Grasberg mine	**Hamersley mine**	**Highland mine**	**Mariana mine**
	MAJ	**MAJ**	**MAJ**	**MAJ**
Overall accuracy [%]	97.29	92.84	92.17	95.88
Kappa Coefficient	0.91	0.85	0.84	0.83
Producer’s accuracy [%]	86.73	85.4	83.01	74.56
User’s accuracy [%]	100	98.89	99.81	99.29
Omission Error [%]	13.27	14.60	16.99	25.44
Commission Error [%]	0	1.11	0.19	0.71
True positives [pixels]	1954	4830	8975	3899
Totals [pixels]	1954	4884	8992	3927
Difference between totals and true positives	0	54	17	28

5.3 Comparison between classifications and crowdsourcing

5.3.1 Comparison by visual interpretation

Classifications and majority polygons were first compared visually. This means, all three classifications for each mine were compared to the corresponding majority polygon by overlaying these two layers. Figure 5-32 shows that when overlaying the index-based classification of Grasberg mine with the corresponding majority polygon, classification and majority polygon overlap only partly. Number 2, indicates grey colored pixels that represent areas that have been covered by the index-based classification and the majority polygon, demonstrating that this area was assigned to the mine class by both methods. Number 1 on the contrary, points out areas that were only covered by the index-based classification, whereas number 3 indicates pixels only being considered mine by the majority polygon. As a first visual impression, it was observed that regarding these two methods, the majority polygon represents a homogeneous polygon (number 3), whereas the index-based classification is composed of several polygons, sometimes distributed all over the AOI, as number 1 indicates. The area covered by both methods (number 2) contains almost the entire index-based classification but not the entire majority polygon. Thus, the majority polygon constitutes a larger polygon than the index-based classification.

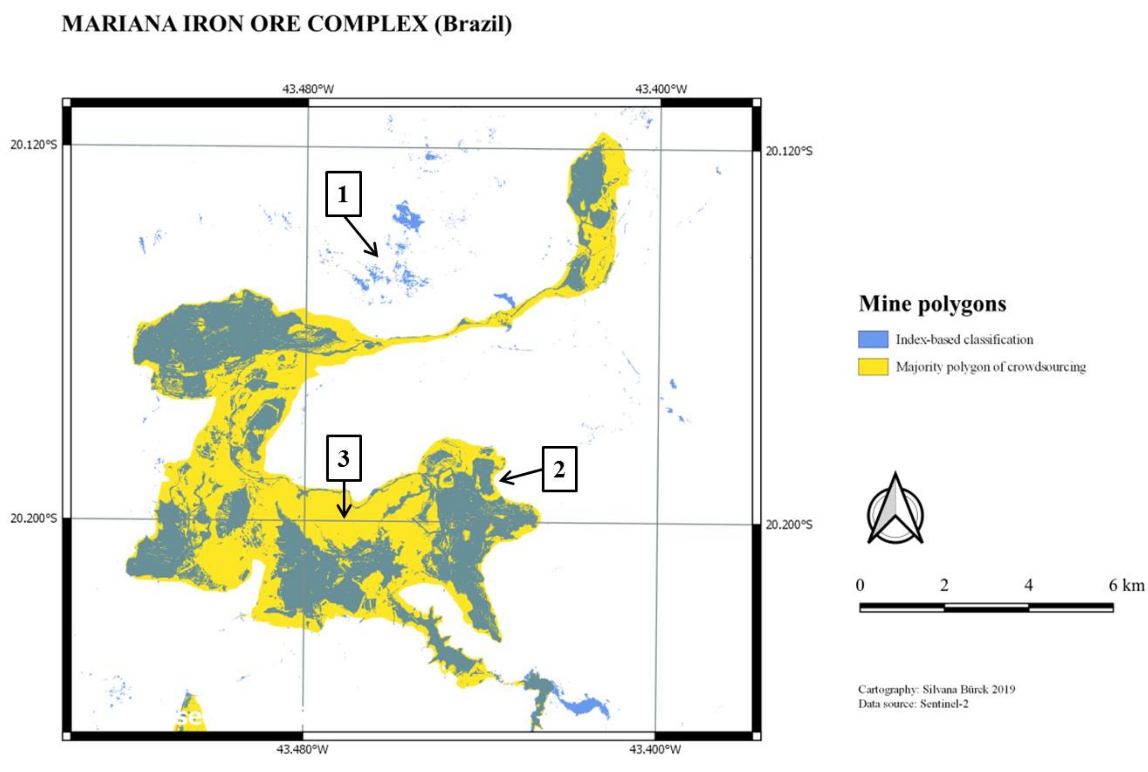

Figure 5-32: Overlay of index-based classification upon the majority polygon for the study site Mariana mine. Numbers exemplify areas covered only by the classification [1], by the majority polygon [3] or by both methods [2]; contains modified Copernicus Sentinel data (2018).

When comparing the pixel-based classification to the majority polygon, similar observations were made, presented in Figure 5-33. Contrary to the majority polygon that is considered to be homogeneous, the pixel-based classification does not represent a uniform shape and is composed of several small polygons spread all over the AOI. As for the index-based classification, this salt & pepper effect is visible in number 1 and is more dominant within the pixel-based classification than in the index-based classification. The area covered by both methods, similarly indicated by number 2, is slightly larger than for the comparison between the index-based classification and the majority polygon, whereby the pixel-based classification is almost entirely embedded within the majority polygon.

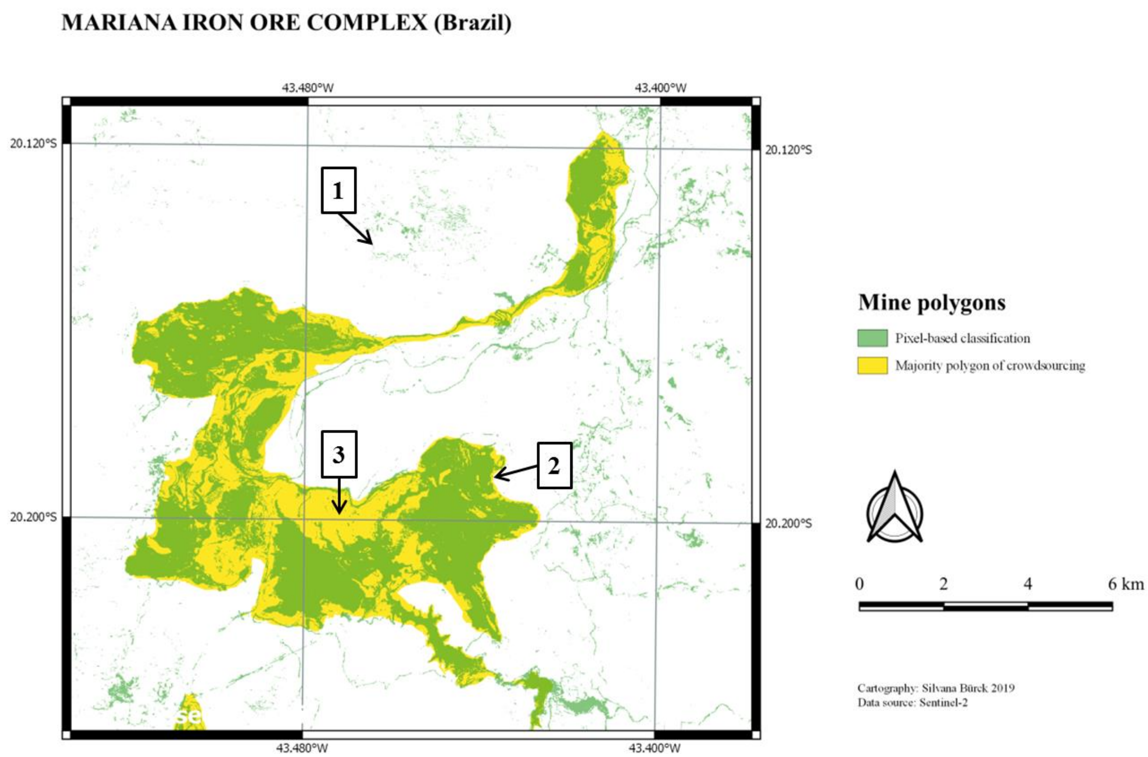

Figure 5-33: Overlay of pixel-based classification upon the majority polygon for the study site Mariana mine. Numbers exemplify areas covered only by the classification [1], by the majority polygon [3] or by both methods [2]; contains modified Copernicus Sentinel data (2018) and modified Aster GDEM v2 (2011).

Regarding the comparison between the object-based classification and the majority polygon, the largest spatial overlap between the two layers compared to the previous comparison was detected as indicated by number 2 within Figure 5-34. As for the other classifications, the object-based classification is composed of several polygons, but they are larger in extent than in the other classifications. Especially in the eastern part of Figure 5-34, the object-based classification is more dominant, indicated by an accumulation of large polygons. These characteristics of each comparison were observed for all four study sites.

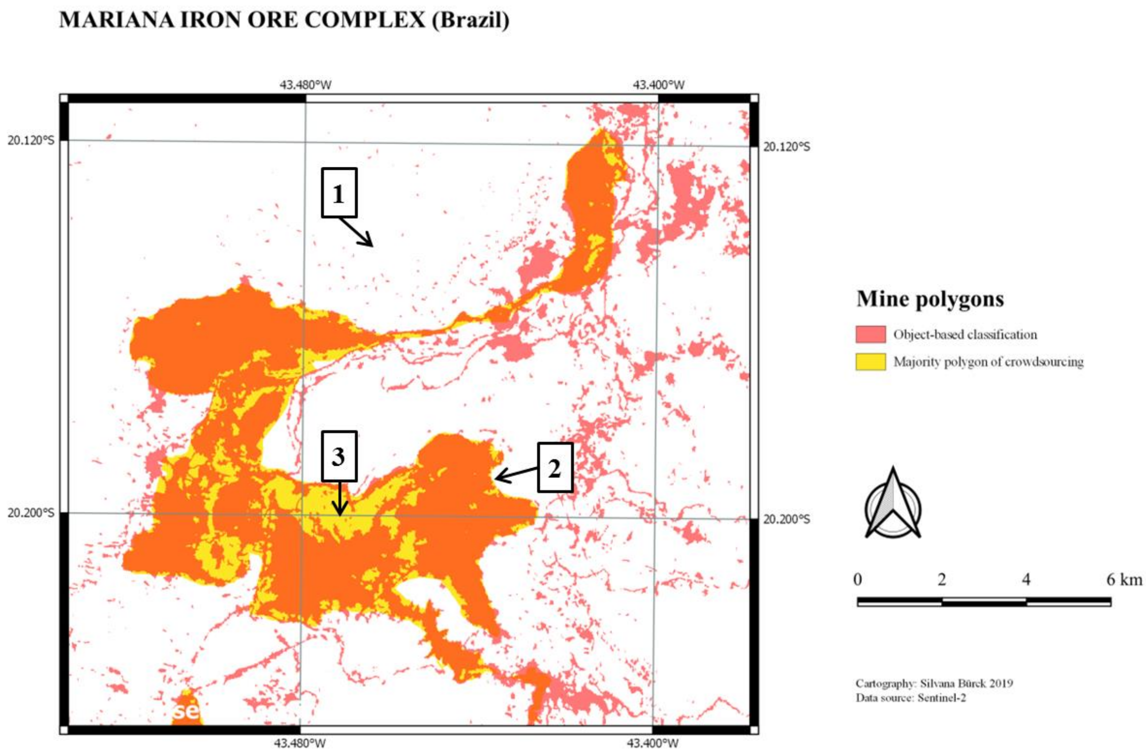

Figure 5-34: Overlay of object-based classification upon the majority polygon for the study site Mariana mine. Numbers exemplify areas covered only by the classification [1], by the majority polygon [3] or by both methods [2] contains modified Copernicus Sentinel data (2018).

5.3.2 Comparison by Intersection over Union

As an overview, IoU values for all comparisons are shown in Figure 5-35 and Table 5-5. On an intra-mine level, lowest IoU values were mostly achieved for the comparison of majority polygons & index-based classifications, higher agreement for the comparisons of majority polygons & pixel-based and object-based classifications. As an example, lowest IoU of 0.35 was achieved by comparing index-based classification & majority polygon of Grasberg mine, whereas the highest IoU of 0.60 was achieved for the comparisons pixel-based classification & majority polygon and object-based classification & majority polygon of Highland mine. Considering IoU on an inter-mine level, for Highland valley mine, mean IoU

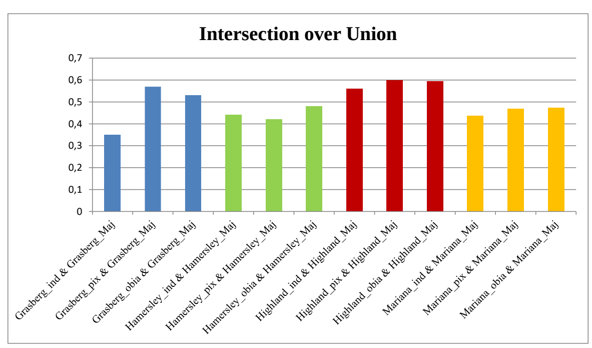

Figure 5-35: IoU values for all 12 comparisons.

value is highest (0.58), indicating that the majority polygon and the classifications are more similar than it is the case for the other study sites. Lower agreement among classifications and majority polygon was obtained for Hamersley mine, where all IoU values are ≤ 0.48. The mean IoU for all comparisons of Hamersley mine is 0.49. For all conducted comparisons the mean IoU is 0.49, indicating that classifications and crowdsourcing are different from each other.

Regarding the IoU of Grasberg mine, almost similar IoU values of 0.57 and 0.53 were obtained for the comparison of the pixel-based classification & majority polygon and for the object-based classification & majority polygon, respectively. Given the fact that according to Everingham et al. (2010), the IoU > 0.5 represents similarity, the pixel-based and object-based classifications are considered to be similar to the majority polygon. When comparing the index-based classification & majority polygon, an IoU of 0.35 indicates that the index-based classification and the majority polygon are less similar. The mean IoU of all comparisons regarding Grasberg mine is 0.48, representing low agreement between classifications and crowdsourcing.

For Hamersley mine, the IoU varies between 0.42 for the comparison of majority polygon & pixel-based classification, 0.48 for the comparison with the object-based classification and 0.44 for the comparison with the index-based classification, respectively. The mean IoU value of 0.44 for this study site indicates that classifications and majority polygon are significantly different from each other.

Concerning Highland mine, the mean IoU value is 0.58, indicating higher agreement between the classifications and the majority polygon for this study site. Lowest IoU values were obtained when comparing the majority polygon & index-based classification, highest IoU values when comparing to the pixel-based classification (0.6). The comparison of the object-based classification & majority polygon resulted in an IoU of 0.59.

The mean IoU value for Mariana mine is 0.46, thereby 0.44 for the comparison index-based classification & majority polygon and 0.47 for the comparisons of the majority polygon to the pixel-based and object-based classifications. Table 5-5 summarizes the comparative results presented.

Table 5-5: Overview of the area of spatial intersection, area of spatial union and intersection over union for all conducted comparisons.

	Conducted Comparisons	Area of spatial intersection [km^2]	Area of spatial union [km^2]	Intersection over Union
Grasberg mine	Index-based classification & majority polygon	67.09	192.234	0.35
	Pixel-based classification & majority polygon	121.22	212.806	0.57
	Object-based classification & majority polygon	139.087	262.096	0.53
Hamersley mine	Index-based classification & majority polygon	174.751	395.987	0.44
	Pixel-based classification & majority polygon	273.908	650.622	0.42
	Object-based classification & majority polygon	301.741	627.505	0.48
Highland mine	Index-based classification & majority polygon	479.332	855.094	0.56
	Pixel-based classification & majority polygon	603.109	1005.325	0.6
	Object-based classification & majority polygon	561.593	942.894	0.6
Mariana mine	Index-based classification & majority polygon	260.494	597.067	0.44
	Pixel-based classification & majority polygon	342.882	730.175	0.47
	Object-based classification & majority polygon	445.484	938.884	0.47

5.3.3 Comparison by area values

Regarding the spatial area of mines derived by index-based, pixel-based, object-based classifications and the crowdsourcing-based majority polygons, the area of the majority polygon is for most comparisons in between the smallest and the largest area (Table 5-6). Index-based classification represents always the smallest polygon, contrary to the object-based classification. The area of the majority polygon is thus either in between the area of the index-based classification and the pixel-based classification or in between the area of the pixel-based and object-based classification. For Grasberg mine, the area of the majority polygon with 17.34 km^2 is in between the area of the pixel-based classification (13.39 km^2) and the object-based classifications (22.78 km^2). For Hamersley mine, the majority polygon (37.67 km^2) is in between the index-based classification (19.4 km^2) and pixel-based classification (54.78 km^2). Only for Highland mine, the area of the majority polygon is largest with 82.27 km^2, contrary to the classifications that cover an area of $\leq$ 78.57 km^2. For Mariana mine, the area of the majority polygon (56.42 km^2) is close to the area of the pixel-based classification (50.88 km^2), whereas the index-based classification represents the smallest area with 29.33 km^2 and the object-based classification thus the largest area (82.01 km^2).

5.3.4 Comparison by accuracy values

For most accuracy metrics, crowdsourcing results achieve either accuracy values in between the classifications or slightly higher accuracy values (Table 5-6). Regarding the overall accuracy, the majority polygon has the highest accuracy values for Grasberg mine (97.29 %) and Hamersley mine (92.84 %). Overall accuracy of the majority polygon of Highland (92.17 %) and Mariana mine (95.88 %) is still in between the minimum (88.37 % for Highland mine; 92.17 % for Mariana mine) and maximum (97.41 % for Highland mine; 97.73 % for Mariana mine) of the classifications. The same is true for the Kappa coefficient, where the coefficient values of the majority polygons are either in between the classification or highest. Only for Mariana mine, the Kappa coefficient value is slightly lower for the majority polygon (0.83) compared to the other classifications that have a Kappa coefficient value ≥ 0.84. For producer's accuracy, the majority polygon has either highest accuracy values as it is the case for Hamersley mine (85.40 %), is in between the accuracy values of the three classifications, in the case for Grasberg mine (86.73 %) or producer's accuracy is lowest, as it is the case for Highland and Mariana mine. User's accuracy values of the majority polygon are always in between the classifications (Hamersley mine, Mariana mine) or higher (Grasberg mine, Highland mine). Regarding the omission error, the majority polygon has highest values for Highland and Mariana mine, in contrast to Grasberg mine, where the omission error of the majority polygon is in between the classifications and Hamersley mine, where the omission error is lowest. On the contrary, the commission error of the majority polygon is lowest (Grasberg mine, Highland mine) or in between the classifications for all study sites (Hamersley mine, Mariana mine). On an intra-mine level, for Grasberg and Hamersley mine, most accuracy values of the majority polygon are either highest or in between the classifications. For the Highland mine the position of accuracy values of the majority polygon range from lowest accuracy values, medium up to highest accuracy values compared to the classifications. Especially for Mariana mine, accuracy values are either in between the classifications or lowest. Table 5-6 gives an overview of all area and accuracy values.

.

Table 5-6: Overview of area and accuracy values for index-based (IND), pixel-based (PIX) and object-based (OBIA) classifications and majority polygons (MAJ). Grey shaded columns refer to crowdsourcing results derived from the majority polygon.

	Grasberg mine				**Hamersley mine**				**Highland mine**				**Mariana mine**			
	IND	**PIX**	**OBIA**	**MAJ**	**IND**	**PIX**	**OBIA**	**MAJ**	**IND**	**PIX**	**OBIA**	**MAJ**	**IND**	**PIX**	**OBIA**	**MAJ**
Overall accuracy [%]	94.18	93.80	90.31	97.29	85.95	77.41	85.05	92.84	97.41	92.80	88.37	92.17	92.17	97.73	97.01	95.88
Kappa Coefficient	0.56	0.92	0.88	0.91	0.54	0.68	0.80	0.85	0.92	0.90	0.83	0.84	0.84	0.88	0.96	0.83
Producer accuracy [%]	47.89	84.51	90.29	86.73	44.12	71.53	74.40	85.4	98.52	99.03	97.22	83.01	83.01	80.89	91.22	74.56
User Accuracy [%]	77.47	92.07	81.21	100	99.63	90.94	98.28	98.89	97.41	92.80	88.37	99.81	99.81	97.73	97.01	99.29
Omission Error [%]	52.11	15.49	9.71	13.27	55.88	28.47	25.60	14.60	1.48	0.97	2.78	16.99	19.11	8.78	4.07	25.44
Commission Error [%]	22.53	7.93	18.79	0	0.37	9.06	1.72	1.11	11.04	1.13	0.41	0.19	0.11	1.30	2.13	0.71
True positives [pixels]	636	1904	2139	1954	1881	4046	4562	4830	4457	10707	11700	8975	1875	4770	6532	3899
Totals [pixels]	821	2068	2634	1954	1888	4449	4642	4884	5010	10829	11748	8992	1877	4833	6674	3927
Difference between totals and true positives	185	164	495	0	7	403	80	54	553	122	48	17	2	63	142	28
Area of mine [km^2]	8.59	13.39	22.78	17.34	19.4	54.78	55.25	37.67	51.17	78.57	68.17	82.27	29.33	50.88	82.01	56.42
Area of mine relative to the entire study site [%]	5.67	8.84	15.04	11.45	4.72	13.34	13.47	9.17	7.93	12.18	10.58	12.75	3.93	6.82	11.00	7.56
Mean area of mine of each study site [km^2]		14.92				43.15				65.97				54.08		

6 Discussion

This section is dedicated to discuss results of the application of each method, the methodology of this study and to determine related strengths and weaknesses. In the first part, main findings regarding the previously presented results as well as their relation to current studies will be discussed. Secondly, main findings regarding the methodology of this study will be outlined. Upon the base of these new findings, strengths and weaknesses of classifications and crowdsourcing will be derived and described in detail in order to give an answer upon the initial research question.

6.1 Main findings regarding the results of classifications, crowdsourcing and the comparison

The following section will aggregate previously presented results in order to derive main findings, discuss them and relate them to current research.

6.1.1 Classifications

Regarding classifications, the presented results have shown that the classification of mines is not strongly dependent on the classification method and on the amount of datasets integrated into the classification process. Evidence therefore has been given by visually interpreting that with all classification methods the mines have been detected and that the class mine occurs almost similar in extent among classifications, regardless of the amount of datasets included. Overall accuracy ≥ 77.41 % for all classifications and Kappa coefficient values ≥ 0.8 for all classifications, except of Grasberg_ind, Hamersley_ind and Hamersley_pix, show that regarding visual interpretation, overall accuracy and Kappa coefficient values, the classification result is not dependent on the classification method and the amount of datasets included, respectively. This main finding cannot be confirmed or denied by current literature, as no such comparative study in the domain of mining has been conducted yet. Concerning comparisons of pixel-based and object-based classifications within other domains, Prudente et al. (2017) achieved almost similar results for pixel-based and object-based classifications as well, thereby confirming classification method independency. Most current studies dedicated to pixel-based and object-based comparison (Belgiu and Csillik 2018; Keyport et al. 2018; Roy et al. 2018; Wang et al. 2018a) found that object-based classification performs slightly better than pixel-based classification regarding accuracy, something that could not be confirmed within this study. Nevertheless, all studies did not integrate index-based classifications either. The current study thus extents the state of the art in this context by comparing three classification methods. Instead of focusing on the comparison of classification methods, some current studies investigated the combination of pixel-based and object-based classifications (Chen et al. 2018d; Xiong et al. 2017). This has not been the scope of this study, but might be of interest for future considerations.

Nevertheless, when taking omission and commission error into account, it has been found that index-based classification is considered to be the classification method performing slightly weaker than pixel-based and object-based classification. For omission and commission error, index-based classifications achieve frequently higher error values, indicating thereby that for this type of classifications a large amount of pixels had been falsely assigned to the classes by excluding or including pixels. Pericak et al. (2018) did not compare index-based classifications to other classification methods, but within their study, they found that an NDVI-based classification for mine area computation achieves high accuracy values, thereby demonstrating high performance of index-based classifications. Their index-based classification differed slightly in their methodology to the index-based classification of this study that was based on NDVI as well. It remains thus to be tested if – when adopting Pericak's methodology for the investigation of Grasberg, Hamersley, Highland and Mariana mine – higher accuracy will be achieved. Similar to this study, Pericak et al. (2018) focused on the implementation of NDVI only. But the observation that other spectral indices such as FMI and CMI have been considered to be not informative enough for an index-based classification, as demonstrated in chapter 4, has been confirmed by Castellanos-Quiroz et al. (2017).

The fact that mines in four different geographic regions could be classified and even achieved high accuracy results, demonstrates possible transferability. Charou et al. 2010 classified different mines as well, thereby further confirming transferability of mine classification. But Charou et al. 2010 included study sites within one country, thereby not demonstrating transferability to different geographic regions, as it has been proven within this study. Regarding their methodology, classification variety has been limited to pixel-based classification. This present study thus extents the investigations of Charou et al. 2010, as a methodological comparison has been conducted and as study sites in different geographic regions have been investigated.

In addition to these findings, visual interpretation has shown that all features indicating a potential mine from LaJeunesse Connette et al. (2016) have been comprised into the class mine. This has been proven by all classifications, which means that all classifications are considered to be able to detect mine features. High user's accuracy $\geq$ 77.47 % confirmed that classifications containing the mine features from LaJeunesse Connette et al. (2016) are close to reality. Hence, this finding supports the study of LaJeunesse Connette et al. (2016) with respect to their proposed mine features. Nevertheless some features, such as water bodies, have been wrongly categorized to the class mine even though they do not belong to the class mine. The classification algorithms of this study do not have contextual and local knowledge, whereby neighborhood relations are not considered.

In order to deal with class belonging, a progressive approach has been chosen for this study as the class mine comprises all features indicating a potential mine from LaJeunesse Connette et al. (2016). As these mine features include even buildings, all buildings within the study site have been classified as mine. Subsequently, the classification result represents an overestimation due to the fact that sometimes buildings, roads or water bodies are not likely to belong to the mine. However, this progressive approach is supported by the assumption that the mines of the four study sites are located in remote areas and thus artificial features such as buildings or roads are primary dedicated to mining activity. As soon as the area of interest is larger, this argument becomes invalid. Regarding the class water, this progressive approach remains challenging, because not all water bodies found within the AOI are of artificial origin. Therefore, I propose that for future work, shape and color of water bodies need to be further investigated as additional indicators. Furthermore, the motivation of the study needs to be taken into account when discussing class belonging. For the motivation of this study − which is the EHP analysis −, a progressive approach is preferred to a conservative, given the fact that environmental consequences are expected to be larger in extent. For a precise assignment of all features, contextual and local knowledge would be required. In this context I propose a rule-based object oriented classification or conditional random field, as these methods can include the factor spatial proximity. Current studies that are related to rule-based classifications or spatial proximity, such as the study from Chen et al. (2018d) and Ma et al. (2017a) might constitute a suitable support regarding this issue. Alam et al. (2019) addressed this challenge by developing a combined methodology of convolutional neural networks and conditional random fields, whereby the latter is expected to provide contextual information. With less effort, but more subjectiveness, reclassification can also be performed in order to add or remove features from the mine, which have not been added or removed by the algorithm itself. Classification of mines is thus dependent on the post-processing. This finding has been further supported by Roy et al. (2018), who achieved higher accuracy values after post-processing.

Furthermore, I found out that the classification of mines depends on the study site. Mines embedded within homogeneous surroundings, such as rocky or sandy, perform generally weaker in accuracy assessment. Regarding overall accuracy, Kappa coefficient values, producer's and user's accuracy as well as omission and commission error, Hamersley mine and partially Grasberg mine achieved lower accuracy. Even visual interpretation has revealed that when focusing on all land use and land cover classes, most differences among classifications occur within Hamersley mine, the mine which is located in the desert. Results have demonstrated that regarding omission and commission error, miss-classifications occurred mostly between the class bare area and mine. Inspections of the spectral signal of these two classes reveal that the spectral signal of bare area and mine is very similar (Figure 6-1). Even though the spectral range of mine is wider than the one of bare area, the spectral signal of bare area is almost entirely covered by the spectral signal of the mine. Both land use and land cover classes have a reflectance peak in band 8 with 0.17 and 0.15 for bare area and mine, respectively. Within the other bands, reflectance values of both classes are moderate. Spectral similarities between classes are thus accompanied by a weaker performance regarding accuracy metrics. Consequently, the classification of homogeneous study sites is considered to be more difficult. This has been confirmed by Lobo et al. (2018), who – on the contrary –, classified a total of 13 mining sites in the Brazilian Amazon and achieved satisfactory accuracy values thereby. Their study sites are considered to represent heterogeneous study sites, given the fact that these study sites are composed of dense forest on the one hand and mining sites on the other hand. Lobo et al. (2018) confirm indirectly that the classification of mines in homogeneous study sites is considered to be more difficult. Even though Charou et al. (2010) investigated mines in different geographic locations within Greece, no correlation between classification results and study site types has been mentioned.

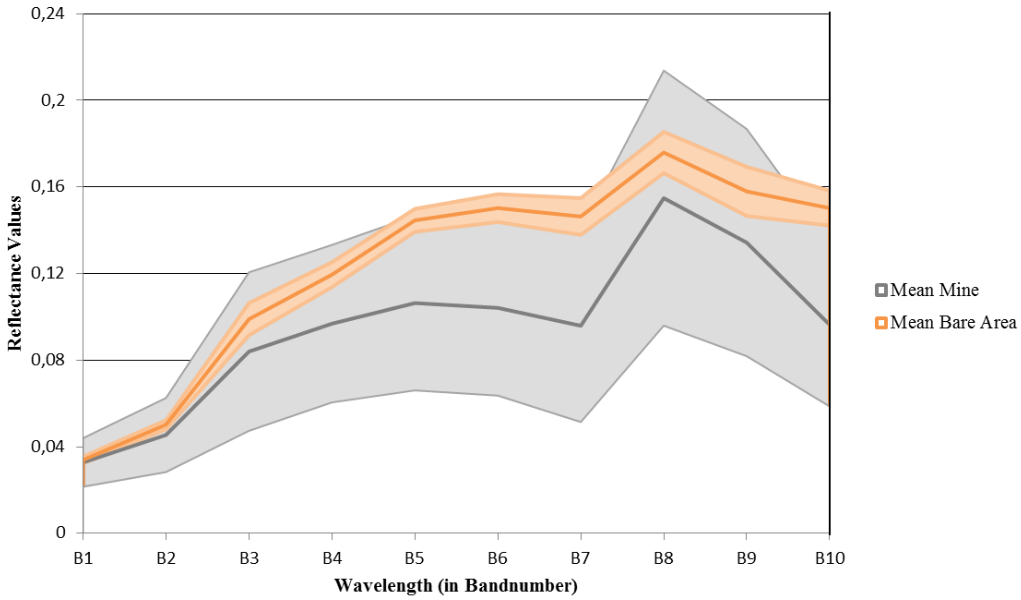

Figure 6-1: Spectral signatures of bare area and mine of Hamersley mine. The spectral signature of bare area is almost entirely embedded into the spectral signature of the mine.

Contrary to visual interpretation, when considering the entire area of the class mine, differences in area among classifications occur. Index-based classifications always represents the smallest mine, whereas object-based classifications represent the largest mine. The reason for this difference between qualitative and quantitative results is that especially for index-based and pixel-based classification the salt & pepper effect is present, thus resulting in a large amount of isolated pixels which have been classified as mine. Wang et al. (2018a) faced the same issue regarding salt & pepper effect for pixel-based classification (Wang et al. 2018a). Visually this can only be recognized when zooming into the classifications, as shown within the results (Figure 5-7). Quantitative area results thus constitute reliable results, as they include isolated pixels in their area value. This means that when considering the mine area, differences among classifications occur. Nevertheless, previously it has been mentioned that high overall accuracy, Kappa coefficient values, producer's and user's accuracy for all classifications demonstrated that the classification of mines is not dependent on the classification method. This contradiction can be explained by having a closer look upon the reference dataset, which is compared with the classifications for obtaining accuracy metrics such as overall accuracy, Kappa coefficient values, producer's and user's accuracy. The reference dataset for each study site has been created by expert knowledge. Thereby, a certain amount of training polygons, which are distributed all over the AOI have been classified by an expert. The total amount of pixels that are covered by the reference dataset for the index-based classification of Grasberg mine is 15084, the total amount of pixels of the entire classification is 1515110. Hence, the reference dataset represents only 0.99 % of the entire study site. Subsequently, when interpreting accuracy results, it needs to be taken into account that all accuracy statements about the classifications account only for the area that has been covered by the reference dataset. Nevertheless, the criteria of Lillesand et al. (2008), who propose a total of 50 training samples for each class for accuracy assessment, has been met. In addition, no further reference dataset or in-situ measurements were available. To sum up, differences among classifications are less visible within the qualitative results, which can be explained by salt & pepper effect, which is not recognizable at first view. The fact that accuracy metrics reveal similarity among classifications represents a tendency, given the fact that reference data does not portray the entire study site. Area computation only reveals differences among classifications.

6.1.2 Crowdsourcing

For crowdsourcing, a main finding derived from the presented results is that a heterogeneous group can recognize open-pit mines in satellite imagery, digitize the delineation of the mine and achieve thereby high accuracy values ≥ 92.17 %. This fact that digitization constitutes a potential method in order to generate geographic information by the crowd, has been further explained by Albuquerque et al. (2016), who define different tasks of crowdsourcing-based geospatial information generation. This main finding is supported by qualitative visual interpretation, where it has been recognized that all volunteers did solely focus on the mine and did not digitize any other part within the satellite imagery, which does not belong to the mine. In addition, all features indicating a potential mine from LaJeunesse Connette et al. (2016) are comprised within the majority polygon, demonstrating that volunteers are able to detect mine features and digitize them. Further evidence is given by high Kappa coefficient values ≥ 0.8, high producer’s and user’s accuracy, low commission error and minor differences between totals and true positives for all majority polygons.

Taking into consideration that mines in different geographic regions have been digitized and thus high accuracy values have been obtained, transferability has been demonstrated. I assume that transferability to other geographic regions will be given as well, as the four study sites already differ strongly among each other because of their location within different ecozones. Transferability of crowdsourcing tasks has been confirmed by Lesiv et al. (2019) who launched a crowdsourcing campaign for the establishment of a global crop field estimation.

Nevertheless, digitization is a subjective process, in which no entire agreement among volunteers exists. Differences in digitizations, as recognized by visual interpretation of all digitizations and the existence of differences in spatial extent between Min and Max polygons, show that volunteers do not digitize in the same way. This is further supported by the frequency distribution figures, which demonstrate, that for all study sites the amount of how often a pixel has been considered to represent mine varies. Within this context, further observations regarding quality issues related to crowdsourcing, such as credibility, can be found in Heipke (2010) and Fritz et al. (2012).

Another main finding is that the majority polygon is a good approximation to reality. Evidence therefore has been given by very high accuracy metrics such as overall accuracy, Kappa coefficient values, producer’s and user’s accuracy and very low commission errors for all four majority polygons. The application of the majority for detailed analysis has been found in current studies (Herfort et al. 2018) as well.

Furthermore, it has been found that additional information about features indicating potential mines and the digitization procedure are required. This further finding is confirmed by the fact that even if all features indicating a potential mine from LaJeunesse Connette et al. (2016) are included within the majority polygon, not all such features within the entire satellite imagery were recognized. Regarding the Min and Max polygon, it has been observed that the Min polygon represents always the pit itself, whereas the Max polygon includes several additional mine features. The lack of information about features indicating potential mines and the digitization task explains why some volunteers accounted only the pit itself as the mine, whereas some other volunteers included further features. Lesiv et al. (2019) prevented this information lack by making volunteers familiar with the topic and the digitization in a workshop. However, in this study visual interpretation of the frequency distribution reveals that only a small amount of volunteers (< 4) digitized in this progressive way, whereas the majority (≥ 9) agreed on the digitization of the mine.

Besides, it has been shown that digitization of open-pit mines within homogeneous study sites is more difficult than within heterogeneous study sites. This finding has been supported by visual interpretation of the difference between Min and Max polygons among all study sites. For Grasberg mine and Hamersley mine, the spatial difference between the Min and Max polygon was largest, indicating difficulties in digitizing these mines. Furthermore, when comparing the frequency distribution figures of all study sites, a higher level of agreement for Highland mine and Mariana mine, demonstrates that the digitization of these two mines has been easier than for Grasberg mine and Hamersley mine. The fact that the majority polygon of Hamersley mine has lowest user's accuracy values, highest commission error values and highest difference between true positives and totals, provides further evidence of difficulties in digitizing mines within homogeneous surroundings. To face this difficulty regarding homogeneous study sites, an initial training workshop of the volunteers, such as proposed by Lesiv et al. (2019), could be implemented. Additionally, one could make use of the strength of crowdsourcing − being mentioned by Heipke (2010) − that volunteers have local knowledge. Digitization tasks of mines can thus be distributed among volunteers according to their localization and thus according to their local knowledge.

Surprisingly, Grasberg mine, being located within rocky surroundings and thus also representing a homogeneous study site, performs best regarding accuracy metrics such as overall accuracy, Kappa coefficient values, producer's and user's accuracy, omission and commission error values. Hence, it can be assumed that digitization results depend further on the order of digitization. Within the instructions for digitization, the procedure has been exemplary explained regarding Grasberg mine. Additionally, Grasberg mine digitization has been the first digitization task. These two facts support the assumption that the digitization result of the first digitization task is better in terms of accuracy metrics than the results of the following digitization tasks. Besides, differentiate task difficulty might also explain why Grasberg mine digitization achieved higher accuracy performance than the other study sites. The fact that task difficulty correlates with geometry complexity and interpretation difficulty (Albuquerque et al. 2016) is of particular interest regarding this issue, as Hamersley mine and Mariana mine are considered to reveal more complex geometries than Grasberg mine and are thus more difficult to interpret. This constitutes a further explanation of better accuracy performance of Grasberg mine.

A further finding has been that the digitization task requires optimization as far as the task it-self is concerned. Visual interpretation of the frequency distribution of Mariana mine has shown that the digitization led to artefacts, when the requirement of the task − that only one polygon shall be created −, will be fulfilled. The digitization task thus needs to be refined to a micro-task, in the same way than

Herfort et al. (2018), who developed micro-tasks out of the complex 3D information extraction. This accounts especially for the digitization of roads. Some volunteers did not fulfill this task requirement and created several polygons. Then additional post-processing is required in order to merge the polygons for further analysis.

6.1.3 Comparison between classifications and crowdsourcing

Visually it has been observed that the majority polygon always is referred to have the lowest amount of mine polygons, contrary to the classifications which contain a large amount of polygons. This has been found out when visually comparing the overlap of classifications and majority polygon in the results. The large amount of polygons of classifications is primary due to salt & pepper effect, which has been observed by Wang et al. (2018a) as well. Nevertheless, when other parameters, such as the perimeter will be computed, the amount of polygons is crucial. In the case of classifications, all polygons need then to be merged to a multi-polygon. This procedure is not required when only one polygon is available, as it is mostly the case for the majority polygons. Focusing on the overall motivation of the study, which is the supply of the parameter “mine area at earth surface”, a uniform polygon is considered to be more fitting, as the mining areas constitute entire areas instead of fragmentary dispersed areas.

A major finding is that the agreement between classifications and crowdsourcing is generally low. This means that the area detected as mine by the classifications differs from the area considered to represent a mine by the crowd. A low mean IoU of 0.49 for all comparisons has confirmed this finding. Contrary to this finding, Albuquerque et al. (2016) compared their crowdsourced classification to automated approaches in the case of building detection and considered both results to be comparable. Nevertheless, differences in the automated classification of small objects have been observed by Albuquerque et al. (2016), whereas crowdsourcing classifications were able to detect even small features. In the case of this study, it remains thus to be investigated if small objects, such as tailing dams, can be detected by both methods or if one method is preferred for this specific task.

Generally, when similarity by a high IoU is proven, both compared methods can be considered to be representative and thus a potential user can choose between the two methods. As soon as discrepancy is confirmed, a potential user needs to find out which method achieves better results. Given the fact that the mean IoU of 0.49 indicates discrepancy between classifications and crowdsourcing, I propose the application of the following decision tree, illustrated in Figure 6-2. Provided that IoU has been calculated, in case of the IoU is ≥ 0.5, the comparison is considered to represent similarity, according to Everingham et al. (2010) and thus method 1 or method 2 can be chosen. If IoU is < 0.5, discrepancy is confirmed. In this case the two methods have to be revised regarding their accuracy performance. The method performing better in accuracy metrics such as overall accuracy, producer’s and user’s accuracy, commission and omission error is than recommended to be chosen. The other method thus will be rejected. When applying the decision tree for this study, the following choice of methods can be recommended. For Grasberg mine the mean IoU is < 0.5. This means results are different and thereby the method with the best accuracy performance will be chosen. Regarding all accuracy metrics, crowdsourcing performs better than classifications. This means that for Grasberg mine, the majority polygon will be considered to be representative for the mine and thereby crowdsourcing is preferred to classifications. The same accounts for Hamersley mine, where IoU is also < 0.5. When taking all accuracy metrics into account, the majority polygon will be considered to be a more accurate representation of the mine and thus the method crowdsourcing will be recommended as well. Highland mine comparison, with an IoU ≥ 0.5 demonstrates similarity, whereby the classifications and the majority polygon can be considered to be representative, thus both methods can be chosen. Discrepancy is achieved for the comparison of classifications and crowdsourcing regarding Mariana mine. Because classifications perform better in terms of accuracy, one of the three classification methods is recommended to be chosen instead of the method crowdsourcing. The conclusion can thus be drawn that the choice of the appropriate method in order to determine the mine area, is dependent on the study site. But taking into account that following this decision tree, crowdsourcing has been preferred to classifications, a general recommendation for the application of crowdsourcing within studies focusing on the computation of mine extent can be made. As this remains a recommendation based on IoU and accuracy values only, a further consideration of strengths and weaknesses of each method is required.

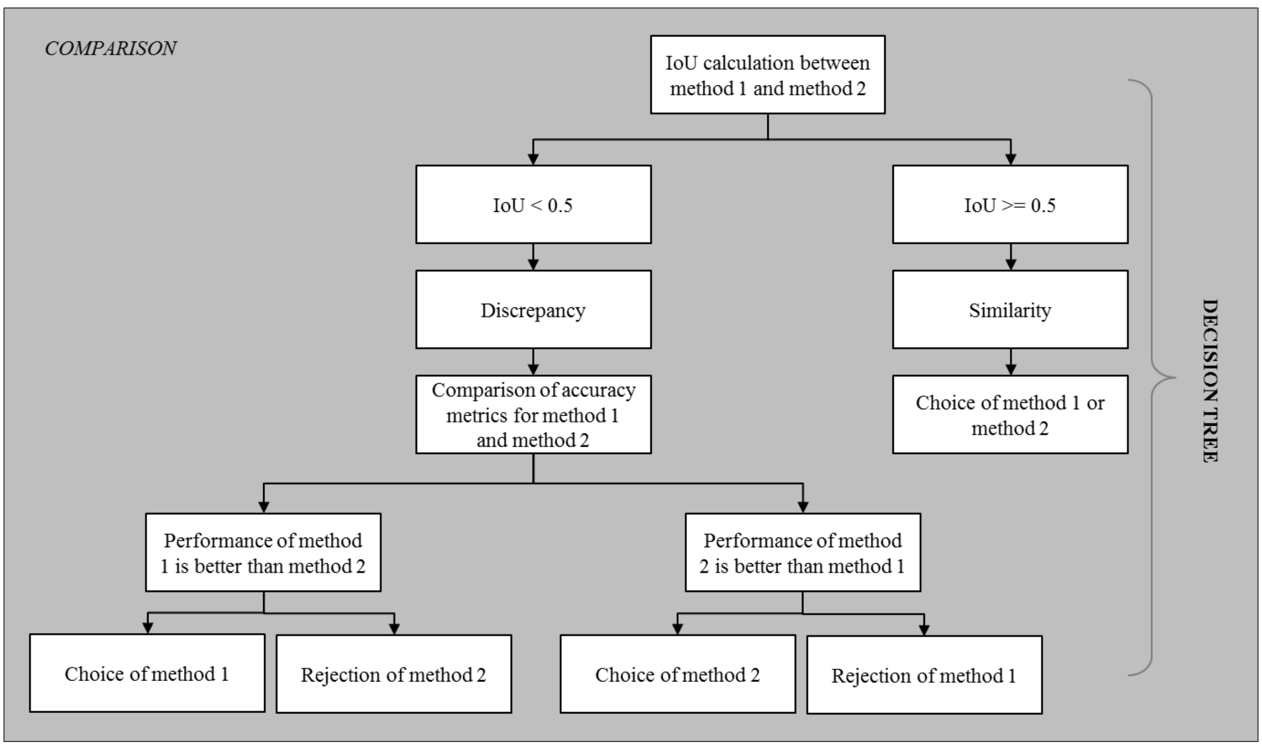

Figure 6-2: Proposed decision tree for supporting method selection.

As previously demonstrated, similarity between classifications and majority polygon depends on the study site. When comparing the IoU on an inter-mine level, Hamersley mine comparisons achieved lower mean IoU values than the other mines, whereas Highland mine comparisons reached highest mean IoU values. For the study site Hamersley mine, which is located in the desert, the IoU was lowest. This indicated discrepancies between classifications and crowdsourcing. Additionally, accuracy values of the majority polygon and the classifications were lowest. These facts support the finding that classification and digitization of mines in homogeneous study sites is considered more difficult. Higher agreement between classifications and crowdsourcing being observed for heterogeneous study sites such as Highland mine are in line with this finding. Besides the fact that classification and digitization of mines depends on the study site only, the geometry of the objects needs to be considered, as this might influence the task difficulty as well (Albuquerque et al. 2016).

Furthermore, when comparing the area values between classifications and crowdsourcing, the presented results have shown that the area being digitized by the majority of the crowd is in between the area of the index-based classifications and the pixel-based or object-based classification, except of Highland mine. That means the majority polygon is at an intermediate position between the conservative and progressive area calculation. In view of this, the majority polygon can be considered to represent a robust mediocrity. Evidence has been given when comparing the area of all classifications and majority polygons to each other. In current research, crowdsourcing results have been compared to one automated classifications method (Albuquerque et al. 2016). This study compares crowdsourcing to three types of classification methods, therefore being able to estimate the position of crowdsourcing among different classification methods. With respect to the finding that crowdsourcing results are at an intermediate position between classifications, this study extents the current state of the art.

The same has been observed for most accuracy metrics, where crowdsourcing results achieved either accuracy values in between the classifications or slightly higher accuracy values. This accounts particularly for overall accuracy, Kappa coefficient values, producer’s and user’s accuracy, and for commission error. Similar to the previous main findings, the crowdsourcing results occur to represent a mediocrity between the classifications. Nevertheless, for some accuracy metrics, such as omission error, crowdsourcing achieved the highest values for Highland and Mariana mine. This observation is probably related to the previously described main finding that the order of task presentation influences accuracy metrics or that geometry complexity plays a significant role (Albuquerque et al. 2016).

6.2 Main findings regarding the methodology of this study

This chapter addresses primary technical issues related to the methodology, which have been met during performance of the methodology. When possible, propositions about how to face these issues have been made.

The classification process of pixel-based and object-based classifications has shown that the classification result is very dependent on the training. Intense training of a class leads to an overestimation of the class, whereas moderate training results in an underestimation. The entire training process is thereby strongly subjective. A fixed amount of training samples for each class also reveals in an imbalance between over- and underestimation because within the study site some land use and land cover classes are more dominant than others. When all classes experience the same intensity of training, classes that in reality only cover a small part of the study site will become overestimated in the classification and classes being dominant in the study site will probably be underestimated. In order to mitigate this subjectiveness in future analyses, I propose to conduct previously an unsupervised classification, as it has been the case within Charou et al. (2010) and then an estimation of the percentage of each land use class being represented in the study site. Subsequently, the intensity of the training, in other words the amount of training samples, can be determined relative to the percentage of each land use class.

Besides the training procedure itself, the reference dataset is considered to be subjective as it is based on expert knowledge only. For an exact accuracy assessment, one needs to get in-situ GPS measurements of the extent of the mine. As no such in-situ measurements exists and a fieldtrip to acquire such measurements would be beyond the scope of this study, expert knowledge has been considered to be the reference for this study. LaJeunesse Connette et al. (2016) pronounce that remote sensing analyses constitute the only way to get spatial information about mining areas which are sometimes located in remote areas or armed conflict zones, thereby challenging the acquisition of in-situ measurement.

Another issue that has been met during the application of the methods is related to the presence of clouds in tropical or subtropical geographic regions. The same issue has been confirmed by Paull et al. (2006). For pixel-based and object-based classifications, the clouds and their corresponding shadows have been classified within this study, but especially for index-based classifications, the cloud issue has been more important. The reason therefore is that the NDVI range of clouds is embedded into the NDVI range of mines (Figure 6-3). The NDVI of clouds ranges from 0.007-0.076, the NDVI of the mine from -0.147-0.204. In order to address this issue, cloud masking has been performed. A common procedure against this issue is the removing of all clouds and the filling-up of the empty spaces with further cloud-free satellite imagery. Time series can be applied in this context so as to remove clouds (Julien and Sobrino 2019). This issue becomes more important when parts of the mine are covered by clouds. For all four study sites, mines have not been covered by clouds, replacing clouds by other imagery has thus not been required.

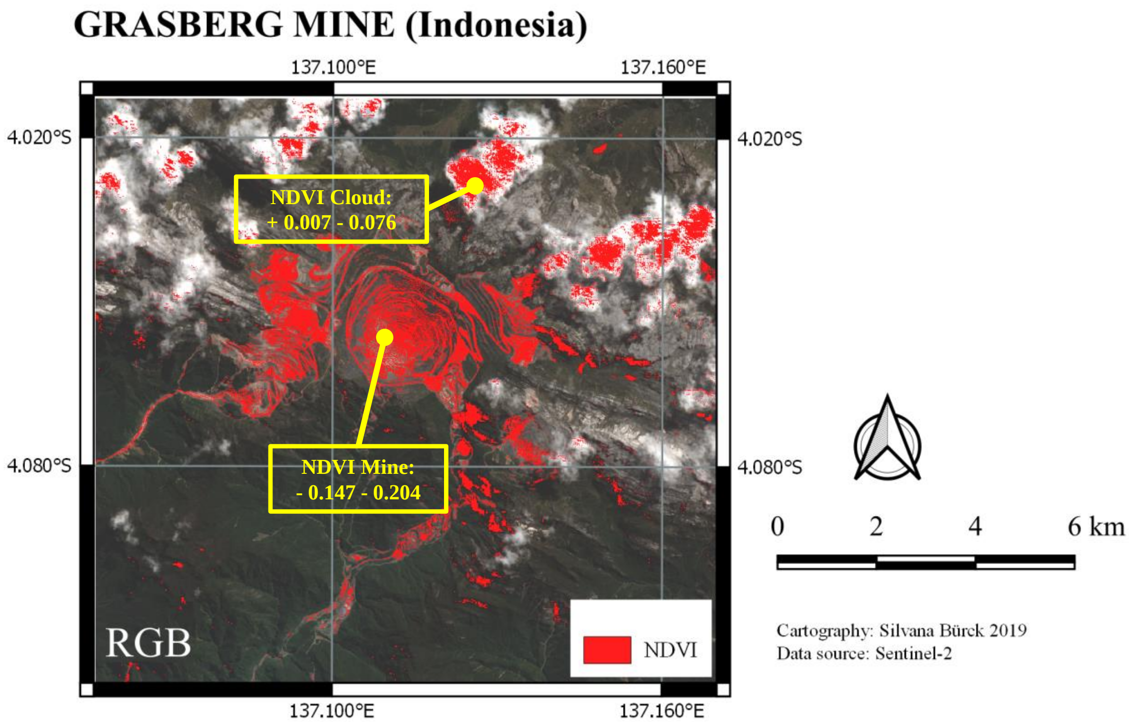

Figure 6-3: Analysis of NDVI values of clouds and the mine. The NDVI range of clouds is within the NDVI range of the mine; contains modified Copernicus Sentinel data (2018).

Other constraints have been met by software availability regarding object-based analysis. For many small scale institutions, NGO's and other organizations, the access to commercial software which enables object-based classification is limited. Therefore, efforts have been made in order to perform all analyses on the base of open-source software. Only for object-based classification this condition could not have been fulfilled as open-source software is still too limited or too experimental for object-based classification. Nevertheless, the emergence of novel sensors and remote sensing analyses (Ghassemian 2016) is accompanied by a constant extension of open-source software in the GIS and remote sensing domain.

Due to its advantages being mentioned within chapter 4, SVM algorithm has been chosen for the pixel-based and object-based classifications of this study. Taking into account that a large amount of current studies in the domain of remote sensing are related to machine learning, further machine learning algorithms, such as random forest (Whyte et al. 2018) remain to be tested. The scope of this study was not to compare classification algorithms, but the comparison of different classification algorithms might be of interest for future investigations as well.

With respect to the applied methods, the different level of effort in terms of complexity and the computation requirements beyond each method need to be considered. Index-based classification is the least effort-intense method, because on a single-source level only the NDVI threshold needs to be set, whereby this classification method is the fastest one. The fact that spectral index analyses provide a method which reduces time and expenditure has been confirmed by Sawut et al. (2018), who investigate heavy metal contents in an open pit mine by spectroscopy and spectral indices. Pixel-based classification needs intensive training and object-based classification requires high computation performance, in addition to an intense training. Contrary to the findings of this study, Lobo et al. 2018 demonstrated that a small training sample with 10 small size polygons of 5 x 5 pixels per class constitutes an appropriate training set for pixel-based classification, thus demonstrating that pixel-based classification can be considered a quick and efficient method as well, while providing accuracy and reduced image processing time. Regarding the finding that object-based classification is considered to be the most effort intense method, Prudente et al. (2017) pronounced that less processing time has been required by applying the Maxver, the so called Maximum Likelihood algorithm.

Within this study, a different amount of datasets has been included into the classifications, thereby performing classifications on single-source or multi-source level. As previously explained, the classification results were not strongly dependent on the amount of datasets being integrated. Instead of this differentiation in source-levels, data fusion might be of potential interest, given the fact that a wide range of data fusion methods, such as the Ehlers fusion (Abdikan et al. 2014), have currently been developed. By increasing spectral and spatial resolution, the classification results can be improved.

As far as crowdsourcing is concerned, technically it needs to be mentioned, that instructions for digitizations need to be revised according to the finding that additional information about features indicating potential mines and the digitization task is required. Therefore, I propose the development of a catalogue of features indicating potential mines with detailed information and exemplary imagery. When launching a crowdsourcing event, precise information about mine features can be given in a workshop, as it has been the case for Lesiv et al. (2019). Within the same context, digitization instructions need to become more precise in order to avoid that volunteers choose wrong saving parameters or file designation, which then requires further post-processing. Further optimization and simplification of the digitization task is needed regarding the fact that participation in the crowdsourcing project is very time consuming for volunteers.

A serious issue regarding crowdsourcing is the participation rate. Difficulties have been met in finding sufficient volunteers for the crowdsourcing project. In order to face this issue, I propose that benefits for the volunteers need to be presented with more detail. Another possibility to cope with this limitation is the launching of a crowdsourcing campaign, where social aspects play a significant role as well. For future crowdsourcing projects, small expense allowances for volunteers or other incentives can also be taken into account. As far as large scale projects are concerned, one could further think of crowdsourcing platforms such as Amazon’s Mechanical Turk, where an integrated participant compensation system for volunteers has been established (Buhrmester et al. 2011).

As far as metadata of the volunteers are concerned, no such background information about the volunteers is available. Information about the prior knowledge of volunteers regarding contextual information about mining or technical information about GIS and digitization is considered to be important for a holistic evaluation of the crowdsourcing results. This would be further helpful in order to identify types of target groups for crowdsourcing. For future projects, a questionary about the socio-economic background and experience of volunteers needs to be included to the crowdsourcing project.

Similar to Hillen and Höfle (2015), who demanded volunteers to give basic information before digitizing, background information is recommended to be requested within future crowdsourcing projects.

For the comparison between classifications and crowdsourcing, IoU has been useful in order to compare the two methods among each other. IoU gives information about how similar or different the results of the methods are. Nevertheless this comparison metric does not consider the similarity of shape for example. Even tough metrics such as the level of agreement, sensitivity, precision, and F1 score have been applied in order to assess the performance of the crowdsourcing results (Albuquerque et al. 2016), they might be of interest for method comparison as well.

Given the fact that for IoU no exact threshold indicating clearly similarity or dissimilarity exists, only relative statements can be made. A proposed threshold has been found within the study of Everingham et al. (2010) that has been adopted for the proposed decision tree. In order to support comparison and to built-up a decision tree, the threshold of 0.5 has been accepted and chosen for this study.

This proposed decision tree is expected to support the choice of the appropriate method for the computation of the mine area of the four study sites. However, when – according to the decision tree – classifications are preferred, a potential user still needs to find out which classification method is considered to be the most suitable one. Therefore, IoU should be computed for the comparisons of the classification methods among each other as well.

Limited significance of IoU has been observed when a potential user needs to decide which method to apply because the IoU presupposes that both methods have already been applied. The IoU is thus no metric supporting decision making of potential methods that have not been applied yet. Nevertheless, it can be applied within this study in order to indicate similarity and discrepancy among the tested methods. The findings of the comparison between classifications and crowdsourcing from this study can be transferred to other studies. Besides focusing on comparing the methods in order to choose between them, both methods can also is applied together instead of separately, thereby profiting from valuable synergies. Classifications could be trained or validated by the crowd. This has been exemplified by Johnson et al. (2017), who integrate crowdsourcing-based training data in automated classifications. That means instead of contrasting the machine to the crowd, they can be combined, according to Johnson et al. 2017. The perspective of Johnson et al. (2017) thus expands the view of this current study, which is dedicated to method comparison only.

6.3 Strengths and Weaknesses

The initial research question was to examine strengths and weaknesses of classifications, among them index-based, pixel-based and object-based classifications on single-source and multisource level, and crowdsourcing that can be applied in order to determine the delineation of the area that is subject to open-pit mining at earth surface in different geographic regions. At first, the qualitative visual interpretation and quantitative comparison by IoU revealed that classifications and crowdsourcing achieve different results. Classifications and crowdsourcing vary among area values and accuracy assessment. By applying the methods and analyzing results, new findings regarding effort, transferability, completeness, implementation, quality and credibility as well as their potential for automatization and further development have been generated. These findings have partially been discussed and related to current studies in the previous chapter. Upon the base of this, strengths and weaknesses, as well as potential opportunities and threats, will subsequently be derived.

6.3.1 Classifications

Regarding classifications, a major strength is related to the fact that all investigated classifications methods are able to classify mines, recognize all features indicating a potential mine, and achieve satisfactory results regarding visual interpretation and accuracy assessment. Thus, mine area computation can be performed with classifications. Classification methods range thereby from low effort up to high effort and from single-source up to multi-source. A further strength is that already with low effort classifications and with a single data source, mines can be classified and achieve satisfactory results. Furthermore, transferability of all classification methods is considered to be a strength. Homogeneous study sites are in fact more difficult to classify, but moderate accuracy is also obtained when classifying homogeneous study sites.

A major weakness of classifications is that classification algorithms − as they have been applied within this study −, have no contextual and local knowledge. They do not include features entirely correctly in the classification result and demonstrate thereby incompleteness. This issue can be faced by rule-based object-based classification, conditional random field or intense post-processing, as thereby neighborhood constellations will be considered. Another weakness of classifications is their subjective character, as the training process regarding pixel-based and object-based classifications is considered to be subjective and strongly influences the classification as well as its credibility. Subjectiveness in the training phase can be reduced by performing training relative to the proportion of the trained land use class, as previously mentioned. A further weakness is that object-based classification is very effort intense. When low effort constitutes a condition, index-based classification or pixel-based classification can be performed. Regarding transferability, for each new study site a new training set for pixel-based and object-based and a newly defined NDVI range is required. This weakness can be mitigated by developing one training set and one NDVI range per ecozone, as mines are likely to resemble within a given ecozone. Besides, cloud issues are challenging, especially for tropical study sites and for index-based classifications, thus effort is required in order to face this issue. Time series of satellite imagery are likely to provide partial cloud-free imagery. In addition, spectral similarities between the mine and the surroundings can result in miss-classifications, requiring effort intense spectral signature separation. Therefore, other characteristics of mines, such as elevation, can be considered with more detail. Furthermore, classifications provide different area values, thus questioning credibility. Pixel-based classification appears to constitute an intermediate position between index-based classifications that tend to an underestimation and object-based classifications, which appear to overestimate the mine area. Regarding index-based and pixel-based classification, the salt & pepper effect is dominant, which requires further intense post-processing when further analysis, such as perimeter computation, will be conducted. Salt & pepper effect can be limited when choosing object-based classification or when post-processing index-based and pixel-based classification more intensely.

Opportunities are related to a potential automatization of classifications, when one characteristic training set or NDVI range set per ecozone is created and subsequently classification of mines within new satellite imagery is performed. Thereby, transferability to other geographic regions is demonstrated. This approach could be extended further in terms of the development of an automatic mine detection model, related to the propositions of Pericak et al. (2018). For this study, the classified mines have been known to be existent. By means of the characteristic training set or NDVI range set, new satellite imagery, where mine existence is not yet guaranteed, can be classified. Instead of classifying existent mines, this might support mine detection and thus provide the required information for a potential global mine database. This can further support the Corine land cover project by providing detailed information about mine extent (Castellanos-Quiroz et al. 2017). Furthermore, the fact that pixel-based and object-based classifications contain other land use classes represents another potential development, as these land use classes are of particular interest regarding monitoring and change detection. Additional opportunities are related to the wide range of classification algorithms, which can be further investigated and the availability of methods that can be applied in order to integrate neighborhood constellations into the classification, such as rule-based object-based classification, conditional random field or intensified post-processing. Thereby, the issues related to incompleteness can be faced.

Risks that might prevent the implementation of classifications and thus their realization are primary related to access limitations, if free availability of software and satellite imagery is prevented. In this case, the establishment of an archive of satellite imagery is recommended in the unlikely case that all satellite imagery becomes commercial. Additionally, risk is related to restricted aces to open-source software. Nevertheless, the emergence and constant development of open-source software might lead to the assumption that tools and software, also open-source, for all classifications will be provided in the near future. A further limitation arises when no cloud-free imagery is available, which means that classifications cannot be realized. Then active sensors, such as Sentinel-1 need to be further investigated, as they penetrate clouds. A major risk is always related to the absence of reference data, which makes quality control very difficult. As demonstrated within this study, a dataset created upon expert knowledge is considered to constitute a sufficient reference, when no in-situ measurements are available.

An overview of strengths and weaknesses, as well as opportunities and threats of classifications is given in Figure 6-4.

CLASSIFICATIONS

Strengths	**Weaknesses**
Successful detection and classification with all methods Area computation is possible with all methods Single-source & low effort methods achieve satisfactory results (IND) Transferability Digitization of homogeneous study sites	Partially effort intense (OBIA) Subjective character (Training) Transferability requirements (Training set per ecozone) Clouds issues Spectral similarities between mine and bare area No contextual knowledge of algorithms Differences regarding area results Salt & pepper effect
Opportunities	**Threats**
Automatization Establishment of a global mine database Mine detection additional to mine classification Automatic mine detection model Integration of neighborhood factor Change detection & monitoring Further classification algorithms	Access limitations Dominance of cloud issues Absence of reference data

Figure 6-4: Matrix of strengths & weaknesses and opportunities & threats of classifications.

6.3.2 Crowdsourcing

A major strength of crowdsourcing (Figure 6-5) is that volunteers can recognize the mines within a given AOI, digitize the delineation of the area which is subject to open-pit mining and achieve thereby high accuracy values. Hence, area computation can be performed with crowdsourcing. Especially the derivation of the polygon that has been assigned to be a mine by the majority represents a good approximation to the real mine, because it contains all features indicating a potential mine. Besides these advantages, the fact that volunteers have contextual knowledge is a major strength. Volunteers consider the factor proximity, their digitizations thus demonstrate completeness. Another strength of this method is its transferability to other geographic regions, proven by the availability of different study sites within this crowdsourcing project. Digitization of mines in homogeneous study sites is in fact more difficult, but nevertheless satisfactory results can be achieved. Additionally, the low amount of polygons is easy to handle and less effort intense regarding further analysis, such as perimeter computation.

Weaknesses of this method are related to the contradiction between precise information provision for volunteers and the fact that participation is already very time consuming. This conflict makes it difficult to realize crowdsourcing projects. By minimizing the crowdsourcing task at maximum, precision in the information and low time consumption of the volunteers can be both realized. Furthermore, digitization by volunteers is highly subjective, thereby questioning credibility. Therefore, the implementation of a questionary is recommended, so as to investigate prior knowledge for an accurate evaluation of the crowdsourcing results. Moreover, the digitization result is dependent on the order of task presentation. When realizing a crowdsourcing project, this needs thus to be considered. Switching the order of task presentation might remedy this issue.

In order to increase participation rate, a future opportunity constitutes the launching of a crowdsourcing event, where the social factor of crowdsourcing will be included. Another opportunity to encourage more people in participation is to connect to crowdsourcing communities, to distribute the invitation for the crowdsourcing project among a larger target group and to keep the project open for a longer period. Especially a crowdsourcing campaign is considered to be a suitable tool in order to achieve a wide range of volunteers that can support the potential development of a global mine database by digitizing mines on global scale. These opportunities might support the realization of a crowdsourcing project. Regarding the analysis of the generated data, potential automatization is related to script-based analysis of the data and polygon post-processing. A novel opportunity and further potential development is related to the dual character of crowdsourcing. The contribution of volunteers by fulfilling a crowdsourced task has so far been considered to be the central objective of this study. Besides data generation, a sensitization of the crowd for environmental issues, such as mining and its footprint within the environment, has taken place. This duality needs to be further investigated, as high potential is seen in raising awareness towards environmental issues by generating geographic data. Crowdsourcing is thus considered to have an additional environmental teaching effect. Furthermore, information about the background of volunteers which can be retrieved by a questionary, is useful in investigating the target group. Acquired knowledge about target groups can then be transferred to other crowdsourcing tasks and support their realization.

Threats are primary related to the quality of the digitized data. Seriousness of the volunteers in the digitization cannot be proven, but is essential for the quality of the data. This could be mitigated by pronouncing the importance of the generated data and its potential implications. A major risk related to crowdsourcing is that participation rate will be too low. Therefore, several opportunities have previously been proposed such as the launching of a crowdsourcing event or the connection to other groups.

CROWDSOURCING

Strengths	**Weaknesses**
Successful detection and digitization by volunteers Area computation is possible with digitizations Majority is a representative approximation Contextual knowledge of volunteers Transferability Digitization of homogeneous study sites Simple handling	Contradiction between precision and time-consumption (Instructions) Subjectivity of volunteers Influence of task order
Opportunities	**Threats**
Enhancement of participation by events Connection to communities Broad target group Longer project duration Establishment of a global mine database Script-based post-processing and analysis Dualism between geospatial data generation & sensitization of volunteers for environmental issues Investigation of target groups	Seriousness of volunteers Participation rate

Figure 6-5: Matrix of strengths & weaknesses and opportunities & threats of crowdsourcing.

7 Conclusion

This section summarizes previous findings and derives the main conclusion with respect to the research objective of this study. Besides, the contribution of this study towards the initial motivation as well as directions for future research will be outlined.

The objective of this study was to compare remote sensing analyses that can be applied for the computation of the spatial extent of mining areas. For this comparative study, index-based, pixel-based and object-based multi-spectral classifications on single-source and multi-source level, as well as crowdsourcing have been applied in order to compute the spatial extent of open-pit mines in different geographic regions. It has been demonstrated that remote sensing analyses, among them classifications and crowdsourcing, can be used in order to detect known open-pit mines in different geographic regions, classify or respectively digitize them with an overall accuracy ≥ 77.41 % and derive the spatial extent. However, the comparison by Intersection over Union (IoU) revealed that results of both methods are different, given a low IoU ≤ 0.49. Classification and crowdsourcing results vary in their area and accuracy value, as well as their visual impression. With respect to area and accuracy values, the majority polygon, which is referred to the polygon being assigned to the mine by the majority of the crowd, is mostly at an intermediate position between the classifications. Taking findings related to the results and the implementation of the methods into account, strengths and weaknesses, as well as opportunities and threats of each method have been derived. Each method has its own strengths and weaknesses, as well as opportunities and threats with respect to effort, transferability, completeness, implementation, quality and credibility as well as their potential for automatization and further development. Classifications convince through their required effort, as already with low-expenditure methods satisfactory results could have been achieved, whereas they are considered challenging regarding transferability, as each time new training need to be performed. In addition, spectral similarities between classes challenge the distinction between features and the absence of contextual knowledge questions completeness. Regarding crowdsourcing, contextual knowledge of volunteers results in the inclusion of correct mine features in digitizations. Difficulties related to this method are primarily related to the contradiction between very precise instructions on the one hand and least expenditure of time for volunteers. The consideration of these strengths and weaknesses is essential in order to choose the appropriate method for mine area computation. Opportunities and threats are expected to guide future research.

Up to now, information about the spatial extent of mining areas has not been available yet for all open-pit mines on global scale, whereby the EHP analysis of open-pit mines remained limited. By providing strengths and weaknesses of methods that can be applied within this context, this study significantly contributes towards an entire EHP analysis of globally distributed open-pit mines.

Nevertheless, some investigations of both methods as well as their combination remain to be pursued. Regarding classifications, it needs to be investigated if the integration of other classification algorithms and classification methods that consider the factor proximity, such as rule-based object-based analysis or conditional random fields face the issue of absence of contextual knowledge within classifications. Given the large variety of classification methods, IoU remains to be applied for the comparisons among classifications, so as to distinguish not only between classifications and crowdsourcing, but also to differentiate between classifications. With respect to further potentials, it needs to be investigated if – by means of a characteristic training or NDVI range set per ecozone – unknown mines can be detected within new satellite imagery. This might set the path towards an automated mine detection model.

As far as crowdsourcing is concerned, the potential of a global mine mapping event needs to be investigated on a short-term in order to confirm global transferability and to establish a global mine database in the long term. Concerning the volunteers, a thorough understanding of the background of volunteers is required so as to evaluate crowdsourcing results entirely and to determine the appropriate target group for the crowdsourcing-based analysis of the open-pit mine extent in different geographic regions. These aspects might support further development of crowdsourcing in the domain of mine area computation.

Concerning the comparison of both methods, further research should assess if both methods could complement each other in an integrated classification-crowdsourcing model, instead of choosing between classifications and crowdsourcing. Rather than opposing machine-based results to human-based results, one could develop a methodology, which fuses the strengths and opportunities of both methods, in order to generate a powerful tool. Within this context, it needs to be assessed in detail in which stage of the analysis the methods could complement each other. For example it is assumed that crowdsourcing could support classifications by providing training, by providing geospatial information when classifications are not accurate enough or by performing the evaluation of the classification results. Synergetic effects of classifications and crowdsourcing in the domain of mine area computation thus constitutes a novel research objective which extends this present study.

8 Appendix

Table 8-1: Spectral mine range of the three calculated indices NDVI, FMI and CMI for each study site.

	Grasberg mine	Hamersley mine	Highland mine	Mariana mine
NDVI range	- 0.85 - 0.08	- 1 - 0.1	- 0.795 - 0.14	- 0.651 - 0.2
FMI range	0.96 - 1.20	1.4 - 1.9	0.9 - 1.26	1.12 - 1.8
CMI range	1.02 - 1.20	1 - 1.2	0.94 - 1.3	1.05 - 1.2

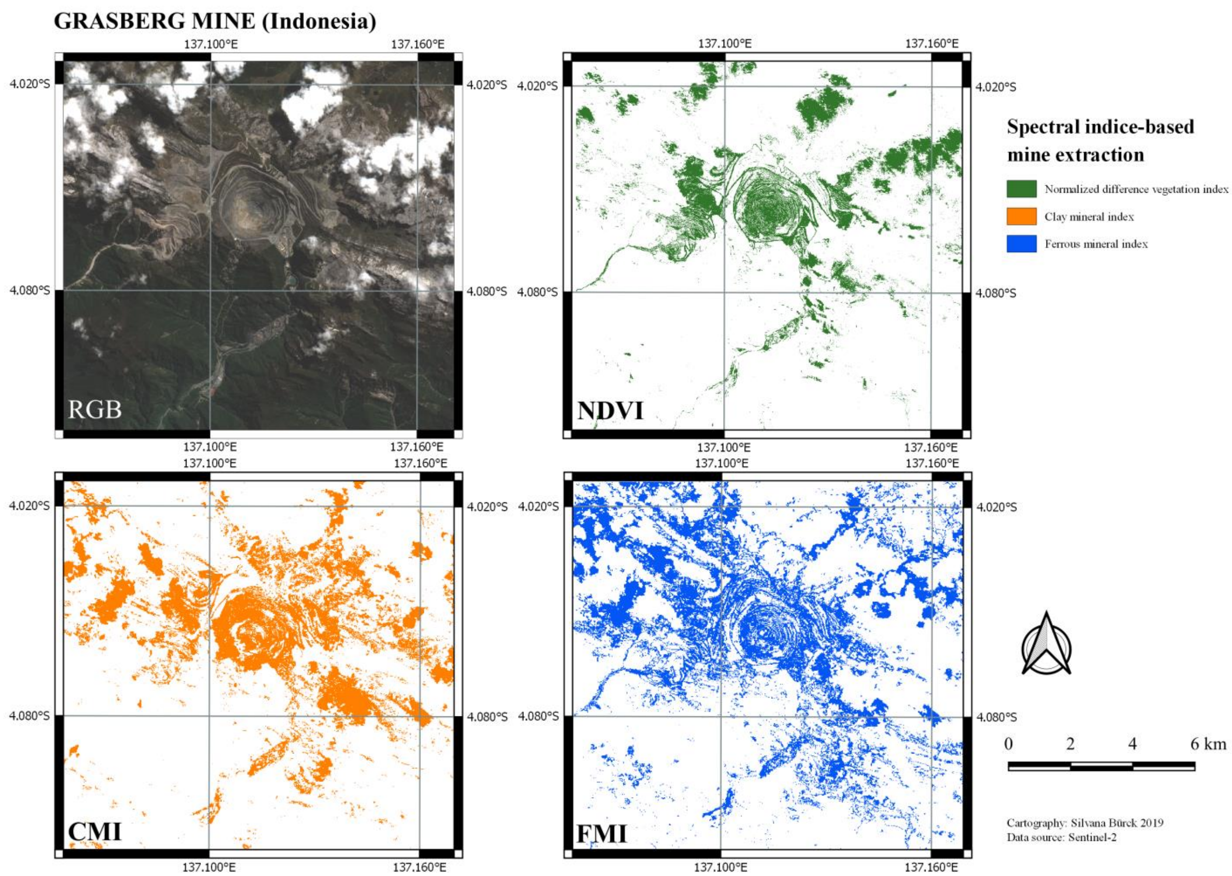

Figure 8-1: Overview of the three calculated indices NDVI, CMI and FMI exemplary for Grasberg mine. All three indices do not cover the same mine area; contains modified Copernicus Sentinel data (2018).

Table 8-2: Omission error of the class mine. This table shows the amount of pixels of other land use classes (in %), which should have been integrated into the class mine. Bold entries refer to Figure 5-14.

Grasberg mine			Hamersley mine			Highland mine			Mariana mine		
IND	**PIX**	**OBIA**	**IND**	**PIX**	**OBIA**	**IND**	**PIX**	**OBIA**	**IND**	**PIX**	**OBIA**
Non-mine 52.11 %	Bare area 1.60 %	Dense vegetation 0.55 %	Non-mine 55.88 %	Sparse vegetation 1.96 %	Shadow 1.42 %	Non-mine 1.48 %	Clouds 0.06 %	Bare area 0.68 %	Non-mine 19.11 %	Clouds 0.99 %	Shadow/ Clouds 0.56 %
-	Clouds 2.44 %	Sparse vegetation 0.55 %	-	Humid areas 3.34 %	Bare area 7.03 %	-	Shadow 0.31 %	Dense vegetation 0.96 %	-	Shadow 1.34 %	Bare area 1.06 %
-	Shadow 11.05 %	Shadow 8.19 %	-	Bare area 22.12 %	Humid areas 16.94 %	-	Bare area 0.43 %	Shadow 0.99 %	-	**Bare area 5.68 %**	Sparse vegetation 1.88 %

Table 8-3: Commission error of the class mine. This table shows the amount of pixels (in %), which have been included into the class mine but belong to the other classes. Bold entries are related to Figure 5-15.

Grasberg mine			Hamersley mine			Highland mine			Mariana mine		
IND	**PIX**	**OBIA**	**IND**	**PIX**	**OBIA**	**IND**	**PIX**	**OBIA**	**IND**	**PIX**	**OBIA**
Non-mine 1.34 %	Shadow 2.20 %	Bare area 4.31 %	Non-mine 99.95 %	Bare area 3.20 %	Sparse vegetation 0.73 %	Non-mine 2.84 %	Sparse vegetation 0.06 %	Sparse vegetation 0.04 %	Non-mine 0.01 %	Bare area 1.47 %	Bare area 2.73 %
	Clouds 2.58 %	Shadow 5.16 %	-	Shadow 8.16 %	Humid areas 0.83 %		Bare area 4.22 %	Bare area 0.75 %	-	-	-
	Bare area 3.27 %	Clouds 8.70 %	-	**Sparse vegetation 9.13 %**	Bare area 2.01 %		Clouds 6.57 %	Clouds 2.21 %	-	-	-

Table 8-4: Overview of training samples for pixel-based classifications.

	Training samples for pixel-based classification			
	Grasberg mine	**Hamersley mine**	**Highland mine**	**Mariana mine**
Shadow [pixels]	4917	2263	6031	21419
Clouds [pixels]	13015	0	2420	9059
Bare Area [pixels]	4454	26239	6658	48888
Sparse Vegetation [pixels]	753	6154	11291	17994
Dense Vegetation [pixels]	3047	0	27328	41300
Mine [pixels]	9338	47732	44630	31587
Humid Areas [pixels]	0	2527	0	0
Total amount of pixels	35524	84915	98358	170247
Area [km^2]	3.55	8.49	9.83	17.02
Area relative to entire study site [%]	2.34	2.07	1.52	2.28

Table 8-5: Overview of training samples for object-based classifications.

	Training samples for object-based classification			
	Grasberg mine	**Hamersley mine**	**Highland mine**	**Mariana mine**
Shadow [pixels]	699	1263	6031	21419
Clouds [pixels]	578	0	2420	9059
Bare Area [pixels]	144	26239	6658	48888
Sparse Vegetation [pixels]	556	6154	11291	17994
Dense Vegetation [pixels]	996	0	2732	41300
Mine [pixels]	970	42267	30290	29542
Humid Areas [pixels]	0	2527	0	0
Total amount of pixels	3943	78450	59422	168202
Area [km^2]	0.39	7.84	5.94	16.82
Area relative to entire study site [%]	0.26	1.91	0.92	2.25

Table 8-6: Spectral attributes that have been included in the object-based classifications; source: Harris Geospatial (2019b), modified.

	Attribute	Description
Spectral attribute	Spectral_Mean	Mean value of the pixels comprising the region in band x
	Spectral_Max	Maximum value of the pixels comprising the region in band x
	Spectral_Min	Minimum value of the pixels comprising the region in band x
	Spectral_STD	Standard deviation value of the pixels comprising the region in band x

Table 8-7: Texture attributes that have been included in the object-based classifications; source: Harris Geospatial (2019b), modified.

	Attribute	Description
Texture attribute	Texture_Range	Average data range of the pixels comprising the region inside the kernel (whose size you specify with the Texture Kernel Size parameter in segmentation)
	Texture_Mean	Average value of the pixels comprising the region inside the kernel
	Texture_Variance	Average variance of the pixels comprising the region inside the kernel
	Texture_Entropy	Average entropy value of the pixels comprising the region inside the kernel

Table 8-8: Spatial attributes that have been included in the object-based classifications; source: Harris Geospatial (2019b), modified.

	Attribute	Description
Spatial attribute	Area	Total area of the polygon, minus the area of the holes. If the input image is pixel-based, the area is the number of pixels in the segmented object. For a segmented object with 20 x 20 pixels the area is 400 pixels. If the input image is georeferenced, the area is in the map units of the input image. For a segmented object with 20 x 20 pixels, where the input image pixel resolution is 2 meters, the total area is 1600 square meters (400 pixels x 2 meters x 2 meters).
	Length	The combined length of all boundaries of the polygon, including the boundaries of the holes. This is different than the Major_Length attribute. If the input image is pixel-based, the length is the number of pixels. For a segmented object with 20 x 20 pixels, the length is 80 pixels. If the input image is georeferenced, the length is in the map units of the input image. For a segmented object with 20 x 20 pixels, where the input image pixel resolution is 2 meters, the length is 160 meters (80 pixels x 2 meters).
	Compactness	A shape measure that indicates the compactness of the polygon. A circle is the most compact shape with a value of 1 / pi. The compactness value of a square is 1 / 2(sqrt(pi)). Compactness = Sqrt (4 * Area / pi) / outer contour length
	Convexity	Polygons are either convex or concave. This attribute measures the convexity of the polygon. The convexity value for a convex polygon with no holes is 1.0, while the value for a concave polygon is less than 1.0. Convexity = length of convex hull / Length
	Solidity	A shape measure that compares the area of the polygon to the area of a convex hull surrounding the polygon. The solidity value for a convex polygon with no holes is 1.0, and the value for a concave polygon is less than 1.0. Solidity = Area / area of convex hull
	Roundness	A shape measure that compares the area of the polygon to the square of the maximum diameter of the polygon. The "maximum diameter" is the length of the major axis of an oriented bounding box enclosing the polygon. The roundness value for a circle is 1, and the value for a square is 4 / pi. Roundness = 4 * (Area) / (pi * Major_Length^2)
	Form_Factor	A shape measure that compares the area of the polygon to the square of the total perimeter. The form factor value of a circle is 1, and the value of a square is pi / 4. Form_Factor = 4 * pi * (Area) / (total perimeter)^2
	Elongation	A shape measure that indicates the ratio of the major axis of the polygon to the minor axis of the polygon. The major and minor axes are derived from an oriented bounding box containing the polygon. The elongation value for a square is 1.0, and the value for a rectangle is greater than 1.0. Elongation = Major_Length / Minor_Length
	Rectangular_Fit	A shape measure that indicates how well the shape is described by a rectangle. This attribute compares the area of the polygon to the area of the oriented bounding box enclosing the polygon. The rectangular fit value for a rectangle is 1.0, and the value for a non-

	rectangular shape is less than 1.0. Rectangular_Fit = Area / (Major_Length * Minor_Length)
Main_Direction	The angle subtended by the major axis of the polygon and the x-axis in degrees. The main direction value ranges from 0 to 180 degrees. 90 degrees is North/South, and 0 to 180 degrees is East/West.
Major_Length	The length of the major axis of an oriented bounding box enclosing the polygon. Values are map units of the pixel size. If the image is not georeferenced, then pixel units are reported.
Minor_Length	The length of the minor axis of an oriented bounding box enclosing the polygon. Values are map units of the pixel size. If the image is not georeferenced, then pixel units are reported.
Number_of_Holes	The number of holes in the polygon. Integer value.
Hole_Area/Solid_Area	The ratio of the total area of the polygon to the area of the outer contour of the polygon. The hole solid ratio value for a polygon with no holes is 1.0. Hole_Area/Solid_Area = Area / outer contour area

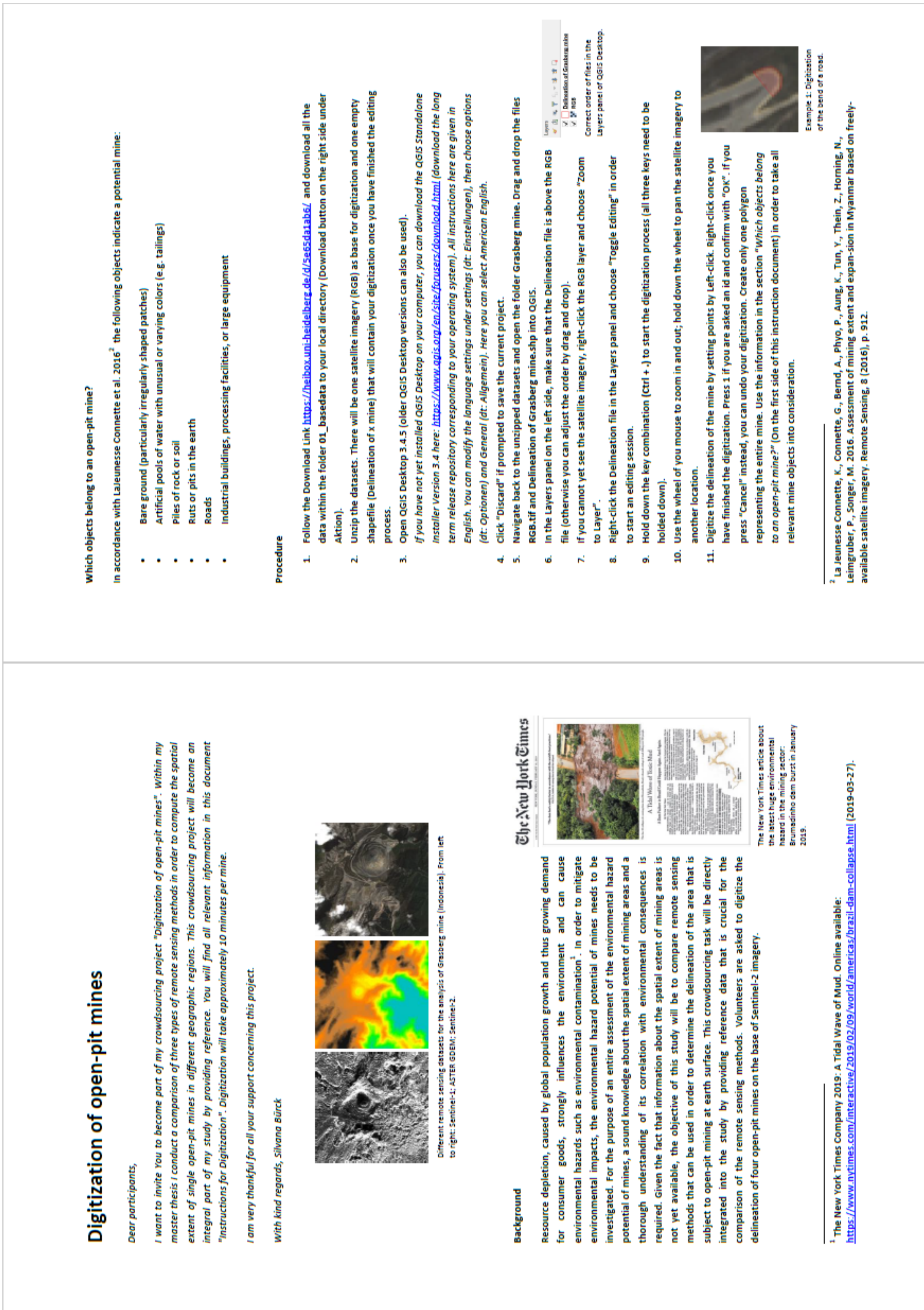

Digitization of open-pit mines

Dear participants,

I want to invite You to become part of my crowdsourcing project "Digitization of open-pit mines". Within my master thesis I conduct a comparison of three types of remote sensing methods in order to compute the spatial extent of single open-pit mines in different geographic regions. This crowdsourcing project will become an integral part of my study by providing reference. You will find all relevant information in this document "Instructions for Digitization". Digitization will take approximately 10 minutes per mine.

I am very thankful for all your support concerning this project.

With kind regards, Silvana Bürck

Different remote sensing datasets for the analysis of Grasberg mine (Indonesia). From left to right: Sentinel-1; ASTER GDEM; Sentinel-2.

Background

Resource depletion, caused by global population growth and thus growing demand for consumer goods, strongly influences the environment and can cause environmental hazards such as environmental contamination[1]. In order to mitigate environmental impacts, the environmental hazard potential of mines needs to be investigated. For the purpose of an entire assessment of the environmental hazard potential of mines, a sound knowledge about the spatial extent of mining areas and a thorough understanding of its correlation with environmental consequences is required. Given the fact that information about the spatial extent of mining areas is not yet available, the objective of this study will be to compare remote sensing methods that can be used in order to determine the delineation of the area that is subject to open-pit mining at earth surface. This crowdsourcing task will be directly integrated into the study by providing reference data that is crucial for the comparison of the remote sensing methods. Volunteers are asked to digitize the delineation of four open-pit mines on the base of Sentinel-2 imagery.

The New York Times

A Tidal Wave of Toxic Mud

The New York Times article about the latest huge environmental hazard in the mining sector: Brumadinho dam burst in January 2019.

[1] The New York Times Company 2019: A Tidal Wave of Mud. Online available: https://www.nytimes.com/interactive/2019/02/09/world/americas/brazil-dam-collapse.html (2019-03-27).

Which objects belong to an open-pit mine?

In accordance with LaJeunesse Connette et al. 2016[2] the following objects indicate a potential mine:

- Bare ground (particularly irregularly shaped patches)
- Artificial pools of water with unusual or varying colors (e.g. tailings)
- Piles of rock or soil
- Ruts or pits in the earth
- Roads
- Industrial buildings, processing facilities, or large equipment

Procedure

1. Follow the Download Link https://heibox.uni-heidelberg.de/d/5e65da1ab6/ and download all the data within the folder **01_basedata** to your local directory (Download button on the right side under Aktion).
2. Unzip the datasets. There will be one satellite imagery (RGB) as base for digitization and one empty shapefile (Delineation of x mine) that will contain your digitization once you have finished the editing process.
3. Open QGIS Desktop 3.4.5 (older QGIS Desktop versions can also be used).
If you have not yet installed QGIS Desktop on your computer, you can download the QGIS Standalone Installer Version 3.4 here: https://www.qgis.org/en/site/forusers/download.html (download the long term release repository corresponding to your operating system). All instructions here are given in English. You can modify the language settings under settings (dt: Einstellungen), then choose options (dt: Optionen) and General (dt: Allgemein). Here you can select American English.
4. Click "Discard" if prompted to save the current project.
5. Navigate back to the unzipped datasets and open the folder **Grasberg mine.** Drag and drop the files **RGB.tif and Delineation of Grasberg mine.shp** into QGIS.
6. In the Layers panel on the left side, make sure that the Delineation file is above the RGB file (otherwise you can adjust the order by drag and drop).
7. If you cannot yet see the satellite imagery, right-click the RGB layer and choose "Zoom to Layer".
8. Right-click the Delineation file in the Layers panel and choose "Toggle Editing" in order to start an editing session.
9. Hold down the key combination (Ctrl + .) to start the digitization process (all three keys need to be holded down).
10. Use the wheel of you mouse to zoom in and out; hold down the wheel to pan the satellite imagery to another location.
11. Digitize the delineation of the mine by setting points by Left-click. Right-click once you have finished the digitization. Press 1 if you are asked an id and confirm with "OK". If you press "Cancel" instead, you can undo your digitization. Create only one polygon representing the entire mine. Use the information in the section *"Which objects belong to an open-pit mine?"* (On the first side of this instruction document) in order to take all relevant mine objects into consideration.

Correct order of files in the Layers panel of QGIS Desktop.

Example 1: Digitization of the bend of a road.

[2] La Jeunesse Connette, K., Connette, G., Bernd, A., Phyo, P., Aung, K., Tun, Y., Thein, Z., Horning, N., Leimgruber, P., Songer, M. 2016. Assessment of mining extent and expan-sion in Myanmar based on freely-available satellite imagery. Remote Sensing, 8 (2016), p. 912.

Figure 8-2: Instructions for digitization I. This document presented the base of the crowdsourcing project.

Example 2: Digitization of Agua Limpa mine (Brazil). Left: View of the entire polygon; Right: Detail view of the delineation.

12. If you want to delete a point of your polygon, activate the Node Tool (the tool is available in the toolbar above the imagery), select the point you want to delete and press the "delete" key of your keyboard.
13. Right-click the Delineation file in the Layers panel and choose "Save Layer Edits".
14. Click "Project" in the top menu toolbar and choose "Exit QGIS" in order to close the session.
15. Click "Discard" if prompted to save the current project.
16. Navigate back to the folder Grasberg mine and highlight all files called Delineation.
17. Right-click and choose "Send to" and then "Zip-compressed folder".
18. Modify the name of the newly created compressed folder according to your initials "Delineation of Grasberg mine_initials". E.g. my name is Silvana Bürck, so I would rename the folder Delineation of Grasberg mine_SB.
19. Open the following Upload link: https://heibox.uni-heidelberg.de/u/d/73c3bd7a08/ .
20. Upload your newly created Zip-compressed folder with the digitization (The upload link is available until 12.04.2019).

    Congratulations, you have just digitized your first mine!
21. Repeat step 5 – 18 for the three other mines.

Further investigated mines. From left to right: Hamersley mine (Australia); Highland Valley mine (Canada); Mariana mine (Brazil).

Contact

Silvana Bürck
E-Mail: silvana.buerck@ifeu.de
Phone: +49 (0)6221 4767 56

Figure 8-3: Instructions for digitization II. This document presented the base of the crowdsourcing project.

9 References

Abbaspour, H., Drebenstedt, C., Paricheh, M., and Ritter, R. (2019). Optimum location and relocation plan of semi-mobile in-pit crushing and conveying systems in open-pit mines by transportation problem. Int. J. Min. Reclam. Environ. *33*, 297–317.

Abdikan, S., Balik Sanli, F., Sunar, F., and Ehlers, M. (2014). A comparative data-fusion analysis of multi-sensor satellite images. Int. J. Digit. Earth *7*, 671–687.

Ahmadi, M.R., and Bazzazi, A.A. (2019). Cutoff grades optimization in open pit mines using meta-heuristic algorithms. Resour. Policy *60*, 72–82.

Ahmadi, M.R., and Shahabi, R.S. (2018). Cutoff grade optimization in open pit mines using genetic algorithm. Resour. Policy *55*, 184–191.

Alam, F.I., Zhou, J., Liew, A.W.-C., Jia, X., Chanussot, J., and Gao, Y. (2019). Conditional Random Field and Deep Feature Learning for Hyperspectral Image Classification. IEEE Trans. Geosci. Remote Sens. *57*, 1612–1628.

Albertz, J. (2009). Einführung in die Fernerkundung: Grundlagen der Interpretation von Luft- und Satellitenbildern (Darmstadt: WBG (Wiss. Buchges.)).

Albuquerque, J., Herfort, B., and Eckle, M. (2016). The Tasks of the Crowd: A Typology of Tasks in Geographic Information Crowdsourcing and a Case Study in Humanitarian Mapping. Remote Sens. *8*, 859.

Asner, G.P., Llactayo, W., Tupayachi, R., and Luna, E.R. (2013). Elevated rates of gold mining in the Amazon revealed through high-resolution monitoring. Proc. Natl. Acad. Sci. *110*, 18454–18459.

Banks, G., Paull, D., and Mockler, S. (2005). The Social and Environmental Impact of Mining in Asia-Pacific: The Potential Contribution of a Remote-Sensing Approach (Canberra: Resource Management in Asia-Pacific Program, Research School of Pacific and Asian Studies, The Australian National University).

Barley, M.E., Pickard, A.L., Hagemann, S.G., and Folkert, S.L. (1999). Hydrothermal origin for the 2 billion year old Mount Tom Price giant iron ore deposit, Hamersley Province, Western Australia. Miner. Deposita *34*, 784–789.

Basommi, P.L., Guan, Q., and Cheng, D. (2015). Exploring Land use and Land cover change in the mining areas of Wa East District, Ghana using Satellite Imagery. Open Geosci. *7*.

Belgiu, M., and Csillik, O. (2018). Sentinel-2 cropland mapping using pixel-based and object-based time-weighted dynamic time warping analysis. Remote Sens. Environ. *204*, 509–523.

Bensaman, B., Furqan, R.A., Rosana, M.F., and Yuningsih, E.T. (2015). Hydrothermal Alteration and Mineralization Characteristics of Gajah Tidur Prospect, Ertsberg Mining District, Papua, Indonesia. 9.

Beretta, F., Shibata, H., Cordova, R., Peroni, R. de L., Azambuja, J., and Costa, J.F.C.L. (2018). Topographic modelling using UAVs compared with traditional survey methods in mining. REM - Int. Eng. J. *71*, 463–470.

Blom, M., Pearce, A.R., and Stuckey, P.J. (2018). Multi-objective short-term production scheduling for open-pit mines: a hierarchical decomposition-based algorithm. Eng. Optim. *50*, 2143–2160.

Bona, D.S., Arymurthy, A.M., and Mursanto, P. (2018). Classification of Limestone Mining Site using Multi-Sensor Remote Sensing Data and OBIA Approach a Case Study: Biak Island, Papua. In 2018 International Conference on Advanced Computer Science and Information Systems (ICACSIS), (Yogyakarta: IEEE), pp. 417–422.

Borie, C., Parcero-Oubiña, C., Kwon, Y., Salazar, D., Flores, C., Olguín, L., and Andrade, P. (2019). Beyond Site Detection: The Role of Satellite Remote Sensing in Analysing Archaeological Problems. A Case Study in Lithic Resource Procurement in the Atacama Desert, Northern Chile. Remote Sens. *11*, 869.

Buhrmester, M., Kwang, T., and Gosling, S.D. (2011). Amazon's Mechanical Turk: A New Source of Inexpensive, Yet High-Quality, Data? Perspect. Psychol. Sci. *6*, 3–5.

Bundesministerium für Umwelt, Naturschutz, Bau und Reaktorsicherheit (BMUB) (2016). Deutsches Ressourceneffizienz-programm II - Programm zur nachhaltigen Nutzung und zum Schutz der natürlichen Ressourcen. 144.

Cai, Y., Guan, K., Peng, J., Wang, S., Seifert, C., Wardlow, B., and Li, Z. (2018). A high-performance and in-season classification system of field-level crop types using time-series Landsat data and a machine learning approach. Remote Sens. Environ. *210*, 35–47.

Carabassa, V., Ortiz, O., and Alcañiz, J.M. (2019). RESTOQUARRY: Indicators for self-evaluation of ecological restoration in open-pit mines. Ecol. Indic. *102*, 437–445.

Cardoso-Fernandes, J., Teodoro, A.C., and Lima, A. (2019). Remote sensing data in lithium (Li) exploration: A new approach for the detection of Li-bearing pegmatites. Int. J. Appl. Earth Obs. Geoinformation *76*, 10–25.

Carlà, T., Farina, P., Intrieri, E., Ketizmen, H., and Casagli, N. (2018). Integration of ground-based radar and satellite InSAR data for the analysis of an unexpected slope failure in an open-pit mine. Eng. Geol. *235*, 39–52.

Carmo, F.F. do, Kamino, L.H.Y., Junior, R.T., Campos, I.C. de, Carmo, F.F. do, Silvino, G., Castro, K.J. da S.X. de, Mauro, M.L., Rodrigues, N.U.A., Miranda, M.P. de S., et al. (2017). Fundão tailings dam failures: the environment tragedy of the largest technological disaster of Brazilian mining in global context. Perspect. Ecol. Conserv. *15*, 145–151.

Castellanos-Quiroz, H.O.A., Ramírez-Daza, H.M., and Ivanova, Y. (2017). Detection of open-pit mining zones by implementing spectral indices and image fusion techniques. DYNA *84*, 42.

Castelo Branco, J., Rebbah, R., Duarte, J., and Baptista, J.S. (2019). Risk Assessment in the Open Pit Mining Industry—A Short Review. In Occupational and Environmental Safety and Health, P.M. Arezes, J.S. Baptista, M.P. Barroso, P. Carneiro, P. Cordeiro, N. Costa, R.B. Melo, A.S. Miguel, and G. Perestrelo, eds. (Cham: Springer International Publishing), pp. 13–21.

Charou, E., Stefouli, M., Dimitrakopoulos, D., Vasiliou, E., and Mavrantza, O.D. (2010). Using Remote Sensing to Assess Impact of Mining Activities on Land and Water Resources. Mine Water Environ. *29*, 45–52.

Chen, B., Huang, B., and Xu, B. (2017). Multi-source remotely sensed data fusion for improving land cover classification. ISPRS J. Photogramm. Remote Sens. *124*, 27–39.

Chen, G., Knibbs, L.D., Zhang, W., Li, S., Cao, W., Guo, J., Ren, H., Wang, B., Wang, H., Williams, G., et al. (2018a). Estimating spatiotemporal distribution of PM1 concentrations in China with satellite remote sensing, meteorology, and land use information. Environ. Pollut. *233*, 1086–1094.

Chen, G., Weng, Q., Hay, G.J., and He, Y. (2018b). Geographic object-based image analysis (GEOBIA): emerging trends and future opportunities. GIScience Remote Sens. *55*, 159–182.

Chen, L., Li, W., Zhang, X., Chen, L., and Chen, C. (2018c). Application of Object-oriented Classification with Hierarchical Multi-Scale Segmentation for Information Extraction in Nonoc Nickel Mine, the Philippines. In 2018 Fifth International Workshop on Earth Observation and Remote Sensing Applications (EORSA), (Xi'an: IEEE), pp. 1–3.

Chen, Y., Zhou, Y., Ge, Y., An, R., and Chen, Y. (2018d). Enhancing Land Cover Mapping through Integration of Pixel-Based and Object-Based Classifications from Remotely Sensed Imagery. Remote Sens. *10*, 77.

Cheng, G., Yang, C., Yao, X., Guo, L., and Han, J. (2018). When Deep Learning Meets Metric Learning: Remote Sensing Image Scene Classification via Learning Discriminative CNNs. IEEE Trans. Geosci. Remote Sens. *56*, 2811–2821.

Cionek, V.M., Alves, G.H.Z., Tófoli, R.M., Rodrigues-Filho, J.L., and Dias, R.M. (2019). Brazil in the mud again: lessons not learned from Mariana dam collapse. Biodivers. Conserv. *28*, 1935–1938.

Climate-Data.org. Online available: https://de.climate-data.org/ (2019-06-14).

Congedo, L. (2018). Semi-Automatic Classification Plugin Documentation. 216. Online available: https://www.google.com/url?sa=t&rct=j&q=&esrc=s&source=web&cd=3&cad=rja&uact=8&ved=2ahUKEwj1tt-PoeniAhXMAmMBHT-9D1gQFjACegQIARAC&url=https%3A%2F%2Fmedia.readthedocs.org%2Fpdf%2Fsemiautomaticclassificationmanual-v5%2Flatest%2Fsemiautomaticclassificationmanual-v5.pdf&usg=AOvVaw3LrRJLaWS5dKUFTc1_It2R (2019-06-14).

Costa, H., Foody, G.M., and Boyd, D.S. (2017). Using mixed objects in the training of object-based image classifications. Remote Sens. Environ. *190*, 188–197.

Domínguez-Haydar, Y., Velásquez, E., Carmona, J., Lavelle, P., Chavez, L.F., and Jiménez, J.J. (2019). Evaluation of reclamation success in an open-pit coal mine using integrated soil physical, chemical and biological quality indicators. Ecol. Indic. *103*, 182–193.

Dong, J., Zhuang, D., Huang, Y., and Fu, J. (2009). Advances in Multi-Sensor Data Fusion: Algorithms and Applications. Sensors *9*, 7771–7784.

Drury, S.A. (1993). Image interpretation in geology (London ; New York: Chapman & Hall).

Duncan, C., Owen, H.J.F., Thompson, J.R., Koldewey, H.J., Primavera, J.H., and Pettorelli, N. (2018). Satellite remote sensing to monitor mangrove forest resilience and resistance to sea level rise. Methods Ecol. Evol. *9*, 1837–1852.

Eck, T.F., Holben, B.N., Reid, J.S., Xian, P., Giles, D.M., Sinyuk, A., Smirnov, A., Schafer, J.S., Slutsker, I., Kim, J., et al. (2018). Observations of the Interaction and Transport of Fine Mode Aerosols With Cloud and/or Fog in Northeast Asia From Aerosol Robotic Network and Satellite Remote Sensing. J. Geophys. Res. Atmospheres *123*, 5560–5587.

Ehlers, M., Klonus, S., Johan Åstrand, P., and Rosso, P. (2010). Multi-sensor image fusion for pansharpening in remote sensing. Int. J. Image Data Fusion *1*, 25–45.

ESA (2014). European Space Agency Copernicus Open Acess Hub 2019. Online available: https://scihub.copernicus.eu/dhus/#/home (2019-06-14).

Espitia-Pérez, L., da Silva, J., Brango, H., Espitia-Pérez, P., Pastor-Sierra, K., Salcedo-Arteaga, S., de Souza, C.T., Dias, J.F., Hoyos-Giraldo, L.S., Gómez-Pérez, M., et al. (2018a). Genetic damage in environmentally exposed populations to open-pit coal mining residues: Analysis of buccal micronucleus cytome (BMN-cyt) assay and alkaline, Endo III and FPG high-throughput comet assay. Mutat. Res. Toxicol. Environ. Mutagen. *836*, 24–35.

Espitia-Pérez, L., Arteaga - Pertuz, M., Soto, J.S., Espitia-Pérez, P., Salcedo-Arteaga, S., Pastor–Sierra, K., Galeano–Páez, C., Brango, H., da Silva, J., and Henriques, J.A.P. (2018b). Geospatial analysis of residential proximity to open-pit coal mining areas in relation to micronuclei frequency, particulate matter concentration, and elemental enrichment factors. Chemosphere *206*, 203–216.

Everingham, M., and Winn, J. (2012). The PASCAL Visual Object Classes Challenge 2012 (VOC2012) Development Kit. 32. Online available: http://host.robots.ox.ac .uk/pascal/VOC/voc2012/devkit_doc.pdf (2019-06-14).

Everingham, M., Van Gool, L., Williams, C.K.I., Winn, J., and Zisserman, A. (2010). The Pascal Visual Object Classes (VOC) Challenge. Int. J. Comput. Vis. *88*, 303–338.

Fernandes, G.W., Goulart, F.F., Ranieri, B.D., Coelho, M.S., Dales, K., Boesche, N., Bustamante, M., Carvalho, F.A., Carvalho, D.C., Dirzo, R., et al. (2016). Deep into the mud: ecological and socio-economic impacts of the dam breach in Mariana, Brazil. Nat. Conserv. *14*, 35–45.

Fritz, S., McCallum, I., Schill, C., Perger, C., See, L., Schepaschenko, D., van der Velde, M., Kraxner, F., and Obersteiner, M. (2012). Geo-Wiki: An online platform for improving global land cover. Environ. Model. Softw. *31*, 110–123.

Froyland, G., Menabde, M., Stone, P., and Hodson, D. (2018). The Value of Additional Drilling to Open Pit Mining Projects. In Advances in Applied Strategic Mine Planning, R. Dimitrakopoulos, ed. (Cham: Springer International Publishing), pp. 119–138.

Ganci, G., Cappello, A., Bilotta, G., Herault, A., Zago, V., and Del Negro, C. (2018). Mapping Volcanic Deposits of the 2011–2015 Etna Eruptive Events Using Satellite Remote Sensing. Front. Earth Sci. *6*.

Garai, D., and Narayana, A.C. (2018). Land use/land cover changes in the mining area of Godavari coal fields of southern India. Egypt. J. Remote Sens. Space Sci. *21*, 375–381.

García-Gonzalo, E., Fernández-Muñiz, Z., Garcia Nieto, P. J., Sánchez, A. and Menéndez, M. (2016). Hard-Rock Stability Analysis for Span Design in Entry-Type Excavations with Learning Classifiers. Materials. *9*. 531. 10.3390/ma9070531.

Georganos, S., Grippa, T., Vanhuysse, S., Lennert, M., Shimoni, M., Kalogirou, S., and Wolff, E. (2018). Less is more: optimizing classification performance through feature selection in a very-high-resolution remote sensing object-based urban application. GIScience Remote Sens. *55*, 221–242.

Ghassemian, H. (2016). A review of remote sensing image fusion methods. Inf. Fusion *32*, 75–89.

Glawion R. (2012). Physische Geographie: ein Lehr- und Übungsbuch (Braunschweig: Westermann).

Gray, P., Ridge, J., Poulin, S., Seymour, A., Schwantes, A., Swenson, J., and Johnston, D. (2018). Integrating Drone Imagery into High Resolution Satellite Remote Sensing Assessments of Estuarine Environments. Remote Sens. *10*, 1257.

Han, W., Feng, R., Wang, L., and Cheng, Y. (2018). A semi-supervised generative framework with deep learning features for high-resolution remote sensing image scene classification. ISPRS J. Photogramm. Remote Sens. *145*, 23–43.

Harris Geospatial (2019a). Harris Geospatial Solutions: Geospatial Data and Analytics. Online available: https://www.harrisgeospatial.com/ (2019-06-14).

Harris Geospatial (2019b). Attribute list. Online available: https://www.harrisgeospatial.com/docs/attributelist.html#texture_attributes (2019-06-14).

Hatje, V., Pedreira, R.M.A., de Rezende, C.E., Schettini, C.A.F., de Souza, G.C., Marin, D.C., and Hackspacher, P.C. (2017). The environmental impacts of one of the largest tailing dam failures worldwide. Sci. Rep. *7*.

Heipke, C. (2010). Crowdsourcing geospatial data. ISPRS J. Photogramm. Remote Sens. *65*, 550–557.

Herfort, B., Höfle, B., and Klonner, C. (2018). 3D micro-mapping: Towards assessing the quality of crowdsourcing to support 3D point cloud analysis. ISPRS J. Photogramm. Remote Sens. *137*, 73–83.

Hillen, F., and Höfle, B. (2015). Geo-reCAPTCHA: Crowdsourcing large amounts of geographic information from earth observation data. Int. J. Appl. Earth Obs. Geoinformation *40*, 29–38.

Hossam, M.A. (2015). High Performance Hyperspectral Image Classification using Graphics Processing Units. Online available: http://rgdoi.net/10.13140/2.1.3025.4887 (2019-06-14).

Hou, X., Liu, S., Cheng, F., Zhang, Y., Dong, S., Su, X., and Liu, G. (2019). Vegetation community composition along disturbance gradients of four typical open-pit mines in Yunnan Province of southwest China. Land Degrad. Dev. *30*, 437–447.

Jaccard, P. (1901). Étude comparative de la distribution florale dans une portion des Alpes et du Jura. Impr. Corbaz Comp. Online available: https://www.e-periodica.ch/digbib/view?pid=bsv-002:1901:37::790 (2019-06-14).

Jackisch, R., Gloaguen, R., Lorenz, S., Zimmermann, R., and Möckel, R. (2018). Drone-Borne Hyperspectral Monitoring of Acid Mine Drainage: An Example from the Sokolov Lignite District. Remote Sens. *10*, 385.

Ji, S., Zhang, C., Xu, A., Shi, Y., and Duan, Y. (2018). 3D Convolutional Neural Networks for Crop Classification with Multi-Temporal Remote Sensing Images. Remote Sens. *10*, 75.

Jia, D., Wang, C., and Lei, S. (2018). Semisupervised GDTW kernel-based fuzzy c-means algorithm for mapping vegetation dynamics in mining region using normalized difference vegetation index time series. J. Appl. Remote Sens. *12*, 1.

Jiang, S., Lian, M., Lu, C., Gu, Q., Ruan, S., and Xie, X. (2018). Ensemble Prediction Algorithm of Anomaly Monitoring Based on Big Data Analysis Platform of Open-Pit Mine Slope. Complexity *2018*, 1–13.

Johansen, K., Erskine, P.D., and McCabe, M.F. (2019). Using Unmanned Aerial Vehicles to assess the rehabilitation performance of open cut coal mines. J. Clean. Prod. *209*, 819–833.

Johnson, B.A., Iizuka, K., Bragais, M.A., Endo, I., and Magcale-Macandog, D.B. (2017). Employing crowdsourced geographic data and multi-temporal/multi-sensor satellite imagery to monitor land cover change: A case study in an urbanizing region of the Philippines. Comput. Environ. Urban Syst. *64*, 184–193.

Julien, Y., and Sobrino, J.A. (2019). Optimizing and comparing gap-filling techniques using simulated NDVI time series from remotely sensed global data. Int. J. Appl. Earth Obs. Geoinformation *76*, 93–111.

Karan, S.K., and Samadder, S.R. (2018a). Improving accuracy of long-term land-use change in coal mining areas using wavelets and Support Vector Machines. Int. J. Remote Sens. *39*, 84–100.

Karan, S.K., and Samadder, S.R. (2018b). Dual-tree complex wavelet transform-based image enhancement for accurate long-term change assessment in coal mining areas. Geocarto Int. *33*, 1084–1094.

Keyport, R.N., Oommen, T., Martha, T.R., Sajinkumar, K.S., and Gierke, J.S. (2018). A comparative analysis of pixel- and object-based detection of landslides from very high-resolution images. Int. J. Appl. Earth Obs. Geoinformation *64*, 1–11.

Kirsch, M., Lorenz, S., Zimmermann, R., Tusa, L., Möckel, R., Hödl, P., Booysen, R., Khodadadzadeh, M., and Gloaguen, R. (2018). Integration of Terrestrial and Drone-Borne Hyperspectral and Photogrammetric Sensing Methods for Exploration Mapping and Mining Monitoring. Remote Sens. *10*, 1366.

Kuchma, T. (2016). COMBINED USE OF SAR AND OPTICAL SATELLITE IMAGES FOR LANDSCAPE DIVERSITY ASSESSMENT. 3.

Kumah, A. (2006). Sustainability and gold mining in the developing world. J. Clean. Prod. *14*, 315–323.

LaJeunesse Connette, K., Connette, G., Bernd, A., Phyo, P., Aung, K., Tun, Y., Thein, Z., Horning, N., Leimgruber, P., and Songer, M. (2016). Assessment of Mining Extent and Expansion in Myanmar Based on Freely-Available Satellite Imagery. Remote Sens. *8*, 912.

Lesiv, M., Laso Bayas, J.C., See, L., Duerauer, M., Dahlia, D., Durando, N., Hazarika, R., Kumar Sahariah, P., Vakolyuk, M., Blyshchyk, V., et al. (2019). Estimating the global distribution of field size using crowdsourcing. Glob. Change Biol. *25*, 174–186.

Li, X., and Shao, G. (2014). Object-Based Land-Cover Mapping with High Resolution Aerial Photography at a County Scale in Midwestern USA. Remote Sens. *6*, 11372–11390.

Li, C., Chen, J., Liao, M., Chen, G., and Zhou, Q. (2018a). Ecological Risk Assessment of Shan Xin Mining Area Based on Remote Sensing and Geography Information System Technology. J. Geogr. Inf. Syst. *10*, 234–246.

Li, H., Yang, H., and Zeng, C. (2018b). Can Crowdsourcing Support Remote Sensing Image Classification? In 2018 26th International Conference on Geoinformatics, (Kunming: IEEE), pp. 1–4.

Li, Z., Jiang, Y., Tao, Z., and He, M. (2019). Monitoring prediction of a rockslide in an open-pit mine and numerical analysis using a material instability criterion. Bull. Eng. Geol. Environ. *78*, 2041–2053.

Lillesand, T.M., Kiefer, R.W., and Chipman, J.W. (2008). Remote sensing and image interpretation (Hoboken, NJ: John Wiley & Sons).

Lin, C.Q., Liu, G., Lau, A.K.H., Li, Y., Li, C.C., Fung, J.C.H., and Lao, X.Q. (2018). High-resolution satellite remote sensing of provincial PM2.5 trends in China from 2001 to 2015. Atmos. Environ. *180*, 110–116.

Lobo, F. de L., Souza-Filho, P.W.M., Novo, E.M.L. de M., Carlos, F.M., and Barbosa, C.C.F. (2018). Mapping Mining Areas in the Brazilian Amazon Using MSI/Sentinel-2 Imagery (2017). Remote Sens. *10*, 1178.

Lozano-Cotrina, E., Berrospi-Elises, E., and Roman-Gonzalez, A. (2018). Detection of Minerals Through the Processing of Satellite Images. In 2018 IEEE XXV International Conference on Electronics, Electrical Engineering and Computing (INTERCON), (Lima: IEEE), pp. 1–4.

Ma, B., Chen, Y., Zhang, S., and Li, X. (2018a). Remote Sensing Extraction Method of Tailings Ponds in Ultra-Low-Grade Iron Mining Area Based on Spectral Characteristics and Texture Entropy. Entropy *20*, 345.

Ma, G., Hu, X., Yin, Y., Luo, G., and Pan, Y. (2018b). Failure mechanisms and development of catastrophic rockslides triggered by precipitation and open-pit mining in Emei, Sichuan, China. Landslides *15*, 1401–1414.

Ma, L., Li, M., Ma, X., Cheng, L., Du, P., and Liu, Y. (2017a). A review of supervised object-based land-cover image classification. ISPRS J. Photogramm. Remote Sens. *130*, 277–293.

Ma, Y., Chen, W., Ma, X., Xu, J., Huang, X., Maciejewski, R., and Tung, A.K.H. (2017b). EasySVM: A visual analysis approach for open-box support vector machines. Comput. Vis. Media *3*, 161–175.

Manhart, A., Dehoust, G., Möck, A., Blepp, M., Schmidt, G., Vogt, R., Kämper, C., Auberger, A., Giegrich, J., Priester, D.M., et al. (2017). Erörterung ökologischer Grenzen der Primärroh-stoffgewinnung und Entwicklung einer Methode zur Bewertung der ökologischen Rohstoffverfüg-barkeit zur Weiterentwicklung des Kritikalitätskon-zeptes (ÖkoRess I). 125. Online available: https://www.umweltbundesamt.de/publikationen/eroerterung-oekologischer-grenzen-der (2019-06-14).

Maxwell, A.E., Warner, T.A., and Fang, F. (2018). Implementation of machine-learning classification in remote sensing: an applied review. Int. J. Remote Sens. *39*, 2784–2817.

McAllister, M.L., Fitzpatrick, P., and Fonseca, A. (2014). Challenges of space and place for corporate 'citizens' and healthy mining communities: The case of Logan Lake, BC and Highland Valley Copper. Extr. Ind. Soc. *1*, 312–320.

Melville, B., Lucieer, A., and Aryal, J. (2018). Object-based random forest classification of Landsat ETM+ and WorldView-2 satellite imagery for mapping lowland native grassland communities in Tasmania, Australia. Int. J. Appl. Earth Obs. Geoinformation *66*, 46–55.

Menabde, M., Froyland, G., Stone, P., and Yeates, G.A. (2018). Mining Schedule Optimisation for Conditionally Simulated Orebodies. In Advances in Applied Strategic Mine Planning, R. Dimitrakopoulos, ed. (Cham: Springer International Publishing), pp. 91–100.

Morales, M., Panthi, K.K., and Botsialas, K. (2019). Slope stability assessment of an open pit mine using three-dimensional rock mass modeling. Bull. Eng. Geol. Environ. *78*, 1249–1264.

Mukherjee, J., Mukherjee, J., Chakravarty, D., and Aikat, S. (2019). A Novel Index to Detect Opencast Coal Mine Areas From Landsat 8 OLI/TIRS. IEEE J. Sel. Top. Appl. Earth Obs. Remote Sens. *12*, 891–897.

Mura, J., Gama, F., Paradella, W., Negrão, P., Carneiro, S., de Oliveira, C., and Brandão, W. (2018). Monitoring the Vulnerability of the Dam and Dikes in Germano Iron Mining Area after the Collapse of the Tailings Dam of Fundão (Mariana-MG, Brazil) Using DInSAR Techniques with TerraSAR-X Data. Remote Sens. *10*, 1507.

Murray, N.J., Keith, D.A., Bland, L.M., Ferrari, R., Lyons, M.B., Lucas, R., Pettorelli, N., and Nicholson, E. (2018). The role of satellite remote sensing in structured ecosystem risk assessments. Sci. Total Environ. *619–620*, 249–257.

NASA (2019). National Aeronautics and Space Administration Earthdata. Online available: https://search.earthdata.nasa.gov/search (2019-06-14).

NASA/METI/AIST/Japan Spacesystems, and U.S./Japan ASTER Science Team. ASTER Global Digital Elevation Model. 2009, distributed by NASA EOSDIS Land Processes DAAC, https://doi.org/10.5067/ASTER/ASTGTM.002. ASTER GDEM is a product of Japan's Ministry of Economy, Trade, and Industry (METI) and NASA.

Natural Earth (2019). Natural Earth. Online available: https://www.naturalearthdata.com/ (2019-06-14).

Navarra, A., Montiel, L., and Dimitrakopoulos, R. (2018). Stochastic strategic planning of open-pit mines with ore selectivity recourse. Int. J. Min. Reclam. Environ. *32*, 1–17.

Neukirchen, F., and Ries, G. (2014). Die Welt der Rohstoffe: Lagerstätten, Förderung und wirtschaftliche Aspekte (Berlin: Springer Spektrum).

Ninomiya, Y. (2003). A stabilized vegetation index and several mineralogic indices defined for ASTER VNIR and SWIR data. In IGARSS 2003. 2003 IEEE International Geoscience and Remote Sensing Symposium. Proceedings (IEEE Cat. No.03CH37477), (Toulouse, France: IEEE), pp. 1552–1554.

Olade, M.. (1977). Major element halos in granitic wall rocks of porphyry copper deposits, Guichon Creek batholith, British Columbia. J. Geochem. Explor. *7*, 59–71.

Olade, M., and Fletcher, K. (1976). Distribution of sulphur, and sulphide-iron and copper in bedrock associated with porphyry copper deposits, highland valley, British Columbia. J. Geochem. Explor. *5*, 21–30.

Ortega, J.H., Rapiman, M., Rojo, L., and Rivacoba, J.P. (2018). A validation of the use of data sciences for the study of slope stability in open pit mines. ArXiv180608426 Phys.

Palchowdhuri, Y., Valcarce-Diñeiro, R., King, P., and Sanabria-Soto, M. (2018). Classification of multi-temporal spectral indices for crop type mapping: a case study in Coalville, UK. J. Agric. Sci. *156*, 24–36.

Panteras, G., and Cervone, G. (2018). Enhancing the temporal resolution of satellite-based flood extent generation using crowdsourced data for disaster monitoring. Int. J. Remote Sens. *39*, 1459–1474.

Pasetto, D., Arenas-Castro, S., Bustamante, J., Casagrandi, R., Chrysoulakis, N., Cord, A.F., Dittrich, A., Domingo-Marimon, C., El Serafy, G., Karnieli, A., et al. (2018). Integration of satellite remote sensing data in ecosystem modelling at local scales: Practices and trends. Methods Ecol. Evol. *9*, 1810–1821.

Paull, D., Banks, G., Ballard, C., and Gillieson, D. (2006). Monitoring the Environmental Impact of Mining in Remote Locations through Remotely Sensed Data. Geocarto Int. *21*, 33–42.

Pericak, A.A., Thomas, C.J., Kroodsma, D.A., Wasson, M.F., Ross, M.R.V., Clinton, N.E., Campagna, D.J., Franklin, Y., Bernhardt, E.S., and Amos, J.F. (2018). Mapping the yearly extent of surface coal mining in Central Appalachia using Landsat and Google Earth Engine. PLOS ONE *13*, e0197758.

Pettorelli, N., Schulte to Bühne, H., Tulloch, A., Dubois, G., Macinnis-Ng, C., Queirós, A.M., Keith, D.A., Wegmann, M., Schrodt, F., Stellmes, M., et al. (2018). Satellite remote sensing of ecosystem functions: opportunities, challenges and way forward. Remote Sens. Ecol. Conserv. *4*, 71–93.

Pohl, C., and Van Genderen, J.L. (1998). Review article Multisensor image fusion in remote sensing: Concepts, methods and applications. Int. J. Remote Sens. *19*, 823–854.

Pour, A.B., and Hashim, M. (2012). The application of ASTER remote sensing data to porphyry copper and epithermal gold deposits. Ore Geol. Rev. *44*, 1–9.

Prakash, A., and Gupta, R.P. (1998). Land-use mapping and change detection in a coal mining area - a case study in the Jharia coalfield, India. Int. J. Remote Sens. *19*, 391–410.

Prudente, V.H.R., Silva, B.B. da, Johann, J.A., Mercante, E., and Oldoni, L.V. (2017). COMPARATIVE ASSESSMENT BETWEEN PER-PIXEL AND OBJECT-ORIENTED FOR MAPPING LAND COVER AND USE. Eng. Agríc. *37*, 1015–1027.

Python Software Foundation (2019). Python Language Reference, version 2.7. Online available: https://www.python.org/ (2019-06-14).

QGIS Development Team (2019). QGIS Geographic Information System. Open Source Geospatial Foundation Project. Online available: https://qgis.org/en/site/ (2019-06-14).

Qian, D., Yan, C., Xiu, L., and Feng, K. (2018). The impact of mining changes on surrounding lands and ecosystem service value in the Southern Slope of Qilian Mountains. Ecol. Complex. *36*, 138–148.

Ramazan, S., and Dimitrakopoulos, R. (2018). Stochastic Optimisation of Long-Term Production Scheduling for Open Pit Mines with a New Integer Programming Formulation. In Advances in Applied Strategic Mine Planning, R. Dimitrakopoulos, ed. (Cham: Springer International Publishing), pp. 139–153.

Raval, S. (2018). Smart Sensing for Mineral Exploration through to Mine Closure. Int. J. Georesources Environ. *4*.

Rose, N.D., Scholz, M., Burden, J., King, M., Maggs, C., and Havaej, M. (2018). QUANTIFYING TRANSITIONAL ROCK MASS DISTURBANCE IN OPEN PIT SLOPES RELATED TO MINING EXCAVATION. 16.

Roy, S., More, R., Kimothi, M.M., Mamatha, S., Vyas, S.P., and Ray, S.S. (2018). Comparative analysis of object based and pixel based classification for mapping of mango orchards in Sitapur district of Uttar Pradesh. *12*, 8.

Sabins, F.F. (1999). Remote sensing for mineral exploration. Ore Geol. Rev. *14*, 157–183.

Safari, M., Maghsoudi, A., and Pour, A.B. (2018). Application of Landsat-8 and ASTER satellite remote sensing data for porphyry copper exploration: a case study from Shahr-e-Babak, Kerman, south of Iran. Geocarto Int. *33*, 1186–1201.

Sampedro, C., and Mena, C.F. (2018). Remote Sensing of Invasive Species in the Galapagos Islands: Comparison of Pixel-Based, Principal Component, and Object-Oriented Image Classification Approaches. In Understanding Invasive Species in the Galapagos Islands, M. de L. Torres, and C.F. Mena, eds. (Cham: Springer International Publishing), pp. 155–174.

Santamarina, J.C., Torres-Cruz, L.A., and Bachus, R.C. (2019). Why coal ash and tailings dam disasters occur. Science *364*, 526–528.

Saralioglu, E., and Gungor, O. (2019). Use of crowdsourcing in evaluating post-classification accuracy. Eur. J. Remote Sens. *52*, 137–147.

Sawut, R., Kasim, N., Abliz, A., Hu, L., Yalkun, A., Maihemuti, B., and Qingdong, S. (2018). Possibility of optimized indices for the assessment of heavy metal contents in soil around an open pit coal mine area. Int. J. Appl. Earth Obs. Geoinformation *73*, 14–25.

Schultz J. (2016). Die Ökozonen der Erde: 23 Tabellen und 5 Kästen (Stuttgart: Verlag Eugen Ulmer).

Selmi, M., Lagoeiro, L.E., and Endo, I. (2009). Geochemistry of hematitite and itabirite, Quadrilátero Ferrífero, Brazil. Rem Rev. Esc. Minas *62*, 35–43.

Sengupta, S., Krishna, A.P., and Roy, I. (2018). Slope failure susceptibility zonation using integrated remote sensing and GIS techniques: A case study over Jhingurdah open pit coal mine, Singrauli coalfield, India. J. Earth Syst. Sci. *127*.

Sheffield, J., Wood, E.F., Pan, M., Beck, H., Coccia, G., Serrat-Capdevila, A., and Verbist, K. (2018). Satellite Remote Sensing for Water Resources Management: Potential for Supporting Sustainable Development in Data-Poor Regions. Water Resour. Res. *54*, 9724–9758.

SNAP (2019). SNAP - ESA Sentinel Application Platform v2.0. Online available: http://step.esa.int/main/ (2019-06-14).

Sonobe, R., Yamaya, Y., Tani, H., Wang, X., Kobayashi, N., and Mochizuki, K. (2018). Crop classification from Sentinel-2-derived vegetation indices using ensemble learning. J. Appl. Remote Sens. *12*, 1.

Stachiw, S., Bicalho, B., Grant-Weaver, I., Noernberg, T., and Shotyk, W. (2019). Trace elements in berries collected near upgraders and open pit mines in the Athabasca Bituminous Sands Region (ABSR): Distinguishing atmospheric dust deposition from plant uptake. Sci. Total Environ. *670*, 849–864.

Thorne, W.S., Hagemann, S.G., and Barley, M. (2004). Petrographic and geochemical evidence for hydrothermal evolution of the North Deposit, Mt Tom Price, Western Australia. Miner. Deposita *39*, 766–783.

United Nations, Department of Economic and Social Affairs, Population Division (2017). World Population Prospects: The 2017 Revision, Key Findings and Advance Tables. Online available: https://www.google.com/url?sa=t&rct=j&q=&esrc=s&source=web&cd=1&cad=rja&uact=8&ved=2ahUKEwjM66LypOniAhWS4IUKHQFWDBQQFjAAegQIABAC&url=https%3A%2F%2Fesa.un.org%2Funpd%2Fwpp%2FPublications%2FFiles%2FWPP2017_KeyFindings.pdf&usg=AOvVaw1QEyf6Of_DPvWz9jiuI9Rh (2019-06-14).

Valderrama-Landeros, L., Flores-de-Santiago, F., Kovacs, J.M., and Flores-Verdugo, F. (2018). An assessment of commonly employed satellite-based remote sensors for mapping mangrove species in Mexico using an NDVI-based classification scheme. Environ. Monit. Assess. *190*.

Vassena, G., and Clerici, A. (2018). OPEN PIT MINE 3D MAPPING BY TLS AND DIGITAL PHOTOGRAMMETRY: 3D MODEL UPDATE THANKS TO A SLAM BASED APPROACH. ISPRS - Int. Arch. Photogramm. Remote Sens. Spat. Inf. Sci. *XLII–2*, 1145–1148.

Vogel, P. (2014). Cumulative environmental impacts of development in the Pilbara region, Advice of the Environmental Protection Authority to the Minister for Environment under Section 16(e) of the Environmental Protection Act 1986. Online available: https://www.google.com/url?sa=t&rct=j&q=&esrc=s&source=web&cd=1&cad=rja&uact=8&ved=2ahUKEwjNnqOVpeniAhXSx4UKHfQJCL0QFjAAegQIARAC&url=http%3A%2F%2Fwww.epa.wa.gov.au%2Fsites%2Fdefault%2Ffiles%2FPublications%2FPilbara%2520s16e%2520advice%2520%2520270814.pdf&usg=AOvVaw0dWGW_-6E_SjpRgcNVGtHj (2019-06-14).

Wang, D., Wan, B., Qiu, P., Su, Y., Guo, Q., and Wu, X. (2018a). Artificial Mangrove Species Mapping Using Pléiades-1: An Evaluation of Pixel-Based and Object-Based Classifications with Selected Machine Learning Algorithms. Remote Sens. *10*, 294.

Wang, R.-Q., Mao, H., Wang, Y., Rae, C., and Shaw, W. (2018b). Hyper-resolution monitoring of urban flooding with social media and crowdsourcing data. Comput. Geosci. *111*, 139–147.

Wasowski, J., Bovenga, F., Nutricato, R., Nitti, D.O., and Chiaradia, M.T. (2018). Advanced satellite radar interferometry for deformation monitoring and infrastructure control in open-cast mines and oil/gas fields. Innov. Infrastruct. Solut. *3*.

Wei, L., Zhang, Y., Zhao, Z., Zhong, X., Liu, S., Mao, Y., and Li, J. (2018). Analysis of Mining Waste Dump Site Stability Based on Multiple Remote Sensing Technologies. Remote Sens. *10*, 2025.

Whyte, A., Ferentinos, K.P., and Petropoulos, G.P. (2018). A new synergistic approach for monitoring wetlands using Sentinels -1 and 2 data with object-based machine learning algorithms. Environ. Model. Softw. *104*, 40–54.

Widzyk-Capehart, E., Barberán, A., Briceño, M.J., Navarro, C., Nguyen, P.M.V., Opazo, C., and Steffen, S. (2019). Collocated Ground Deformation and Pore Pressure Measurements in Open Pit Mines: Laboratory Testing and Analysis of Wireless Sensing Platform. In Proceedings of the 27th International Symposium on Mine Planning and Equipment Selection - MPES 2018, E. Widzyk-Capehart, A. Hekmat, and R. Singhal, eds. (Cham: Springer International Publishing), pp. 381–391.

World Trade Organization (2017). Trade Profiles 2017. Online available: https://www.wto.org/english/res_e/booksp_e/trade_profiles17_e.pdf (2019-06-14).

Wu, Q., Liu, K., Song, C., Wang, J., Ke, L., Ma, R., Zhang, W., Pan, H., and Deng, X. (2018). Remote Sensing Detection of Vegetation and Landform Damages by Coal Mining on the Tibetan Plateau. Sustainability *10*, 3851.

Xiang, J., Chen, J., Sofia, G., Tian, Y., and Tarolli, P. (2018). Open-pit mine geomorphic changes analysis using multi-temporal UAV survey. Environ. Earth Sci. *77*.

Xiaolin Zhu, Fangyi Cai, Jiaqi Tian, and Trecia Williams (2018). Spatiotemporal Fusion of Multisource Remote Sensing Data: Literature Survey, Taxonomy, Principles, Applications, and Future Directions. Remote Sens. *10*, 527.

Xiong, J., Thenkabail, P., Tilton, J., Gumma, M., Teluguntla, P., Oliphant, A., Congalton, R., Yadav, K., and Gorelick, N. (2017). Nominal 30-m Cropland Extent Map of Continental Africa by Integrating Pixel-Based and Object-Based Algorithms Using Sentinel-2 and Landsat-8 Data on Google Earth Engine. Remote Sens. *9*, 1065.

Xu, X., Gu, X., Wang, Q., Gao, X., Liu, J., Wang, Z., and Wang, X. (2018). Production scheduling optimization considering ecological costs for open pit metal mines. J. Clean. Prod. *180*, 210–221.

Xu, Z., Xu, E., Wu, L., Liu, S., and Mao, Y. (2019). Registration of Terrestrial Laser Scanning Surveys Using Terrain-Invariant Regions for Measuring Exploitative Volumes over Open-Pit Mines. Remote Sens. *11*, 606.

Yan, G., Mas, J. -F., Maathuis, B.H.P., Xiangmin, Z., and Van Dijk, P.M. (2006). Comparison of pixel-based and object-oriented image classification approaches—a case study in a coal fire area, Wuda, Inner Mongolia, China. Int. J. Remote Sens. *27*, 4039–4055.

Yang, W., Ai, T., and Lu, W. (2018a). A Method for Extracting Road Boundary Information from Crowdsourcing Vehicle GPS Trajectories. Sensors *18*, 1261.

Yang, Y., Erskine, P.D., Lechner, A.M., Mulligan, D., Zhang, S., and Wang, Z. (2018b). Detecting the dynamics of vegetation disturbance and recovery in surface mining area via Landsat imagery and LandTrendr algorithm. J. Clean. Prod. *178*, 353–362.

Yu, L., Xu, Y., Xue, Y., Li, X., Cheng, Y., Liu, X., Porwal, A., Holden, E.-J., Yang, J., and Gong, P. (2018). Monitoring surface mining belts using multiple remote sensing datasets: A global perspective. Ore Geol. Rev. *101*, 675–687.

Zhang, F., Li, J., Zhang, B., Shen, Q., Ye, H., Wang, S., and Lu, Z. (2018). A simple automated dynamic threshold extraction method for the classification of large water bodies from landsat-8 OLI water index images. Int. J. Remote Sens. *39*, 3429–3451.

Zhang, M., Zhou, W., and Li, Y. (2017). THE ANALYSIS OF OBJECT-BASED CHANGE DETECTION IN MINING AREA: A CASE STUDY WITH PINGSHUO COAL MINE. ISPRS - Int. Arch. Photogramm. Remote Sens. Spat. Inf. Sci. *XLII-2/W7*, 1017–1023.

Introductory quote:

Kelley, K. W. (1988). The home planet. Reading, Mass.: Addison-Wesley [u.a.], 250.